Interrelation and plasticity of inter- and intrahemispheric corticocortical connections, and the relation between ocular dominance columns and callosal connections in rat visual cortex

Robyn Laing

A dissertation
submitted in partial fulfillment of the
requirements for the degree of

Doctor of Philosophy

University of Washington
2014

Reading Committee:
Jaime F Olavarria, Chair
Helen Sherk
Steven L Buck

Program Authorized to Offer Degree:
Department of Psychology

University of Washington

Abstract

Interrelation and plasticity of inter- and intrahemispheric corticocortical connections, and the relation between ocular dominance columns and callosal connections in rat visual cortex

Robyn Laing

Chair of Supervisory Committee:
Professor Jaime F Olavarria
Department of Psychology

Interhemispheric callosal connections are present throughout areas 17 (V1; striate cortex) and 18a (lateral extrastriate cortex) of the rodent visual cortex, are topographically organized, and form a variety of patterns including strips, patches, and bridges as they share relationships to the underlying structures in cortex. Previous studies have shown that the retina plays a role in the development of topographically organized areas in the cortex. Here, we investigated the relationship between callosal connections and the underlying structures in the rat visual cortex, as well as the influence that the retina plays on these connections.

In Chapter 1, we examine both the structural and functional properties of ocular dominance territories and interhemispheric callosal connections in primary visual cortex. We demonstrate a novel finding that rats have patchy callosal connections and segregated ocular dominance columns. Furthermore, in the central portion of V1, callosal connections overlap with ipsilateral ocular dominance columns and at the lateral border of V1, callosal connections overlap with contralateral domains, as has previously been described in the cat. These results suggest that development of cortical modular architecture is more conserved among rodents, carnivores and primates than previously thought.

In Chapter 2, we investigated the role that retinal input plays in the development of interhemispheric callosal connections and ipsilateral striate-extrastriate connections. We found that after bilateral enucleation, the patterns of striate-extrastriate connections and

interhemispheric callosal connections were abnormal. While striate-extrastriate projections consisted of multiple well-defined fields that were largely confined to acallosal regions as they do in normal rats, these projections were highly irregular and variable, as were the acallosal regions observed in extrastriate cortex.

In Chapter 3, we investigated the role that the eyes play in the topography of striate-extrastriate connections. Using multiple, single injections of different tracers placed at different locations in striate cortex, we were able to map out the patterns of projections to extrastriate cortex. In lateral extrastriate cortex of normal rats, the representation of the naso-temporal axis of visual loci mirrors the representation of this axis in V1. We found that the correlation between the distance from injection sites to the lateral border of V1 and the distance from this border to the labeling patterns in area 18a was strong in controls and much weaker in neonatally enucleated rats, suggesting that the eyes play a role in the development of mediolateral topography during neonatal life.

TABLE OF CONTENTS

LIST OF FIGURES

ACKNOWLEDGEMENTS

I wish to acknowledge the following people for their roles in my development as a scientist, the production of this work and my journey through graduate school.

My advisor Jaime Olavarria for teaching me to think and work like a scientist, for helping me to develop my writing skills, and for always believing in me.

Helen Sherk for her support and advice over the years, as well as for invaluable assistance with our experimental setup.

Steve Buck for support and advice that was provided to me during my time in graduate school.

My fellow lab mate Adrian Andelin for his invaluable help and friendship over the years.

My many gifted undergraduate students who worked with me during the long years of graduate school.

The Vision Training Grant at the University of Washington, Department of Biological structure for my financial support over the last three years.

Finally, I would like to thank my significant other Christopher Moss, for his patience, love and support throughout graduate school.

DEDICATION

I would like to dedicate this work to my parents, Thomas and Judy Laing. Without their love and constant support of my education and pursuit of science, this accomplishment would have never been possible.

INTRODUCTION

The discovery of modularity in the cerebral cortex (Mountcastle, 1957) opened new ways of thinking about how cortical architecture might relate to function. For instance, it led to the idea that modules may represent basic functional units, and that sensory cortex could be understood as an orderly assembly of repeating columnar modules performing similar operations on topographically organized sensory input. Such modules have been termed the cortical column. In primary visual cortex (V1, area 17), modular systems, such as orientation columns (aggregates of cells selective for the same orientation of edges or bar-like stimuli) and ocular dominance columns (ODCs, aggregates of cells with the same eye preference), have been extensively studied in a variety of mammalian species (reviewed in Horton and Adams, 2005; Van Hooser, 2007). These studies revealed that while these modular systems are evident in carnivores and primates, there is little evidence of their existence in other orders such as rodents (Drager, 1975; Gordon and Stryker, 1996; Antonini et al., 1999; Kaschube et al., 2010), suggesting that within the visual cortex, mammals can be broadly divided into species that have columnar architecture and those that do not (Horton and Adams, 2005; Horton and Hocking, 1996).

Chapter 1 challenges the notion that rodents lack columnar organization in the visual cortex. Preliminary studies in our lab showed that connections through the corpus callosum in the Long Evans rat were patchy. Based on the relationship between patchy callosal connections and ODCs that was previously described in the cat (Olavarria, 2001), we predicted that rats also have ODCs. While some studies have suggested a degree of segregation (Thurlow and Cooper, 1988;) between ipsilateral and contralateral cells in rat visual cortex, ODCs have otherwise never before been discovered or described in the rat (reviewed by Horton and Hocking, 1996). Such a finding would provide scientists with a new, rodent model to study ODCs and the mechanisms which specify their development as well as their plasticity. Here, we use transneuronal tracing, in situ hybridization and electrophysiology methods to examine the ocular dominance territories as well as callosal connections in rat V1.

While a tremendous amount of research has focused on rodent V1, much less is known about V2. Numerous studies have determined that area 18 of the rat and mouse is subdivided into multiple visual areas, each of which receive direct input from area 17 (Montero, 1973; Espinoza and Thomas, 1983; Wang and Burkhalter, 2007). Anatomical tracing studies supported the

notion that these regions are also separate cortical areas. In the mouse, at least 9 regions have been shown to contain a complete topographic map of the visual field (Wang and Burkhalter, 2007), while in the rat, 10 such areas have been described (Montero, 1993). It has also been demonstrated that callosal connections in area 18 form acallosal islands, which correspond to extrastriate areas (Olavarria and Montero, 1984; Olavarria and Montero, 1989), suggesting that the development of callosal connections and extrastriate areas is related. However there is little research examining the development of either the topography of these extrastriate areas, or the structures of callosal connections interconnecting these areas.

In area 17, it has been shown that the eyes are necessary for the proper development of the callosal map during a critical period which ends by postnatal day 6 (P6; Olavarria et al., 1987; Olavarria and Hiroi, 2003). However, the role that the eyes play in the development of callosal connections in extrastriate areas is not well understood. In Chapter 2, we investigated the role that retinal input plays in the development of interhemispheric callosal connections and ipsilateral striate-extrastriate connections. We focused our analysis on 7 different regions which have previously been described in area 18a. Using anatomical methods, callosal connections and striate-extrastriate projections were labeled and analyzed in both normal and enucleated rats. We predicted that enucleation performed before P6 would affect the patterns of callosal connections in area 18 as well as the interplay between callosal connections and extrastriate areas. Finally, Dong et al. (2004) found that in mice, feedback projections developed later than feedforward striate-extrastriate projections. Therefore we also compared projection patterns from anterograde and retrograde tracer injections in striate to extrastriate cortex as well as the size of areas 17 and 18a in normal and enucleated animals.

In Chapter 3, we focused our investigation on the role that the eyes play in the topography of striate-extrastriate connections. In most of the lateral extrastriate regions of normal rats, the representation of the naso-temporal axis of visual loci mirrors the representation of this axis in V1 (Montero, 1998; Wang and Burkhalter, 2007). To determine whether the eyes are necessary for this mediolateral topography of striate-extrastriate projections, we used multiple, single injections of different tracers placed at different locations in striate cortex to map out the patterns of projections to extrastriate cortex. This technique allowed us to examine the mediolateral retinotopic map in normal and enucleated rats. We predicted that animals which

were enucleated neonatally would have an abnormal pattern of mediolateral topography in extrastriate cortex.

CHAPTER 1 IDENTIFICATION OF EYE-SPECIFIC DOMAINS AND THEIR RELATION TO CALLOSAL CONNECTIONS IN PRIMARY VISUAL CORTEX OF LONG EVANS RATS

ABSTRACT

Ocular dominance columns (ODCs) exist in many primates and carnivores, but it is believed that they do not exist in rodents. Using a combination of transneuronal tracing, in situ hybridization for Zif268 and electrophysiological recordings, we show that inputs from both eyes are largely segregated in the binocular region of V1 in Long Evans rats. We also show that, interposed between this binocular region and the lateral border of V1, there lies a strip of cortex that is strongly dominated by the contralateral eye. Finally, we show that callosal connections co-localize primarily with ipsilateral eye domains in the binocular region and with contralateral eye input in the lateral cortical strip, mirroring the relationship between patchy callosal connections and specific sets of ODCs described previously in the cat. Our results suggest that development of cortical modular architecture is more conserved among rodents, carnivores and primates than previously thought.

This chapter was previously published in Cerebral Cortex (June, 2014) and used with permission.

INTRODUCTION

In primary visual cortex (V1, area 17), ocular dominance columns (ODCs, aggregates of cells with the same eye preference) and orientation columns (aggregates of cells selective for the same orientation of edges or bar-like stimuli) have been extensively studied in a variety of mammalian species (Tootell et al., 1988; reviewed in Horton and Hocking 1996; Van Hooser 2007). These studies revealed that while ocular dominance and orientation columns are evident in many carnivores and primates, there is little evidence of their existence in V1 of other orders such as rodents (Dräger 1975; Metín et al. 1988; Fagiolini et al. 1994; Gordon and Stryker 1996; Antonini et al. 1999; Girman et al. 1999; Ohki et al. 2005; Ohki and Reid 2007). This apparent difference between animal groups suggests that mammals can be broadly divided into species that have columnar architecture in visual cortex and those that do not (Horton and Hocking 1996; Van Hooser 2007). Surprisingly, response tuning properties of visual cortical neurons do not seem to depend on the existence of orientation columns because these properties are remarkably similar in animals with and without orientation columns (Girman et al. 1999; Van Hooser et al. 2005; 2006). These observations have cast doubt on the idea that wiring of functional visual cortical circuits follows the same master plan in all species (Horton and Adams 2005; Van Hooser 2007). In addition, the lack of ocular dominance and orientation columns in the gray squirrel – a diurnal, highly visual rodent whose brain size compares to that of animals with ocular dominance and orientation columns – implies that absence of columnar architecture in visual cortex in rodents cannot be attributed solely to their small brain or nocturnal habit (Van Hooser et al. 2005; 2006). Instead, these studies have led to the idea that in animals like rodents, functional architecture in visual cortex is fundamentally different from that in carnivores and primates.

In the cat, visual callosal connections form patches that are closely correlated with ocular dominance columns (Olavarria 2001; 2002). Prompted by preliminary observations that callosal connections are also patchy in rat V1 we set out to investigate whether callosal patches reflect an underlying pattern of ocular dominance domains that has not been previously described in the rat. We examined this possibility using a combination of anatomical and functional approaches. We found that inputs from both eyes segregate into eye-specific domains in a binocular region of V1. Moreover, we found that in this region callosal patches correlate primarily with ipsilateral eye domains. Surprisingly, our results also show that between this binocular region and the

lateral border of V1 lies a narrow, callosal rich region that is dominated nearly exclusively by the contralateral eye.

MATERIALS AND METHODS

Normal adult Long Evans hooded rats (*Rattus norvegicus*, Charles River Laboratories) were used and procedures were performed according to protocols approved by the Institutional Animal Care and Use Committee at the University of Washington and Vanderbilt University, and are in accordance with the animal care guidelines of the National Institutes of Health, USA.

Intraocular and intracortical injections of anatomical tracers, and histochemical processing

Intraocular and intracortical tracer injections were performed under anesthesia induced and maintained with isoflurane (5% and 2.5%, respectively) in air. Retino-thalamo-cortical projections were revealed following intravitreal injections of the transneuronal tracer horseradish peroxidase conjugated to wheat-germ agglutinin (WGA-HRP; Sigma Co.). Due to its transneuronal transport property, demonstrated at the ultrastructural level (Itaya and Van Hoesen 1982), this tracer has been widely used in studies of retino-thalamo-cortical projections in a variety of species, including rats (Itaya and Van Hoesen 1982; Gerfen et al. 1982; Kageyama et al. 1990), cats (Anderson et al. 1988; Olavarria 2001), ferret (Ruthazer et al. 1999; White et al. 1999), and monkeys (Horton and Hocking 1996). Moreover, cortical patterns of WGA-HRP labeling interdigitate with patterns labeled from the opposite eye with tritiated proline - another widely used transneuronal tracer - in cats (Hata and Stryker 1994) and monkeys (Horton and Hocking 1996), providing evidence that WGA-HRP patterns represent ODCs. A total volume of 6 μl of 3% WGA-HRP in saline was pressure injected over approximately 15 min through glass micropipettes (50-100 μm tip diameter). The injection site was approximately 2.0 mm posterior to the corneal limbus, at a depth of approximately 2.0 mm. Callosal connections were labeled following multiple intracortical injections of either horseradish peroxidase (HRP, Sigma Co, 25% in saline; total volume = 4.0 μl), biotinylated biodextran amine (BDA, 10 kDa, 10% in DW, Molecular Probes, Eugene, OR, total volume = 4 μl), or rhodamine-tagged latex beads (RB; LumaFlour, Naples, FL, concentrated stock solution, total volume = 4 μl). Previous studies at both light and electron microscopic levels have demonstrated that HRP is transported both

anterogradely and retrogradely (Trojanowsky et al. 1981), while BDA (10 kDA) is transported mainly anterogradely, although some retrograde labeling may occur (Reiner et al. 2000). The fluorescent tracer RB is transported retrogradely (Katz et al. 1984).

For all intracortical tracers used, evenly spaced injections (0.2 μl each) were delivered at a depth of about 800-1000 μm in occipital cortex. The tracers were pressure injected through glass micropipettes (50-100 μm tip diameter) over an area extending approximately 2-7 mm lateral to midline suture, and 0.0-6.0 mm anterior to lambda suture. During the tracer injections, the dura was kept intact and moist with saline. Following the injections, the bone chip was repositioned and the skin was sutured by planes.

Four days following intraocular injections of WGA-HRP and 2-3 days following intracortical injections of anatomical tracers (HRP, BDA, or RB) animals were deeply anesthetized with pentobarbital sodium (100 mg/kg i.p.) and perfused through the heart with 0.9% saline followed by 4% paraformaldehyde (PFA) in 0.1M phosphate buffer (PB) (pH 7.4). Cortical mantles were either separated from the brains and flattened for sectioning in the tangential plane or left intact for sectioning in the coronal plane. The flattened cortices were left between glass slides for 24 hours in 0.1 M PB, after which time the tissue was transferred to a 4% PFA in 0.1M PB, 20% sucrose solution for approximately 1 additional hour. Tissue blocks to be sectioned in the coronal plane were kept in 4% PFA in 0.1M PB and 20% sucrose for one or more days. All tissue was cut on a freezing microtome at 60 μm thickness and the sections were collected in 0.1M PB. Sections from brains containing WGA-HRP or unconjugated HRP were reacted for HRP with 3,3,5,5 tetramethyl benzidine as the chromogen (Mesulam 1978). BDA labeling was revealed using the standard Avidin-Biotin-Peroxidase protocol (Vectastain Elite ABC kit, Vector Laboratories, Burlingame, CA) and 0.01% H_2O_2 in 0.05% 3-3′ diaminobenzidine, with cobalt or nickel intensification; sections were then mounted, dehydrated, defatted, and coverslipped. Tangential sections examined only for the fluorescent tracer RB were mounted on slides and analyzed under epifluorescence without further processing. In some experiments combining WGA-HRP and RB, sections processed for WGA-HRP were often also analyzed for epifluorescence because the fluorescent labeling in these sections was similar to that in sections not processed for WGA-HRP. This allowed a direct correlation of the distribution of RB and WGA-HRP labeling in the same section.

In situ hybridization (ISH) for Zif268

In three rats, monocular injections of tetrodotoxin (TTX) were administered under general anesthesia induced with a mixture of ketamine (60-90 mg/kg) and xylazine (6-9 mg/kg), and maintained with isoflurane (1-5%). A total volume of 5 μl of TTX (1 mM) was slowly injected into the vitreous of the left eye with a Hamilton Syringe fitted with a glass pipette. Rats recovered and moved freely in their home cages for a period of twenty-four hours, after which time they were anesthetized with ketamine/xylazine followed by an overdose of pentobarbital (120 mg/kg) and perfused intracardially with 4% PFA in 0.1 M PB. The cortical mantles were separated from the brain and flattened. The tissue was postfixed overnight in 4% PFA/30% sucrose/PB at 4°C and cryoprotected in 30% sucrose/PB at 4°C for 1-2 additional nights. Once frozen, the flattened tissue was cut tangentially to the pial surface on a sliding microtome at 40 μm thickness. The sections were kept in a cryoprotectant solution (30% glycerol, 30% ethylene glycol, 40% 0.1 M phosphate-buffered saline) at -20°C.

Preparation of probes

Plasmids with inserts of specific sequences to rat Zif268 and *ROR*β were prepared with the conventional TA-cloning technique. The sequences of primer sets to clone rat Zif268 were cccaggacaattgaaatttgct (forward) and aaggcaccaagacgtgaaac (reverse), targeting 1878-2678 of NM_001964 including primers. Those for *ROR*β were aaagcaagcacattggagag (forward) and gtcaatgacgtgcccgttgg (reverse), targeting 278-957 of XM_001098940. The sequences were amplified by RT-PCR from rat whole brain cDNA (Zyagen, San Diego, CA) and inserted into pCR®II-TOPO plasmid vectors (Invitrogen, Carlsbad, CA). Those plasmids were amplified by transfecting into competent cells (*E. coli*) (Invitrogen), and purified. Digoxigenin (DIG)-labeled antisense and sense riboprobes were prepared from the plasmids using a DIG-dUTP labeling kit (Roche Diagnostics, Indianapolis, IN). RNA Probes were then purified with ProbeQuant G-50 Micro Columns (GE Healthcare Life Science, Pittsburg, PA).

Colorimetric in situ hybridization (ISH)

Free-floating sections were soaked in 4% PFA/0.1 M PB (pH 7.4) overnight at 4°C, permeabilized with 0.3% Triton-X for 20 min at room temperature and treated with 3μg/ml proteinase K for 30 min at 37°C. After acetylation, the sections were incubated in hybridization buffer [5×standard saline citrate (SSC: 150 mM NaCl, 15 mM Na citrate, pH 7.0), 50% formamide, 2% blocking reagent (Roche Diagnostics), 0.1% *N*-lauroylsarcosine (NLS), 0.1%

sodium dodecyl sulphate (SDS), 20 mM maleic acid buffer; pH 7.5] containing 1.0 μg/ml DIG-labeled riboprobe at 60°C overnight. Hybridized sections were washed by successive immersion in wash buffer 1 (2×SSC, 50% formamide, 0.1% NLS; 60°C, 20 min, twice), RNase A buffer [10 mM Tris-HCl, 10 mM ethylenediamine-*N*,*N*,*N'*,*N'*-tetraacetic acid (EDTA), 500 mM NaCl; pH 8.0] containing 20 μg/ml RNase A (37°C, 30 min), 2×SSC/ 0.1% NLS (37°C, 20 min) and 0.2×SSC/0.1% NLS (37°C, 15 min). Hybridization signals were visualized by alkaline phosphatase (AP) immunohistochemical staining using a DIG detection kit (Roche Diagnostics). Sections were mounted onto glass slides, dehydrated through a graded series of increasing ethanol concentrations followed by xylene, and then coverslipped with Permount. The sense probes detected no signals stronger than background (Fig. 1.9B).

Electrophysiology

Electrophysiological recordings were performed under urethane anesthesia (1200 mg/kg i.p.) supplemented with ketamine (76 mg/kg i.m.). Atropine sulfate (0.1 mg/kg i.p.) was used to reduce tracheal secretion, and dexamethasone (0.001 mg/g s.c.) to prevent brain edema. Body temperature was maintained at 37°C with a heating pad. Pupils were dilated with atropine sulfate ophthalmic solution (1%, Bausch and Lomb), and artificial tears (polyethylene glycol eye drops) and silicone oil were used to protect the corneas and the cerebral cortex, respectively. An area of occipital cortex extending from 2 to 7 mm in the mediolateral direction, and from the lambda suture to 5 mm in the anteroposterior direction was exposed leaving the dura intact. Multiunit activity was recorded with glass-insulated tungsten electrodes (1-2 MΩ; FHC) oriented perpendicularly to the cortical surface at depths of about 400-600 μm. Signals were filtered and amplified with conventional electrophysiological instrumentation, displayed on an oscilloscope and an audio monitor, and stored in a computer. Visual stimuli consisted of hand-held light bars either flashed or swept across the visual field at a distance of 30 cm from the rat's eyes. Each eye was stimulated separately while the non-stimulated eye was covered. Visual responses elicited from an eye ceased when the eye was covered, indicating that covering of the eyes was effective in preventing visual stimulation. Electrode penetrations, spaced at least 200 μm apart, were arranged in a grid over the lateral half of V1. At each recording site, the ocular preference of the multiunit activity was rated on the Hubel and Wiesel's 1-7 scale (Hubel and Wiesel 1962), according to which responses in ocular dominance group 1 were driven only by the contralateral

eye while responses in ocular dominance group 7 were driven only by the ipsilateral eye. Binocular responses were rated in between, with 4 indicating about equal responsiveness to both eyes.

Two-three days prior to recording from one hemisphere, the opposite hemisphere received multiple, evenly spaced injections of HRP to label the pattern of visual callosal connections. In a separate group of rats, HRP was injected intracortically in one hemisphere, and 2-3 days later the splenium of the corpus callosum was transected at the beginning of a recording session on the opposite hemisphere. The splenium was transected by making a parasagittal cut with a #11 scalpel blade in the hemisphere opposite to the recordings, 1 mm lateral to the midline, 3 mm deep, and extending posteriorly from 3 to 6 mm measured from the bregma suture. Rats with and without callosal transection were perfused immediately at the end of the recording sessions, and the recorded hemispheres were flattened for tangential sectioning. The callosotomy was inspected in coronal sections and only cases with a complete transection of the splenium were analyzed. In four rats, cortical cytoarchitecture and visual responsiveness was assessed in the HRP injected hemisphere 2-3 days after the injections. Finally, in two additional rats, the splenium was transected *before* the HRP injections, and care was taken to prevent HRP from spilling into the cut. Two days later the animals were perfused and the presence of HRP labeling in both hemispheres was analyzed in coronal sections.

Data acquisition and analysis

Identifying the border of V1 in anatomical tracer experiments

The cytoarchitectonic criteria typically used to identify the border of V1 in coronal sections (Krieg 1946; Caviness 1975; Zilles et al. 1980) cannot be easily applied in tangential sections. We therefore used the myelination pattern, which can be readily displayed in tangential sections. Previous studies show that cytoarchitectonic and myeloarchitectonic criteria for identifying V1 are in close agreement (e.g., Olavarria and Van Sluyters, 1984). Before histochemical processing for anatomical tracers, unstained tangential sections were scanned to identify the myelin pattern (Richter and Warner 1974; Laing et al. 2012). In these images, the transition from dense myelination in V1 to reduced myelination at the border of V1 was delineated with the aid of the filter "trace contour" in Adobe Photoshop CS5 (Adobe Systems, CA) (Fig. 1.1). The myelin pattern was optimally displayed in tangential sections passing

through layer 4 (approximately 500-650 μm deep) and was confirmed in two or more sections from the same animal (Fig. 1.1). Further information for identifying the border of V1 was provided by the relationship that is known to exist between this border and distinct features of the callosal pattern in V1 (Olavarria and Van Sluyters 1985, Laing et al. 2012).

Following histological processing for anatomical tracers, digital images of labeling patterns were obtained by scanning the sections at 2400 dpi using an Epson 4990 scanner. The distribution of callosal cells labeled retrogradely with the fluorescent tracer RB was analyzed using a microscope equipped with a motorized stage (LEPCO) controlled by a Dell XPS T500 computer and a graphic system (Neurolucida, MicroBrightField, Williston, VT). High-magnification images of anatomical tracer labeling or cortical cytoarchitecture were obtained using a DMR Leica microscope coupled to a Leica DC 300F digital camera.

Digitized images of anatomical tracer and myelin labeling patterns obtained from each animal were carefully aligned with each other in Adobe Photoshop, using the border of V1, the edges of the sections, radial blood vessels and other fiducial marks as reference. Specific labeling patterns were reconstructed by merging series of carefully aligned neighboring sections. Noise and high pass filters were applied to these patterns to remove gradual changes in staining density across the entire image. Thresholded version of these patterns were then prepared, making sure that they accurately represented the labeling pattern observed in the tissue sections. Quantitative comparisons of anatomical features were evaluated with Student's *t*-test using Bonferroni corrections as needed (significance set at $p < 0.01$). Area measurements were not corrected for potential tissue shrinkage.

The patterns of eye-specific WGA-HRP labeling and callosal connections were reconstructed from series of tangential sections and correlated with each other as described previously (Olavarria 2001). The distribution of callosal labeling was compared with thresholded images of the patterns of eye-specific domains, and the χ^2 test (1 df, significance set at $p < 0.01$) was used to test whether the distribution of callosal connections in both eye-specific domains was different from chance. Counts of RB-labeled cells were estimated by dividing the total pixel count for scored RB cells by the average number of pixels in a single cell. When callosal connections were labeled with BDA, chi-square was calculated after the analyzed region was divided into 100 equal units.

In the ISH experiments, V1 was identified using the silver procedure for myelin fibers (Gallyas 1979) in a set of tangential sections. The location of layer 4 was identified by the high expression of *ROR* β mRNA (Hirokawa et al. 2008). Images of myelin and Zif268 expression patterns were captured with a Nikon Eclipse E800M microscope using a high-density CCD color digital camera, DXM1200F (Nikon, Tokyo, Japan). The brightness and contrast of the images were adjusted using Photoshop CS3 Extended (Adobe Systems, CA), and the overall patterns of Zif268 mRNA expression in both hemispheres were reconstructed from 3-5 tangential sections by carefully aligning consecutive sections guided by radial blood vessels and tissue edges.

In the electrode recording experiments, the locations of recording sites with reference to local blood vessels were marked on digital images of the intact cortical surface taken at the beginning of the recording sessions. These images were later correlated with images of the most superficial tangential sections, and the recording sites were matched to the pattern of electrode penetrations observed in these sections. Superficial sections were aligned with deeper sections using the pattern of penetrating blood vessels, section borders and other landmarks. Following histological processing, the recording sites were assigned to specific regions in V1 that were identified by the patterns of HRP-labeled callosal connections and myelination. Only penetrations judged to be oriented perpendicularly to the cortical surface were analyzed. To evaluate the ocular preference of responses within each of the analyzed regions, a Contralateral Bias Index (CBI) was calculated using the formula:

CBI = $[(n1 - n7) + 2/3(n2 - n6) + 1/3(n3 - n5) + N]/2N$, where N is the total number of recorded sites and nx is the number of sites in an ocular dominance group x. This index ranges from 0.0 to 1.0, values that indicate complete dominance by the ipsilateral or the contralateral eye, respectively. CBIs for the cortical regions analyzed in intact brains were compared using Bonferroni-corrected repeated measures Student's t-tests (significance set at $p < 0.01$). CBIs from intact and callosotomized brains were compared using Bonferroni-corrected independent samples Student's t-tests (significance set at $p < 0.01$). Figures were prepared using Adobe Photoshop CS5 and all imaging processing used, including contrast enhancement and intensity level adjustments, were applied to the entire images.

RESULTS

Input from the ipsilateral eye forms separate patches in rat primary visual cortex

Our preliminary observation of callosal patches in V1 led us to hypothesize that input from the ipsilateral eye is segregated into specific domains in the rat, and that these domains correlate with callosal patches, as occurs in the cat (Olavarria 2001; 2002). To test whether inputs from the ipsilateral eye form eye-specific domains in V1, we injected WGA-HRP into one eye and examined the resulting pattern of retino-thalamo-cortical input to V1. In the hemisphere ipsilateral to the injected eye, labeling was found in discrete patches located within a restricted portion, about 1.0 mm wide, of V1 (Figs. 1.1A,B, 1.3, 1.5). However, in all cases analyzed, we observed that WGA-HRP labeling was absent or markedly reduced in a narrow strip of cortex, approximately 0.22 mm in width, that directly adjoined the lateral border of area 17. To aid in the identification of the layer distribution of WGA-HRP labeling observed in tangential sections, we also visualized the labeling pattern in coronal sections (Fig. 1.2) (see also Itaya and Van Hoesen 1982; Gerfen et al. 1982; Kageyama et al. 1990). The WGA-labeling patterns illustrated in Figure 1A,B are from sections cut at the level of layer 4, where the pattern is most distinct (see also Fig. 3C, Fig. 2). Labeling was also seen in sections through lower layer 3 (Fig. 1.3B, Fig. 1.2), but the pattern was less distinct. In deeper sections, the pattern was weak or not visible at the level of layer 5 (Fig. 1.3D, Fig. 1.2), but it was again visible in sections through layer 6 (Figure 1.3E, Fig. 1.2). The labeling pattern in sections through layer 6 resembled the pattern observed in sections through layer 4 (cf. Fig. 1.3C, E), suggesting that patterns of geniculate input to both layers are in register with each other, as occurs in the cat (LeVay and Gilbert 1976).

Tripartite subdivision of V1

Based on the pattern of ipsilateral transneuronal WGA-HRP labeling described above, we recognized three main subdivisions within V1: 1) The Central Segment (CS), defined as the area containing the ipsilateral eye-specific domains (outlined by dashed lines in Fig. 1A,B). We estimate that the surface area occupied by ipsilateral eye domains is about a third of the total surface area of the CS (see below). 2) The Medial Segment (MS), located medial to the CS, presumably represents the peripheral monocular visual field. 3) The Lateral Segment (LS), located between the CS and the lateral border of V1.

Examination of WGA-HRP labeling in the superior colliculus (SC) and dorsal lateral geniculate nucleus (dLGN) showed the typical patterns of retinal projections to these nuclei in the rat (Fig. 1.1F). Ipsilateral to the injected eye, labeling was restricted to one or more densely labeled patches in dorsomedial regions of the dLGN, while contralaterally the labeling was uniformly dense throughout the dLGN, except for a small dorsomedial region that presumably corresponds to the ipsilateral eye recipient zone. Similarly, weak, patchy input was seen in the ipsilateral SC, while dense, uniform labeling occupied the contralateral SC. These observations make it unlikely that the patchy distribution of ipsilateral eye input in V1 is due to obvious anomalies in retino-thalamic projections, or incomplete or uneven uptake of the tracer by retinal ganglion cells.

Patchy callosal connections in rat primary visual cortex

Previous studies report that the distribution of callosal connections in visual cortex peaks at the border region between areas 17 and 18a and extends some distance into these areas (e.g., Cusick and Lund 1981; Olavarria and Van Sluyters 1985). However, in preliminary experiments we observed that callosal connections in V1 are often markedly inhomogeneous in the tangential plane. In the present study we carefully examined the distribution of callosal cells and fibers in V1 as revealed by multiple, evenly spaced intracortical injections of several anatomical tracers, including HRP (Figs. 1.4A,B, 1.10A, Fig. 1.10C), BDA (Fig. 1.4C, 1.6G, 1.7C), or RB (Fig. 1.6C, 1.6I). We observed that, independent of the tracer used, two callosal regions could be readily recognized in tangential sections through area V1 in the hemisphere opposite to the injections: a medial callosal region, approximately 1.0 mm wide at the widest part, where callosal connections typically formed distinct, densely labeled patches of different shapes and sizes (arrows in Fig. 1.4A-C), and a lateral region, indicated by the dashed line in Figs. 1.4A-C, 1.6, 1.10A, where callosal connections form a band approximately 0.22 mm wide abutting the border of V1. In most rats examined this band was homogeneously labeled throughout its anteroposterior extent, but occasionally the labeling was less dense at one or two discrete sites. By its location and width, the lateral callosal band corresponds closely with the LS described above (cf. Figs. 1.1 and 1.4; see below). In agreement with previous descriptions of the laminar distribution of labeled callosal connections (e.g., Olavarria and Van Sluyters 1985), we observed that the callosal pattern was apparent in tangential sections through layers 2-6, although it

appeared somewhat sharper at depths that likely correspond to layer 4 (about 500 µm deep). The patchy appearance of the callosal pattern in tangential sections is not likely due to incomplete or uneven infiltration and transcallosal transport of the tracers because the dLGN ipsilateral to the cortical injections was uniformly labeled with the tracer used in the experiments (Fig. 1.11).

As noted above, both the patchy medial region and the lateral band were observed in the patterns of callosal labeling regardless of the tracer used. At higher magnification, retrogradely labeled somas and dendritic branches were observed with HRP (Fig. 1.4D-G, Fig. 1.10C), retrogradely labeled somas were observed with RB (Fig. 1.6I), while dense networks of labeled fibers, likely including axonal fibers and terminations, and some dendritic branches, were observed with BDA (Fig. 1.4H). These observations are in agreement with previous descriptions of the transport properties of HRP (Trojanowsky et al. 1981), BDA (Reiner et al. 2000) and RB (Katz et al. 1984), and confirm that regions giving rise and receiving visual callosal connections are in close spatial register in rat V1 (e.g., Cusick and Lund 1981; Olavarria and Van Sluyters 1985).

Ipsilateral-eye domains correlate with callosal patches in rat V1

The pattern of ipsilateral eye domains resembled the pattern of callosal patches in the medial callosal region. Patches of ipsilateral eye input and of callosal connections tended to be circular or oval in shape, and often the largest patches were located at mid anteroposterior levels (Figs. 1.1, 1.2). However, more complex shapes that sometimes appeared to be formed by the fusion of nearby patches were also observed. Callosal and ipsilateral eye patches were arranged anteroposteriorly into either single or double strings of patches (Figs. 1.1, 1.4, 1.6A,E, 1.10A).

To assess the similarity between patches of callosal connections and of ipsilateral eye input quantitatively, we measured the size and number of callosal patches and ipsilateral eye domains in different group of rats. On average, ipsilateral eye domains analyzed in 7 rats measured 0.12 mm^2 (SEM = 0.0082 mm^2) in size, and their number ranged from 7 to 12 (M = 9.3, SEM = 0.81). Callosal patches analyzed in 7 rats measured 0.12 mm^2 (SEM = 0.0084 mm^2) in size and their number ranged from 6 to 12 (M = 8.0, SEM = 0.76). We found no significant differences between ipsilateral eye domains and callosal patches when size of patches ($p = 0.68$) and number of patches ($p = 0.27$) were compared across groups (Fig. 1.5A,B, respectively). Furthermore, when the surface area occupied by ipsilateral eye domains (33.9 +- 0.06%) and

callosal patches (34.6+-0.02%) was compared in the CS (Fig. 1.5C), no significant difference was observed ($p = 0.96$).

To test the hypothesis that ipsilateral eye domains are spatially correlated with callosal patches, we labeled both projections in the same animal. Figure 1.6 illustrates results from two animals that received an intraocular injection of WGA-HRP into the right eye, and intracortical injections of either RB (Fig. 1.6A-D) or BDA (Fig. 1.6E-H) into the left hemisphere. In the first case, the pattern of ipsilateral eye-specific domains is shown in panels A and B, while the pattern of callosal connections labeled with RB is shown in panel C. These patterns are superimposed in panel D, with the areas of overlap colored yellow. Similarly, in the second case panels E and F show the ipsilateral eye-specific domains, and panel G shows the pattern of callosal connections labeled with BDA. Panel H shows the superimposition of both patterns, with the areas of overlap colored yellow. In both rats, callosal patches were significantly correlated with ipsilateral eye-specific domains in the areas analyzed (outlined by dashed grey lines in Fig. 1.6D,H) (χ^2, $p < 0.01$). Note that the area analyzed excludes the LS, where callosal connections typically form a homogeneous band. Similar results were obtained in 2 other rats in which callosal connections were studied following multiple injections of RB (χ^2, $p < 0.01$). These results show that callosal patches are in spatial correlation with the ipsilateral eye domains, as it occurs in the cat (Olavarria 2001). In addition, they show that the lateral, homogeneously labeled band of callosal connections overlaps with the LS (indicated by the black dashed line in Fig. 1.6).

Areas of reduced contralateral eye input in V1 correlate with callosal patches

We next investigated whether contralateral eye input to the CS occupies territories that are complementary to, and interdigitated with, the ipsilateral eye domains. If so, one would expect that contralateral eye input would be reduced or absent in areas of ipsilateral eye input. Moreover, since ipsilateral eye domains overlap with callosal patches, areas of reduced contralateral eye input should also correlate with patches of callosal connections.

Contralateral WGA-HRP labeling was densely distributed throughout V1 except for small areas of reduced labeling in the CS (n = 3). Further, intracortical injections of tracers in the opposite hemisphere of the same animals revealed that the areas of reduced contralateral labeling were significantly correlated with patches of callosal input. Figure 1.7 illustrates results from the right hemisphere of an animal that received an intraocular injection of WGA-HRP into the left

eye, and intracortical injections of BDA into the left hemisphere. Areas of reduced contralateral eye input (Fig. 1.7A) are outlined in green in Figure 1.7B, while BDA-labeled callosal regions in the same hemisphere are shown in Figure 1.7C (red outline). In Figure 1.7D, the outline of the callosal pattern (red line) is superimposed to a thresholded representation of the pattern of WGA-HRP labeling, in which the areas of reduced labeling appear white. Analysis of these data shows that callosal patches are significantly correlated with areas of reduced contralateral eye input in the CS (χ^2, $p < 0.01$). Plots of the labeling density (Fig. 1.7E) show that the increase in the density of callosal labeling (red trace) corresponds precisely with a reduction of input from the contralateral eye (green trace). These results provide anatomical evidence of partial segregation between contralateral and ipsilateral eye input in the CS. In addition, they show that the LS receives strong input from the contralateral eye, and confirm data in Figure 6 illustrating that the LS overlaps with a dense band of callosal connections in lateral V1.

In summary, our anatomical data provide evidence that the CS receives largely segregated input from both eyes, while the MS and LS are exclusively or primarily innervated by direct projections from the contralateral eye. In addition, our analysis of the correlation between retino-thalamo-cortical projections and callosal connections indicates that callosal patches in the CS overlap with ipsilateral eye domains, while the lateral callosal band overlaps with contralateral eye input to the LS.

Functional segregation of contralateral and ipsilateral eye domains in V1 demonstrated with ISH for Zif268

Do the patterns of eye-specific inputs demonstrated anatomically result in neural responses in V1 that are also eye-specific? We addressed this question by analyzing the patterns of expression of the immediate early gene Zif268, which is rapidly and transiently induced by neuronal activity (Sheng and Greenberg 1990; Chauhuri et al. 1995; 1997; Markstahler et al. 1998; Caleo et al. 1999; Horton et al. 2000; Takahata et al. 2009; 2014; van Brussel et al. 2009). Previous analysis of Zif268 mRNA expression after monocular inactivation with either intraocular injections of TTX, monocular deprivation or enucleation have revealed Zif268 activation patterns that closely resemble the patterns of ocular dominance columns demonstrated with anatomical methods (e.g., Chaudhuri et al. 1995; 1997; Horton et al. 2000; Takahata et al. 2009; 2014). We therefore used Zif268 induction to map functional activation driven by each eye

in V1 and compared the resulting maps with anatomical patterns of geniculocortical projections. Studies using coronal sections have reported that the basal expression of Zif268 is relatively high in V1 of normally behaving rats, and that labeling is visible in all layers, except layer 1, but most prominently in layers 4 and 6 and least densely in layer 3 and 5 (Caleo et al. 1999; Schlingensiepen et al. 1991).

In three rats, TTX was injected into one eye to down regulate the expression of Zif268 mRNA in territories innervated by that eye. We observed a striking similarity between the patterns of Zif268 activation within V1 and the distribution of eye specific domains revealed by the transneuronal transport of WGA-HRP (cf. Figs. 1.1, 1.8B). In the hemisphere ipsilateral to the active eye (Fig. 1.8B), strong Zif268 activation was restricted to a number of distinct, densely labeled patches resembling those revealed by WGA-HRP labeling. The size of Zif268 patches measured in three rats was not significantly different from the size of patches labeled with WGA-HRP ($p = 0.46$). Moreover, patches labeled by the two methods were restricted to the CS.

Equally striking was the similarity between the Zif268 staining pattern observed in the hemisphere contralateral to the active eye and the pattern of WGA-HRP transport from the contralateral eye. Here, the pattern of Zif268 activation was strong throughout V1 except in a number of small patches in the CS that, judging by their location and number, likely correspond to regions innervated by the inactivated ipsilateral eye (Fig. 1.8A). In both hemispheres, the patterns of Zif268 labeling in V1 were more distinct at the levels of layer 4 (Fig. 1.8F) and 6 (Fig. 1.8H) than at the levels of layers 2-3 (Fig. 1.8D) and 5 (Fig. 1.8G). Finally, consistent with previous studies in normal rats (Caleo et al. 1999), in a control animal we observed a strong and homogenous pattern of Zif268 throughout V1, without obvious periodicity in labeling density (Fig. 9).

It is interesting to note that while the active eye induced strong Zif268 expression in the contralateral LS (Fig 1.8A), it failed to induce obvious Zif268 expression in the ipsilateral LS (Fig. 1.8B). These results were unexpected because they suggest that the binocular zone does not extend to the lateral border of V1 as is commonly believed. Instead, our results provide evidence that the LS in hooded rats is predominantly monocular.

Electrophysiological mapping of ocular dominance preference in normal and callosotomized rats

Our analysis of the patterns of Zif268 activation in rats monocularly injected with TTX suggests that the functional patterns of eye-specific representation in V1 are relayed through eye-specific projections demonstrated with WGA-HRP. However, we showed that callosal patches co-localize with ipsilateral eye domains revealed with WGA-HRP, and that the LS overlaps with a dense, homogeneous band of callosal connections. An obvious question is whether both the ipsilateral eye-driven activity observed in the CS and the contralateral eye-driven activity observed in the LS are relayed through the callosum, rather than through direct retino-thalamo-cortical projections. We addressed this question by recording visual responses in V1 electrophysiologically, both in intact rats and in rats that underwent callosotomy at the beginning of the recording session (see Materials and Methods).

In both intact and callosotomized rats, electrode penetrations orthogonal to the brain surface were arranged in a grid over the lateral half of V1. The multiunit activity driven by visual stimulation of each eye was compared at each site and the ocular preference was rated on the Hubel and Wiesel's 1-7 scale (Hubel and Wiesel 1962). Two or three days prior to the recordings, these rats received intracortical injections of HRP in order to label the callosal connections in the recorded hemisphere. This allowed correlating the electrode penetrations with eye-specific regions identified in the callosal pattern in V1. Intraocular injections of WGA-HRP were not used to identify these regions in order to avoid the risk of retinal damage, which could have interfered with the recording of evoked responses from the injected eye.

In both experimental groups, electrode penetrations were assigned to one of three groups. In the CS, penetrations that were located outside callosal patches were grouped as "interpatch", penetrations that were located within callosal patches were grouped as "on patch". The third group consisted of penetrations that fell within the LS. Penetrations that could not be assigned to one of these regions with certainty were not included. Figure 1.10A,B illustrates an experiment performed in a rat with intact callosum, in which the location of recording sites (colored dots in A, B, respectively) were identified with reference to the callosal pattern in the same animal. These data illustrate that penetrations within patches tended to have higher Hubel & Wiesel scores (stronger ipsilateral eye responses) than those falling either between patches or within the LS.

Data pooled from all penetrations assigned to each cortical region show that in both intact and callosotomized rats the binocularity assessed using the scale of Hubel & Wiesel (1962)

changed markedly depending on the region that was recorded (Fig. 1.10E,F). These data were analyzed by comparing the CBIs for each region in both intact and callosotomized rats (Fig. 1.10G). Consistent with our functional analysis using ISH for Zif268 (Fig. 1.8), in intact rats we found that CBIs were significantly higher on interpatch (M = 0.88, SEM = 0.02, n = 12) and LS (M = 0.93, SEM = 0.03, n = 9) regions when compared to CBIs for patches (M = 0.51, SEM = 0.04, n = 11) ($p < 0.01$, Bonferroni-corrected repeated measures Student's t-tests). No significant differences were found between the interpatch region and LS ($p > 0.01$). In callosotomized rats we found that the region-specific CBIs (interpatch: M = 0.85, SEM = 0.05, n = 7; LS: M = 0.96, SEM = 0.02, n = 9; patch: M = 0.51, SEM = 0.03, n = 12) were no significantly different from the corresponding values in intact rats ($p > 0.01$, Bonferroni-corrected independent samples Student's t-tests). These results provide evidence that the ocular dominance preference assessed within callosal regions in the CS and LS does not depend primarily on activity relayed through the callosal commissure.

A possible confound of our callosotomy test is that the HRP injections may cause extensive cortical damage, essentially obliterating callosal input to the recorded hemisphere in the control group. To address this possibility, we examined the cytoarchitecture of V1 and cell responsiveness in 4 rats that received multiple, evenly spaced injections of HRP in visual cortex of one hemisphere. Recording from lateral V1 in the injected cortex was performed 2-3 days following the HRP injections. HRP labeling in the contralateral hemisphere and ipsilateral thalamus was revealed as in the experiments described above. We observed that cytoarchitectonic changes produced by the HRP injections were restricted to the injection tracks, without obvious changes in the surrounding cortex. Moreover, in all 4 rats stimuli-evoked cell responses in lateral V1 were comparable in strength to responses recorded from lateral V1 in a rat not injected with HRP (Fig. 1.11). These observations provide evidence that visual responsiveness was maintained in the HRP injected hemisphere.

In two additional rats, the splenium was transected *before* the intracortical injections of HRP. Strong HRP labeling was present in the cortex, thalamus and superior colliculus of the injected hemisphere, while no labeling was observed in visual cortex of the opposite hemisphere (Fig. 1.10D), confirming the effectiveness of our procedure for transecting the callosal commissure. No physiological data were collected from these two rats.

DISCUSSION

Using a combination of anatomical tracers we have demonstrated clear patchiness in the distribution of eye specific retino-thalamo-cortical projections and callosal connections in V1 of Long Evans rats. Moreover, we found that eye-specific and callosal patches bear a systematic relationship with each other, as well as with functional representations of each eye assessed with both ISH for Zif268 expression and electrophysiological methods. Although recordings within ipsilateral eye domains in V1 had significantly higher Hubel & Wiesel scores (stronger ipsilateral eye responses) than those falling either between patches or within the LS, sites exclusively dominated by the ipsilateral eye were relatively uncommon within ipsilateral domains (Fig. 1.10). These observations suggest that, as in the cat (Hubel and Wiesel, 1962; Shatz et al., 1977), input from both eyes may overlap to some extent in layer 4. In the rat this overlap may be more evident for penetrations within ipsilateral eye domains due to the small size of these domains compared to the size of contralateral eye domains within the CS.

Previous studies in rodents and ferrets

Previous studies in rats using transneuronal techniques have not described eye-specific domains possibly because they sectioned the brain in the coronal plane, an approach that is not optimal for detecting the relatively small periodicities we describe (Gerfen et al. 1982; Itaya and Van Hoesen 1982; Itaya 1988; Kageyama et al. 1990). Moreover, most of these studies did not use Long Evans rats. Although the existence of cortical patches dominated by one eye has been suggested in studies using physiological techniques (Caleo et al. 1999) or changes in glucose metabolic activity (Thurlow and Cooper 1988), these studies were not primarily focused on this issue and did not attempt to demonstrate eye-specific segregation with anatomical methods. Caleo et al. (1999) revealed the pattern of Zif268 immunostaining in rat visual cortex after monocular injections of TTX, but they do not report the existence of patchy staining in the binocular region, possibly because they displayed the labeling data as revealed in single coronal sections. Finally, a small-scale (<100 μm) honeycomb pattern has been described at the layer 1-2 border in visual cortex of Wistar albino rats (Ichinohe et al. 2003), but its relationship with the patterns of thalamic or callosal projections described here, if any, remains to be investigated.

In mice, no cortical organization related to ocular dominance has been reported by studies using various techniques (Dräger 1974, Antonini et al. 1999; Kalatsky and Stryker 2003; Mrsic-

Flögel et al. 2007; van Brussel et al. 2009). However, a study in knockout mice lacking the transmembrane glycoprotein Ten-m3 showed interdigitation of ipsilateral and contralateral eye domains in V1 (Merlin et al. 2012). These authors hypothesize that segregation of eye domains is likely linked to abnormalities associated with the dramatic expansion of the ipsilateral projection. It will be interesting to determine to what extent the mechanisms mediating the segregation of eye domains in these mutant mice compare with those giving rise to the eye specific segregation we have shown in normal, Long Evans rats.

The LS resembles a cortical strip in ferret V1 that adjoins the 17/18 border and receives subcortical input only from the contralateral eye (White et al. 1999; Ruthazer et al. 1999). The temporal retina in the ferret projects to both hemispheres (Vitek et al. 1985; Morgan et al. 1987), and the crossed projection likely innervates this continuous contralateral eye domain, conveying a representation of central portions of the ipsilateral visual field (White at al. 1999). The temporal retina in the rat also projects bilaterally (Lund et al. 1974; Reese and Cowey 1987), and the contralateral projection is thought to innervate a lateral strip in V1 (Lewis and Olavarria 1995). Our results are consistent with this interpretation and suggest that the LS is the target of projections from the contralateral temporal retina. Thus, the LS could be considered as a single contralateral eye domain that is likely homologous to the continuous contralateral eye band observed in ferret V1.

Functional role of ocular dominance columns

The fact that ODCs have been predominantly described in predator and primate species (reviewed by Horton and Hocking, 1996) lead to the assumption that they may be required for stereopsis (reviewed by Adams and Horton, 2009). However, the apparent correlation between ODCs and higher order species has been challenged by data from numerous studies in several species. For example, while tree shrews do not have ODCs, they do have OD layers such that geniculocortical afferents terminating in layer IV are stacked though still segregated (Casagrande and Harting, 1975), indicating that if a clustering of right and left eye inputs is important, it is not necessary that it be arranged in a columnar fashion. An even stronger blow to the theory is that ODCs are absent in many animals that have strong stereoscopic vision. ODCs are absent in many individual (but not all) owl monkeys and capuchins (reviewed by Livingstone, 1998) and a similar variability was described in squirrel monkeys (Adams and Horton, 2003). Marmosets on

the other hand, only have a transient expression of ODCs; they are present early in life, but later desegregate and disappear (Spatz, 1989). While this result may suggest that ODCs are only necessary for a temporary function (Markstahler et al., 1998), this result still does not take into account animals that lack ODCs altogether. Furthermore, our finding of the existence of ODCs in the rat provide additional evidence that ODCs might not be involved in stereopsis. While rats do have binocular cells, they only have a small binocular field and in general are not believed to rely heavily on vision. Taken together, this apparent lack of a correlation between ODCs and higher order vision suggests that ODCs may not be involved in stereopsis.

If ODCs are not necessary for any level of stereopsis, then what is their role? It has been postulated that ODCs are simply an epiphenomena serving no functional significance (Livingstone, 1996) or a developmental by-product of the mechanisms underlying map formation (reviewed by Lowel, 1994). Indeed, as reviewed by Horton and Adams (2005), the entire concept of the cortical column does not appear to serve any role. Several other systems present examples of this. In particular, rats lack orientation columns, yet the orientation tuning of their cells is still comparable to that of the macaque (reviewed by Horton and Adams, 2005) indicating that there is no functional purpose in clustering cells tuned to similar orientations.

Comparison with studies in the cat

In the cat, callosal connections correlate with contralateral ODCs within a narrow strip known as the 17/18 transition zone (TZ), and with ipsilateral ODCs in regions of V1 located immediately medial to the TZ (Olavarria 2001; 2002; Alekseenko et al. 2005). Olavarria (1996) proposed that callosal linkages between these cortical regions are stabilized during development by influences delivered by bilateral projections from temporal retina. This mechanism would not only induce the formation of callosal patches, but also be responsible for the correlation of callosal patches with either contralateral or ipsilateral ODCs in different regions of V1 (see Fig. 9B in Olavarria 2001).

Since the temporal retina also projects bilaterally in the rat (Lund et al. 1974; Reese and Cowey 1987) it is possible that a similar mechanism operates in this rodent. Figure 1.12 illustrates our view of the relationship between retinal projections, eye-specific domains and point-to-point callosal connectivity (Lewis and Olavarria, 1995) in Long Evans rats. The temporal retina of the right eye (colored dark grey) projects both to ipsilateral eye domains in the

right CS (dark grey circular areas) and to the LS in the left hemisphere (dark grey strip). These cortical regions map the same sector of the left hemifield (colored dark grey) and are interconnected via callosal regions that overlap the dark grey circular areas in the CS of the right hemisphere, and the dark grey LS in the left hemisphere. Thus, as in the cat (Olavarria 2001; 2002), callosal connections in the rat correlate preferentially with ipsilateral eye domains in the CS and with contralateral eye input in the LS. Note that callosal connections link retinotopically matching, but anatomically non-matching, locations (Lewis and Olavarria 1995; Olavarria 1996; 2001; Olavarria and Hiroi, 2003; Bosking et al. 2000).

Binocularity in V1 does not depend on callosal input

Figure 1.12 also illustrates that input from the ipsilateral eye to the ipsilateral eye domains in CS, as well as input from the contralateral eye to the LS can potentially be routed through the callosal commissure. Consistent with this diagram, split optic chiasm experiments in the cat indicate that callosal connections convey contralateral eye input to the TZ (Berlucchi and Rizzolatti 1968; Lepore and Guillemot 1982; Rochefort et al. 2007). In addition, Cerri et al. (2010) showed that callosal connections convey ipsilateral eye input to the binocular region in rat V1. These authors recorded from V1 after injecting TTX into the ipsilateral thalamus to block crossed and uncrossed retinal projections and reported that the inactivation primarily reduced the responses driven by the contralateral eye.

However, in agreement with previous studies in hooded rats (Adams and Forrester 1968; Silveira et al. 1989; but see Restani et al. 2009) and cat (Minciacchi and Antonini 1984), we found that section of the callosum did not significantly alter the ocular dominance map in the CS and LS, indicating that binocularity at sites within callosal territories does not depend significantly on callosal input. Although at first sight these results appear to contradict the previous studies mentioned in the paragraph above, they are consistent with the hypothesis that callosal fibers link cortical sites that are under the influence of the same temporal retina (see Fig. 1.12), as well as with the prediction that section of the callosal commissure would not have a significant effect on binocularity in V1 (Olavarria 2001; 2002). As illustrated in Figure 1.12, callosal input to either the LS or to ipsilateral eye domains largely duplicates the direct retino-thalamo-cortical input to these cortical regions originating from the same temporal retina. Thus,

either the callosal connections or the retino-thalamo-cortical projection would be able to sustain visual cortical activity when the other pathway is abolished.

Why is the LS largely monocular?

Studies in albino rats (Diao et al. 1983) and sheep (Pettigrew et al. 1984) show that a region corresponding to the LS is highly binocular, and that input from the ipsilateral eye to this region comes through the callosum. In contrast, we found that the LS is strongly dominated by the contralateral eye in spite of the fact that the LS is richly innervated by the callosum. Why are callosal connections in hooded rats unable to relay indirect input from the ipsilateral eye to the LS? Figure 1.12 illustrates that the LS in the left hemisphere (dark grey strip) cannot receive transcallosal input from the retinotopically matched nasal retina in the ipsilateral eye (colored light grey) because the regions innervated by this eye in the contralateral, right CS (light grey areas) are largely acallosal. However, if both the light and dark grey territories were intermixed in the right CS, as it would occur in an animal without ocular dominance domains, then input from the left hemiretina (light grey) arriving to the right CS would have access to the left LS through the callosum, leading to an increased binocularity in the left LS. Thus, our findings in Long Evans rats raise the possibility that albino rats and sheep lack segregated ocular dominance domains in V1, a possibility that is consistent with our preliminary results in albino rats (unpublished data) and with previous findings in the sheep (Pettigrew et al. 1984). In this context, our observation that callosal connections do not relay significant input from the ipsilateral eye to the LS further supports our findings that eye-specific domains are functionally segregated in Long Evans rats.

In conclusion, we have shown that Long Evans rats have anatomically and functionally segregated eye-specific domains and patchy callosal connections. We also showed that patches of callosal connections correlate with specific sets of ocular dominance domains just as they do in the cat. These observations suggest that at least some aspects of the modular architecture of rat visual cortex develop according to principles observed in higher species. They also raise the possibility that modular architecture in visual cortex is more conserved among rodents, carnivores and primates than previously thought. Our findings offer a new model for studying aspects of neural circuitry relevant to the emergence of modular architecture in visual cortex, as

well as molecular and other factors involved in the development and plasticity of binocular vision.

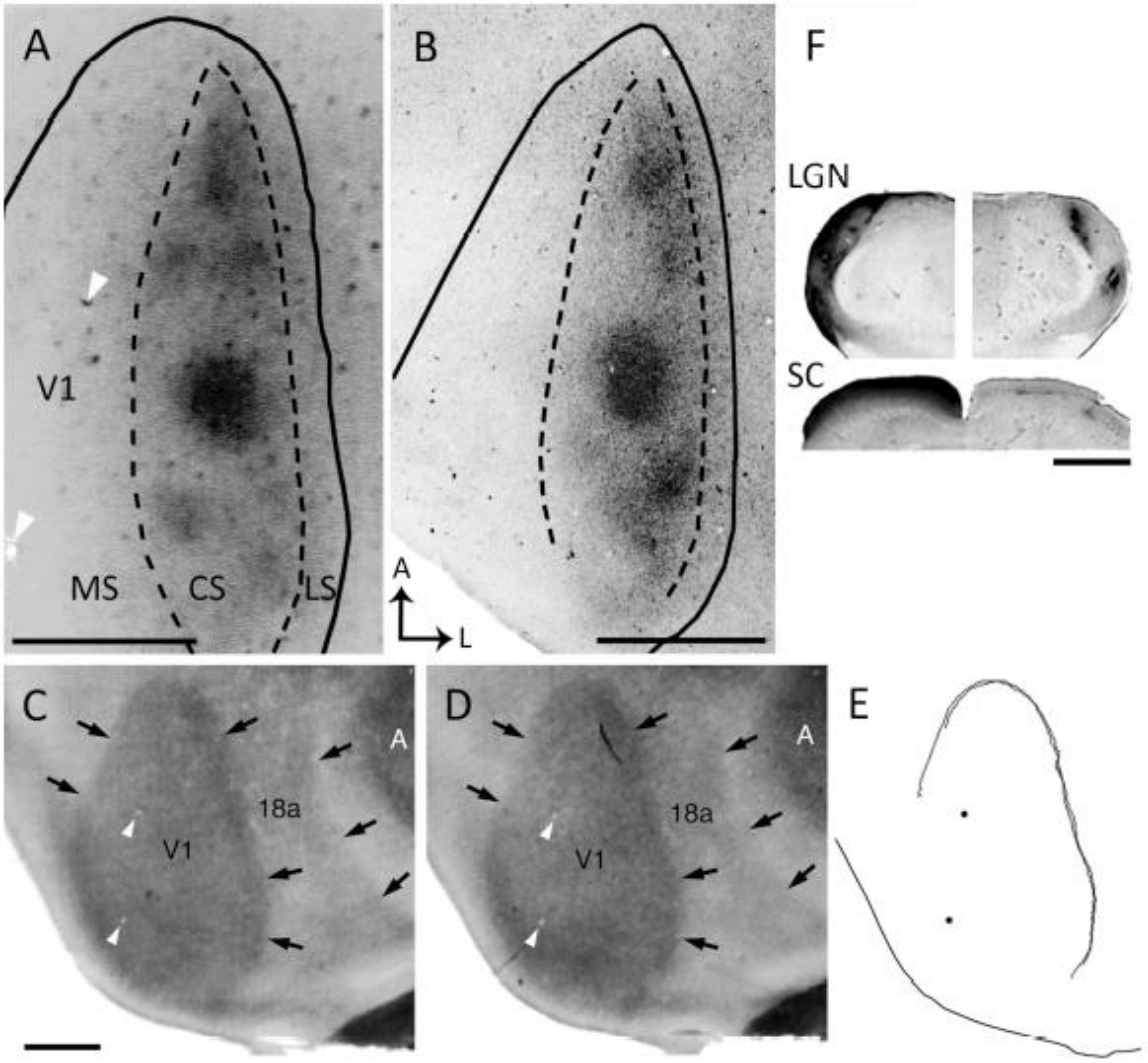

Figure 1.1. Ipsilateral eye dominance domains in V1 demonstrated by transneuronal transport of WGA-HRP. (A, B) Tangential sections from two rats show dark patches of densely labeled axonal terminations. The black lines indicate the border of V1 as determined from the myelin pattern (see Materials and Methods). Dashed lines delineate the subdivision of V1 into medial (MS), central (CS) and lateral (LS) segments. (C, D) Myelin patterns from two tangential sections taken at the level of layer 4 (approximately 500 and 540 μm deep, respectively) from case shown in A. Arrows indicate the borders of V1 and area 18a as determined from the myelin pattern. An area of dense myelination corresponding to primary auditory cortex (A) is visible lateral to area 18a. (E) Contours of area V1 delineated from the myelin patterns in C and D using the filter "trace contour" in Adobe Photoshop (see Materials and Methods). These contours were used to draw the border of V1 in A. Black dots mark blood vessels that are also indicated in A, C

and D (white arrowheads). Note that panel A is slightly rotated clockwise with respect to panels C-E. (F) Subcortical WGA-HRP labeling in case shown in A. Coronal sections through the dorsal lateral geniculate nucleus (LGN; top image), and superior colliculus (SC; bottom image) illustrating the contralateral (left) and ipsilateral (right) WGA-HRP labeling patterns. Dorsal is up. Scale bars = 1.0 mm.

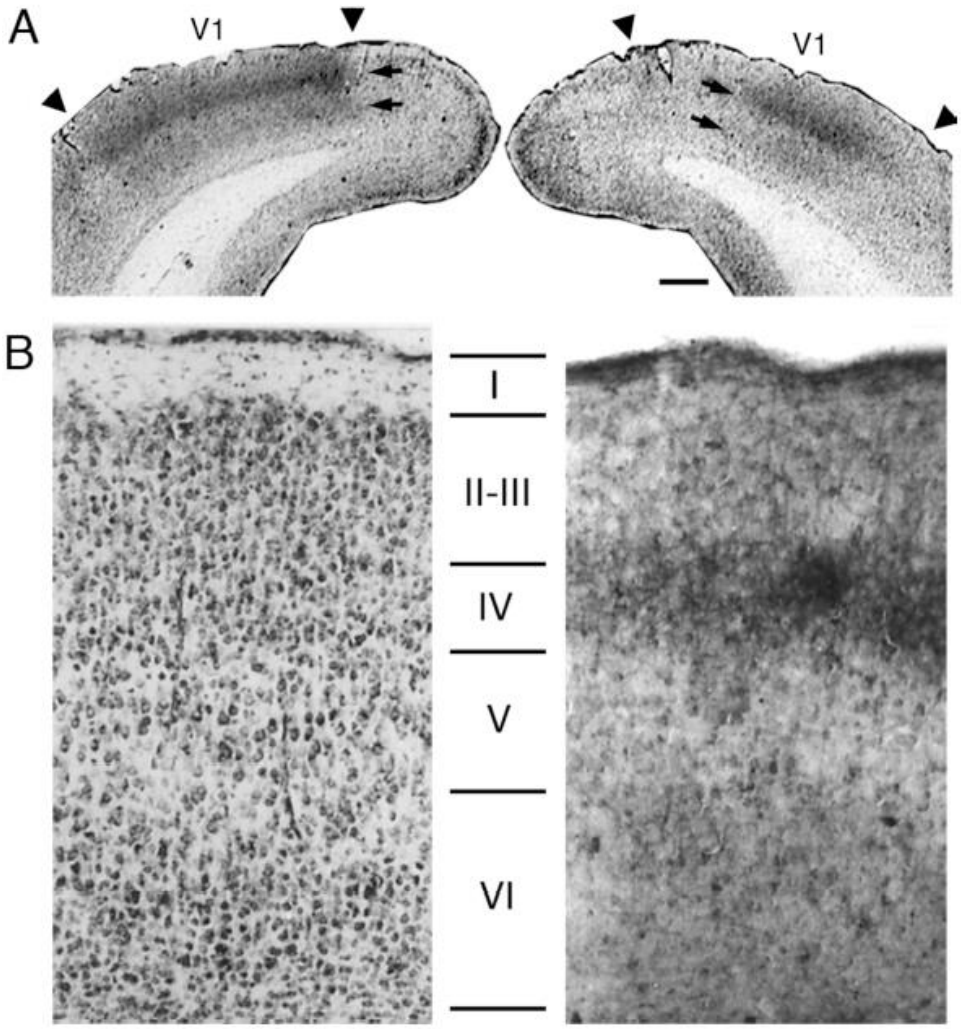

Figure 1.2. Pattern of HRP-labeling across cortical layers. (A) Patterns of labeling in the hemispheres contralateral (left) and ipsilateral (right) to the eye injected with WGA-HRP. Upper and lower arrows point to dense labeling in layers IV and VI, respectively. Black triangles indicate borders of V1. (B) Magnified views of cytoarchitecture (left panel) and WGA-HRP labeling (right panel) from V1 ipsilateral to the injected eye. Roman numerals indicate cortical layers. Scale bars = 500 μm.

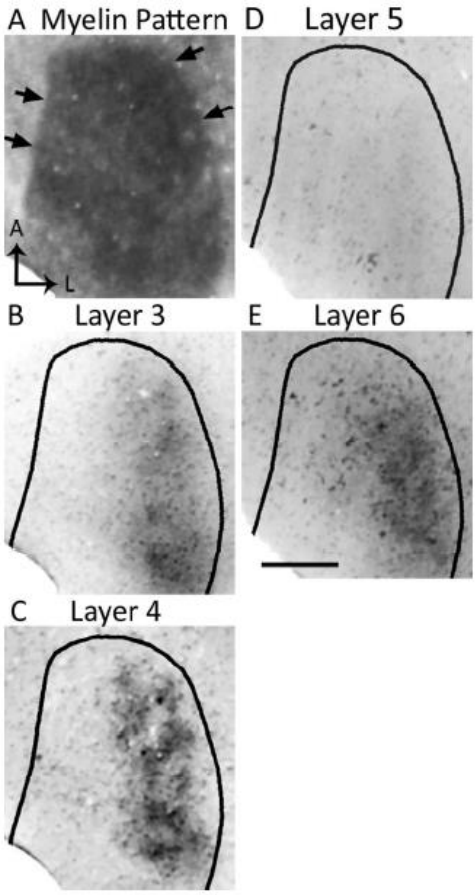

Figure 1.3. Patterns of transneuronal WGA-HRP labeling at different depths in V1 following an injection of the enzyme into the ipsilateral eye. (A) Myelin pattern in section cut at approximately 540 μm deep. Arrows indicate border of V1. (B-E) The pattern of WGA-HRP labeling was most distinct in sections through layer 4 (C, 480 μm) and less distinct in sections through lower layer 3 (B, 360 μm). The pattern was weak or not visible at the level of layer 5 (D, 720 μm), but it was again visible in sections through layer 6 (E, 900 μm). The labeling pattern in sections through layer 6 resembled the pattern observed in sections through layer 4 suggesting that they are in register. Scale bar = 1.0 mm.

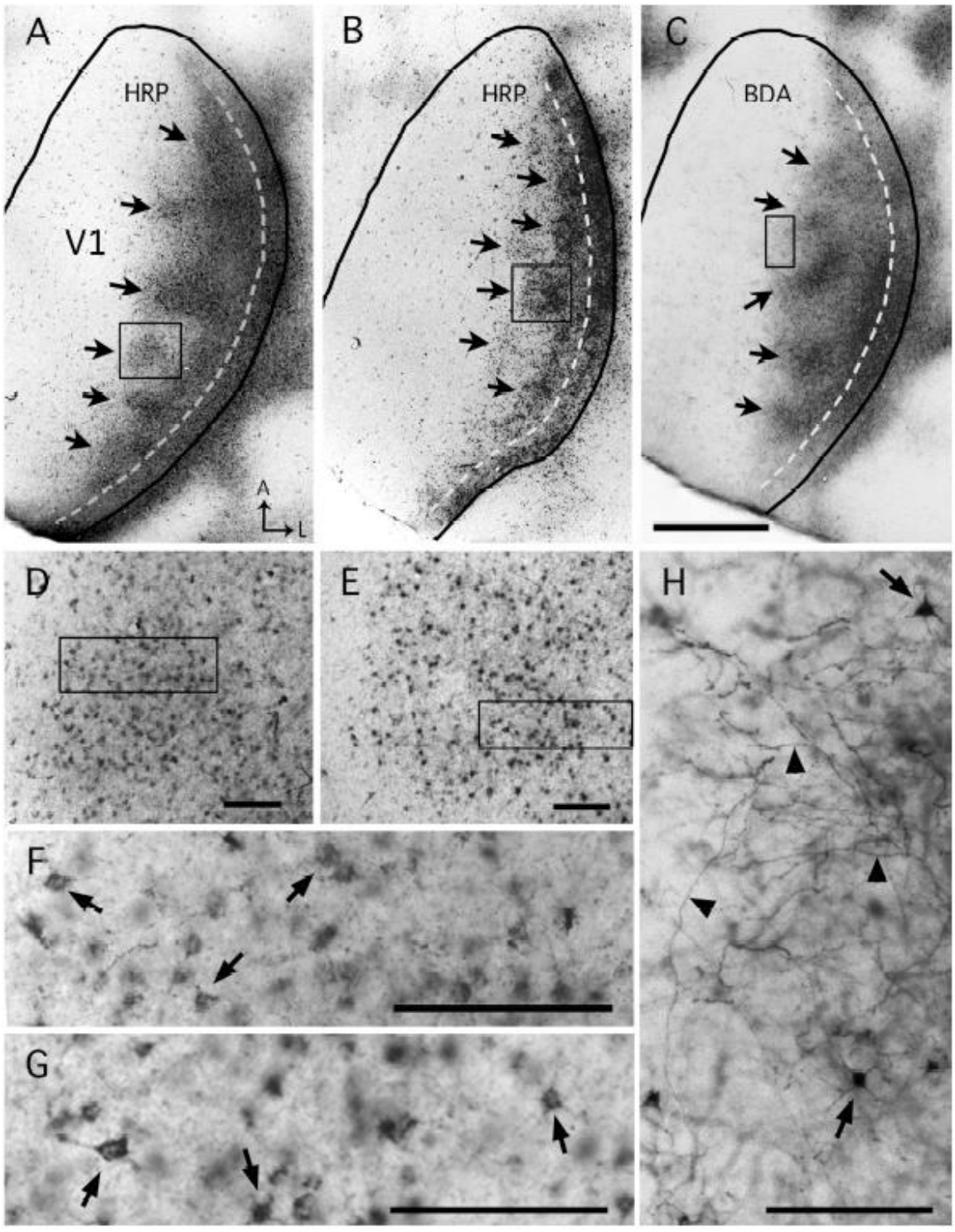

Figure 1.4. Patchy callosal connections demonstrated in tangential sections through the right V1 following multiple intracortical injections of HRP (A, B) or BDA (C) into the left hemisphere. The black lines indicate the border of V1. Dark areas in lateral V1 correspond to dense accumulations of transported tracer. This labeled callosal region consists of a series of patches

located medially (arrows in A, B, C) and a densely labeled band adjacent to the lateral border of V1 (dashed lines in A, B, C). Panels D and E are higher-magnification views of the callosal patches within the boxes in A and B, respectively, and the boxes in D and E are shown at higher magnification in F and G, respectively. Higher magnification views of HRP-labeled regions show primarily retrogradely labeled somas (dark dots in D and E) and finer labeling likely contained in axons and dendrites (Trojanowsky et al. 1981). Arrows in F and G indicate retrogradely HRP-labeled somas. Panel H is a high-magnification view of the BDA-labeling within the box in C, and it illustrates that BDA (10 kDA) primarily labels fibers (black arrowheads) that likely transported BDA anterogradely, and occasionally somas and dendrites (arrows) (Reiner et al. 2000). A: anterior, L: lateral. Scale bar in C = 1.0 mm; in D-H = 100 μm.

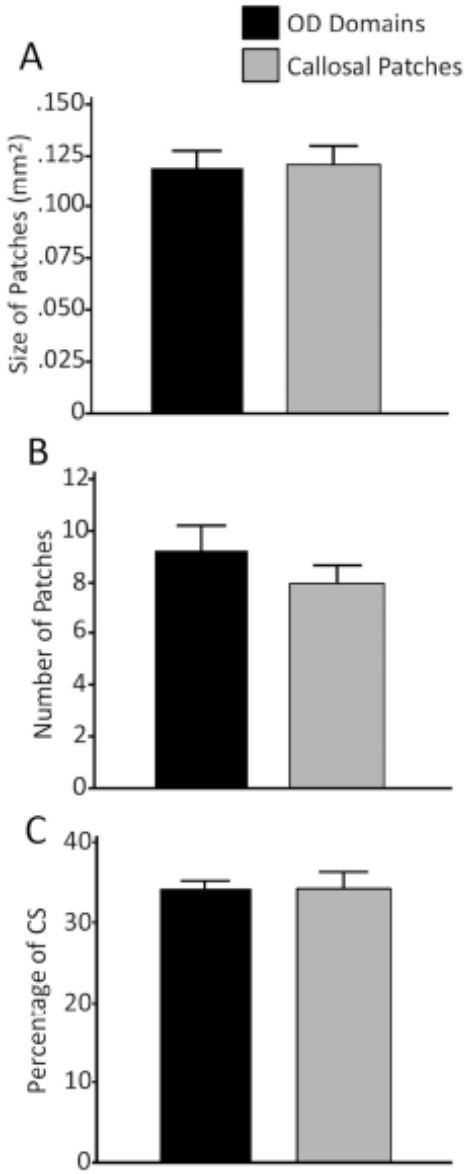

Figure 1.5. Comparison of callosal patches and ipsilateral eye domains. (A) Size of callosal patches demonstrated with intracortical injections of tracers and ipsilateral eye domains demonstrated with intraocular injections of WGA-HRP in different groups of rats (N = 7 per group). Mean sizes (and SEM) were calculated by measuring the area of labeled regions in thresholded versions of the labeling patterns demonstrated in tangential sections. B. Comparison of the number (mean +/- SEM) of ipsilateral eye domains and callosal patches within the CS. (C) Percentage of the surface area of CS that is occupied by ipsilateral eye domains and callosal patches. No significance was found when the size of patches, number of patches and the percentage of the CS occupied by the patches were compared between the two groups ($p > 0.01$).

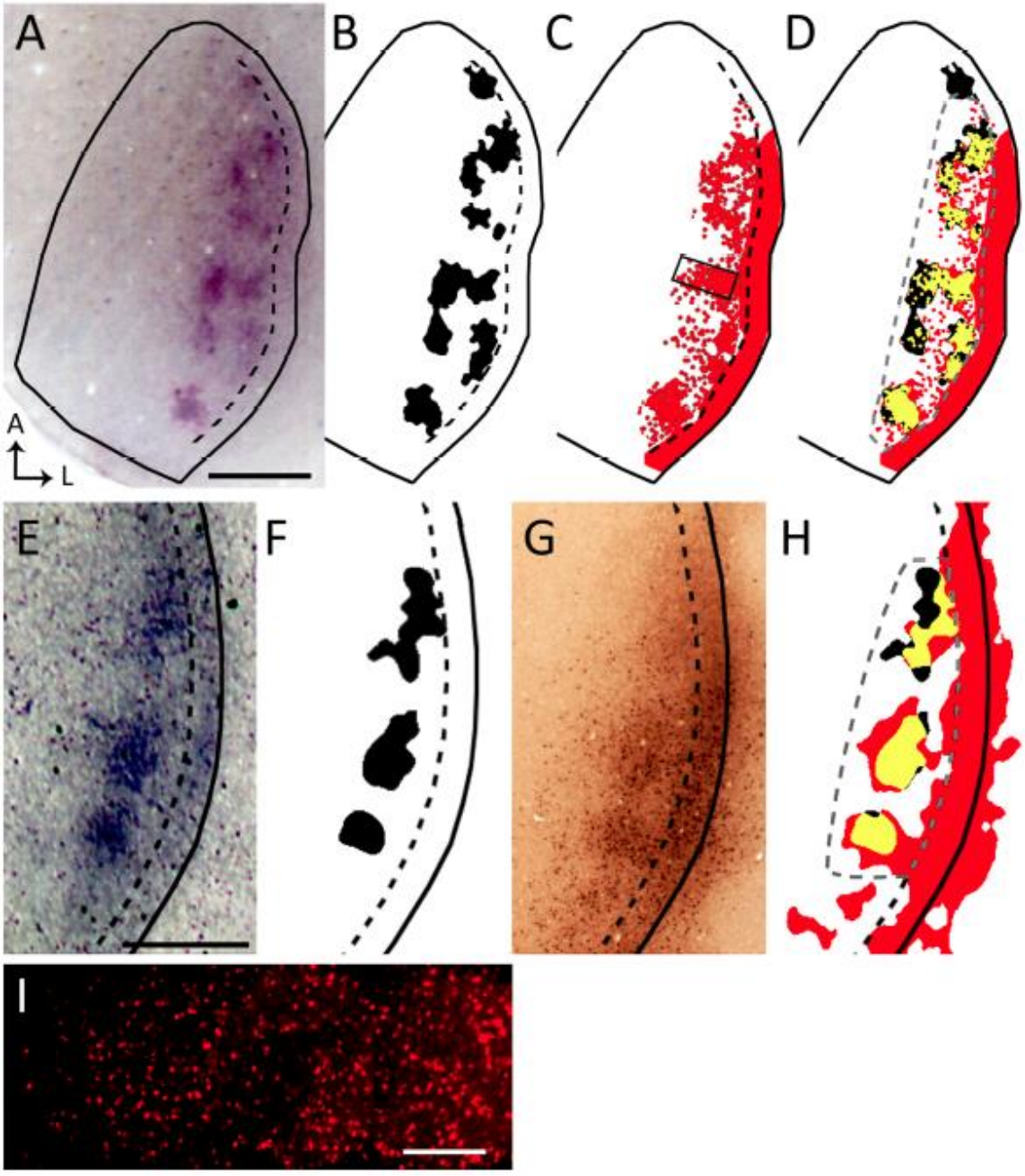

Figure 1.6. Data from two rats (A-D and E-H) illustrate that ipsilateral eye domains correlate with callosal patches in the same animal. Solid black lines indicate the border of V1. Dashed black lines indicate estimated border between the CS and LS. WGA-HRP labeled ipsilateral eye domains (A, E; thresholded version shown in black in B and F, respectively) were correlated in the same animal with callosal connections demonstrated with RB (red areas in C) or with BDA (G), thresholded version colored red in H). High magnification images captured under epifluorescence of the callosal patch within the box in C show RB-labeled cells bodies (I),

illustrating that this tracer is transported retrogradely (Katz et al., 1984). In D and H, the patterns of callosal connections are shown superimposed to the patterns of ipsilateral eye domains from the same animal, and the overlapping regions are colored yellow. Statistical analysis of the correlation was performed in the area outlined by the dashed grey line in D and H (χ^2, $p < 0.01$). Scale bars = 1.0 mm. (I) Image captured under epifluorescence of callosal cell labeled retrogradely with RB in the region within the box in Fig. 5C. This image is a montage from one of the tangential sections used in the reconstruction of the RB-labeled callosal pattern shown in Fig. 5C. Scale bar = 100 μm.

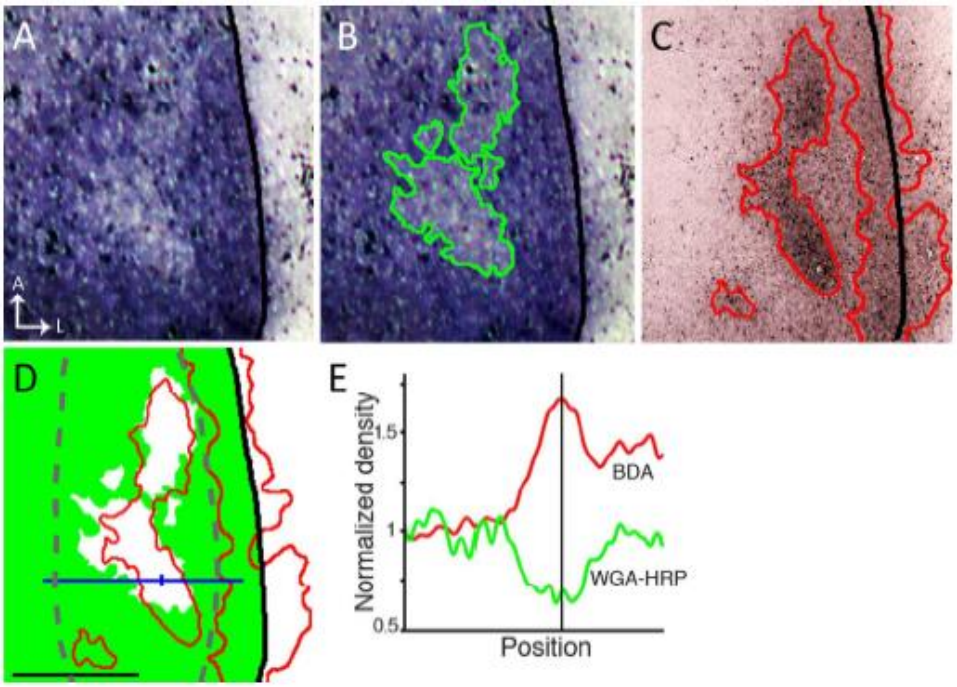

Figure 1.7. Areas of reduced contralateral eye input in V1 correlate with callosal patches. (A) Areas of reduced WGA-HRP labeling in the hemisphere contralateral to the eye injected with WGA-HRP. (B) The green line outlining these areas was determined by thresholding the labeling pattern in A. (C) Pattern of callosal connections in the same animal demonstrated by multiple intracortical injections of BDA in the opposite hemisphere. Densely labeled callosal regions are outlined by red lines determined by thresholding the image. (D) The outline of the callosal pattern (red line) is shown superimposed to a thresholded version of the WGA-labeling pattern in B, in which densely labeled areas are colored green while the areas of reduced WGA-labeling appear white. Note that only callosal patches in the CS correlate with areas of reduced WGA-HRP labeling. Statistical analysis of the correlation was performed in the area outlined by the dashed grey line (χ^2, $p < 0.01$). The area occupied by the densely labeled band of callosal connections at the LS receives strong input from the contralateral eye. (E) Plots of the labeling density at the level indicated by the blue line in D show that the increase in the density of BDA callosal labeling (red curve) corresponds precisely with a reduction of input from the contralateral eye (green curve). The vertical line in E corresponds to the tick mark on the blue line in D. Scale bar = 1.0 mm.

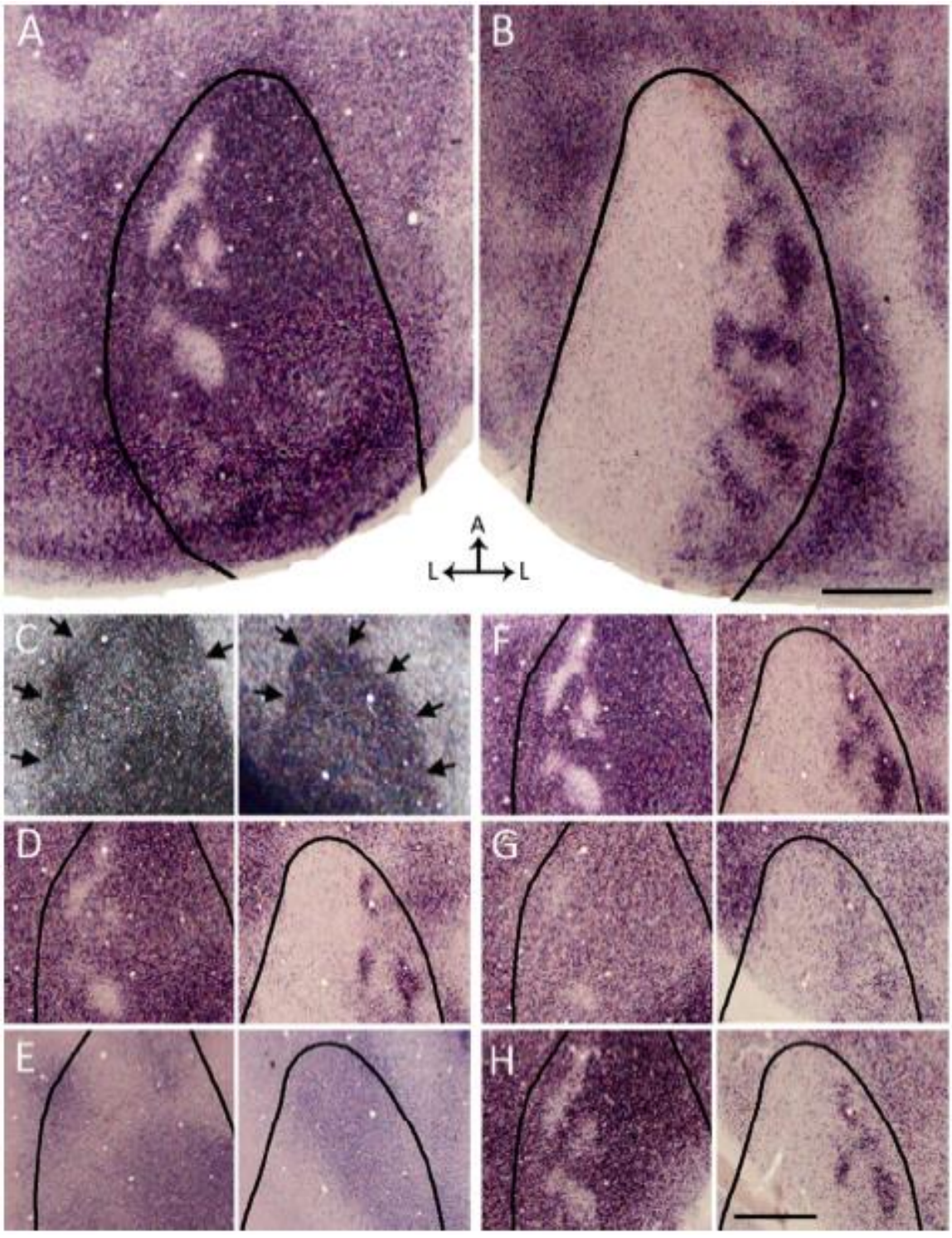

Figure 1.8. Functional segregation of contralateral and ipsilateral eye domains in V1 demonstrated with ISH for Zif268 after an injection of TTX into the left eye, leaving only the right eye active. (A, B) Overall patterns of Zif268 expression in the left (A) and right (B) hemispheres reconstructed from 3 and 4 tangential sections, respectively. Areas of strong Zif268

expression, corresponding to activity driven by the right eye, appear darkly stained. In the left V1 (A), pale patches presumably correspond to domains innervated by the silent left eye. In the right V1 (B), dark patches presumably correspond to domains driven by the active right eye. The black outlines indicate the border of V1 as revealed in the myelin pattern. (C-H) Left and right images in each pair are from the left and right hemispheres, respectively. (C) Pattern of myelination used to determine the border of V1 (arrows). The complete myelination patterns for V1 were available for delineating the border of V1 in A, B. (D) Pattern of Zif268 expression in supragranular layers. (E) Pattern of ROR β labeling in section through layer 4 (Hirokawa et al. 2008). (F) Pattern of Zif268 expression is strongest at the level of layer 4, immediately below the section stained for ROR β (E). (G) The pattern of Zif268 expression weakens and becomes less discernible at approximately the level of layer 5, but it becomes stronger in sections through layer 6 (H). Scale bars = 1.0 mm.

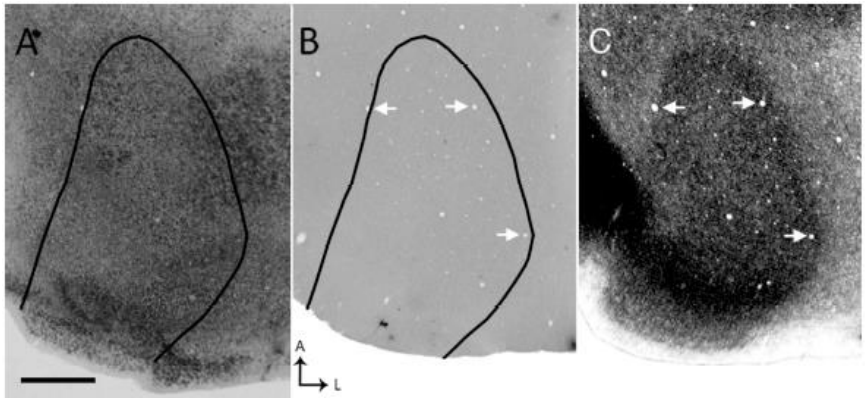

Figure 1.9. Pattern of Zif268 expression in visual cortex of control rat. (A) Overall pattern of Zif268 expression in the right hemisphere reconstructed from 4 tangential sections. A strong and homogeneous pattern of Zif268 expression is observed throughout V1, without obvious patchiness in labeling density. (B) ISH with the sense probes yielded no signals stronger than background. The black outlines in (A) and (B) indicates the border of V1 as visualized in a tangential section stained for myelin (C). Arrows point to the same blood vessels in B and C to facilitate the correlation of the V1 border in B with the myelin pattern in C. Scale bar = 1.0 mm.

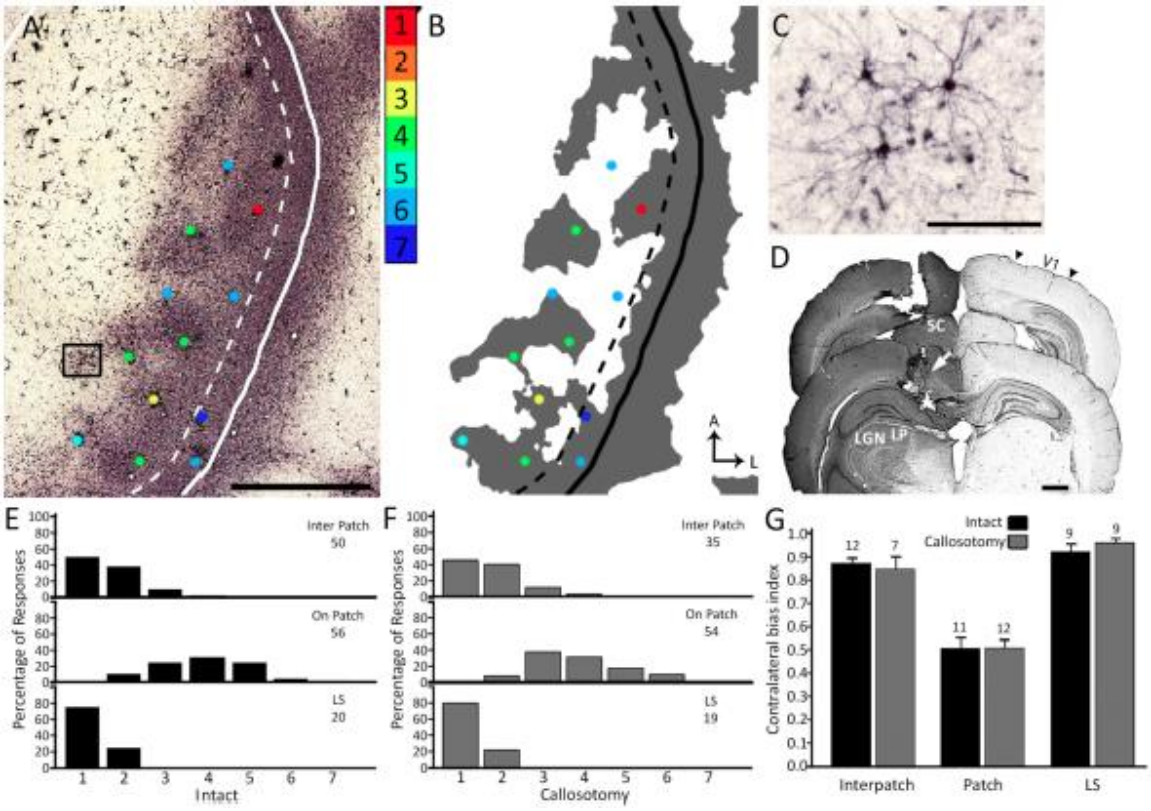

Figure 1.10. Electrophysiological mapping of ocular dominance preference in intact and callosotomized rats. (A) Pattern of callosal connections in the right V1 demonstrated after multiple injections of HRP into the opposite hemisphere in an intact rat. HRP-labeled cells in the region indicated by the box are shown at higher magnification in C. Speckles in medial regions of V1 represent reaction artifact. (B) Thresholded version of the callosal pattern. The dashed line in A and B indicates the approximate border between the CS and the LS, while the solid line indicates the border of V1. Dots in A and B indicate electrophysiological recording sites in the same animal. In B, the Hubel and Wiesel rating for ocular preference is indicated by the color of each dot (see inset in B). (C) High-magnification view of HRP-labeled callosal cells located in the region within the box in A. Retrogradely labeled somas and dendrites appear darkly stained. (D) Effectiveness of the callosotomy procedure. The sections shown were taken 6.0 mm (back panel) and 4.2 mm (front panel) from bregma. White arrow shows transection of the corpus callosum. Black arrowheads indicate borders of V1. LGN = lateral geniculate nucleus, LP = lateral posterior nucleus. (E, F) Recording sites were classified into three groups depending on whether they fell on a patch or interpatch regions of the CS, or within the LS. The histograms represent the percent of sites assigned to each of the seven Hubel and Wiesel ocular dominance

classes in each of these regions in intact (E) and callosotomized rats (F). The number of sites recorded in each region is indicated. (G) Comparison of contralateral bias indices (mean +/- SEM) for the interpatch, patch and LS regions in intact and callosotomized rats (see Results for statistical analysis). The number of rats analyzed in each group is indicated. Scale bar in A,D = 1.0 mm; in C = 100 μm.

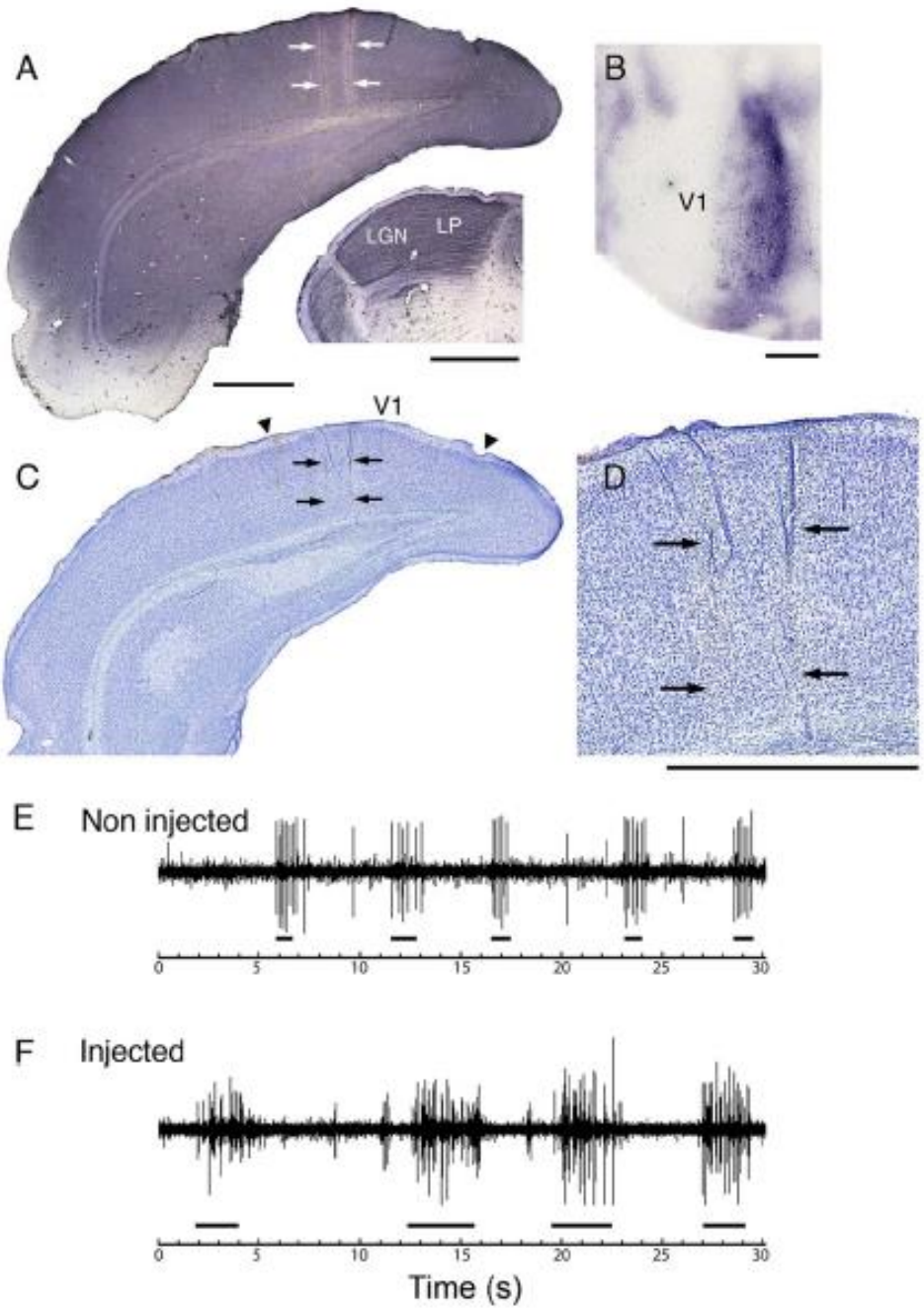

Figure 1.11. Cytoarchitecture and cell responsiveness in V1 following multiple intracortical injections of HRP. (A) Coronal section through the injected cortex showing widespread HRP labeling. White arrows indicate the tracks of two of the HRP injections. The inset shows widespread HRP labeling in the thalamus ipsilateral to the HRP injections in the same animal. (B) Pattern of HRP-labeled callosal connections in V1 revealed in tangential sections from the opposite hemisphere in the same animal. (C) Nissl-stained section through the injected hemisphere in the same animal. (D) Magnified view taken from (C). Black arrows in (C) and (D)

indicate the location of injection tracks shown in (A). (E, F) Examples of responses driven by the contralateral eye in lateral V1 from (E) rat not injected with HRP, and (F) from rat injected with HRP shown in (A-D). The black line segments indicate when light stimulus was present. LGN = lateral geniculate nucleus, LP = lateral posterior nucleus. Scale bars = 1.0 mm.

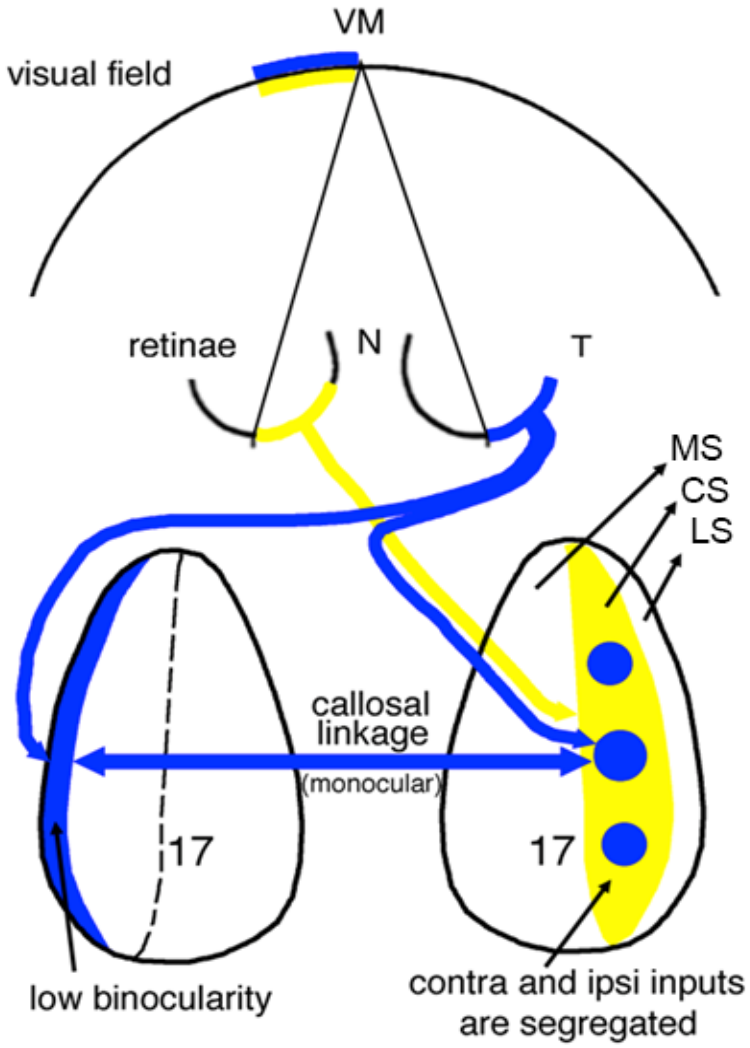

Figure 1.12. Diagram relating the patterns of retinal projections to eye-specific domains in V1 and to the callosal linkages established between these domains. For simplicity only projections from the right temporal (blue) and left nasal (yellow) retinas are shown and the geniculate relay stations have been omitted. This diagram summarizes our finding that callosal connections correlate preferentially with ipsilateral eye domains in the CS (blue circular areas in the right CS) and with contralateral eye input in the LS (blue strip at left). The pathway colored yellow illustrates that input from the left nasal retina to the right CS is distributed preferentially to non-callosally connected regions (yellow regions) surrounding the ipsilateral eye domains, being therefore unable to convey ipsilateral eye input transcallosally to the left LS. This diagram helps

explain our observation that LS in hooded rats is strongly dominated by the contralateral eye. Dashed line indicates the medial border of the CS. T, temporal; N, nasal; MS, medial segment; CS, central segment; LS, lateral segment. Diagram is based on our present results as well as previous studies of the point-to-point callosal connectivity in rat visual cortex (Lewis and Olavarria 1995; Olavarria and Hiroi 2003).

CHAPTER 2 : ROLE OF RETINAL INPUT ON THE DEVELOPMENT OF STRIATE-EXTRASTRIATE PATTERNS OF CONNECTIONS IN THE RAT

ABSTRACT

Previous studies have shown that retinal input plays an important role in the development of interhemispheric callosal connections, but little is known about the role retinal input plays on the development of ipsilateral striate-extrastriate connections and the interplay that might exist between developing ipsilateral and callosal pathways. We analyzed the effects of bilateral enucleation performed at different ages on both the distribution of extrastriate projections originating from restricted loci in medial, acallosal striate cortex, and the overall pattern of callosal connections revealed following multiple tracer injections. As in normal rats, striate-extrastriate projections in rats enucleated at birth consisted of multiple, well-defined fields that were largely confined to acallosal regions throughout extrastriate cortex. However, these projections were highly irregular and variable, and they tended to occupy correspondingly anomalous and variable acallosal regions. Moreover, area 17, but not area 18a, was smaller in enucleates compared to controls, resulting in an increase in the divergence of striate projections. Anomalies in patterns of striate-extrastriate projections were not observed in rats enucleated at P6, although the size of area 17 was still reduced in these rats. These results indicate that the critical period during which the eyes influence the development of striate-extrastriate, but not the size of striate cortex, ends by P6. Finally, enucleation did not change the time course and definition of the initial invasion of axons into grey matter, suggesting that highly variable striate projections patterns do not result from anomalous pruning of exuberant distributions of 17-18a fibers in grey matter.

This chapter was previously published in the Journal of Comparative Neurology (March, 2012) and used with permission.

INTRODUCTION

During embryonic development, occipital cortex becomes parcellated into striate cortex (area 17, primary visual cortex, V1), and a number of extrastriate areas that will later acquire more or less complete representations of the opposite visual hemifield. During a subsequent phase of development, topographically organized intrahemispheric connections are established between striate cortex and extrastriate areas, as well as between sets of extrastriate areas, giving rise to hierarchical networks specialized in the processing of specific attributes of the visual scene (Van Essen and Maunsell, 1983; Maunsell, 1992; Wang et al., 2011). In addition, highly specific patterns of interhemispheric callosal connections develop between visual areas in both hemispheres (Innocenti, 1991; Olavarria and Van Sluyters, 1985). What determines the topographic organization of intra and interhemispheric connections? Studies in anophthalmic rodents (Olavarria et al., 1984; Olavarria et al., 1988; Bravo and Inzunza, 1994) have shown that the distributions of both striate-extrastriate and visual callosal connections are abnormal in these animals, indicating that the eyes play an important role in the specification of these pathways. Early retinal deafferentation also affects the development of corticocortical connections in other species, including monkeys (Dehay et al., 1996; Dehay et al., 1989), cats (Innocenti and Frost, 1980; Olavarria and Van Sluyters, 1995), hamsters (Fish et al., 1991; O'Brien and Olavarria, 1995; Rhoades and Dellacroce, 1980) and opossum (Karlen et al., 2006). However, studies of visual callosal patterns in rats and mice have revealed that the eyes are necessary only during a brief time at the beginning of pathway formation, rather than during the entire developmental period (Olavarria et al., 1987; Olavarria and Hiroi, 2003). These authors showed that although the callosal pathway is very immature at postnatal day 6 (P6) (Olavarria and Van Sluyters, 1985), removal of the eyes at this age or later does not prevent the development of normal callosal patterns. In contrast, removal of the eyes at P4 or earlier results in patterns that are strikingly abnormal in both their overall distributions and point-to-point topography (Olavarria et al., 1987; Olavarria and Hiroi, 2003). These and similar studies in the ferret (Bock et al., 2012) show that lack of retinal input during a brief period induces permanent alterations in the overall distribution and topography of the visual callosal pathway. Thus, the period identified by delaying enucleation represents a unique developmental stage during which retinal input is critically needed for specifying the normal layout and topography of corticocortical connections. Mapping out this critical period is therefore important for identifying the retinally driven

mechanisms that operate at this developmental stage, and for investigating how they lay down the blueprints for normal maps of corticocortical connectivity.

The term *critical period* used here refers to a well-defined developmental stage during which presence of a specific factor (in this case the retinae) is critically required (hence *critical* period) for development to proceed normally (Erzurumlu and Killackey, 1982). These critical periods typically occur at early stages of development, and have been described in various systems at different levels of the neuroaxis (see e.g., Belford and Killackey, 1980). It is important to note that these critical periods differ from periods occurring later in life, during which functional and anatomical changes reflect changes in sensory experience that do not necessarily require end organ damage (Erzurumlu and Killackey, 1982). For example, in rat visual cortex, vision deprivation experiments have demonstrated a period of ocular dominance plasticity that extends approximately from P18 to well into the second month of life (Fagiolini et al., 1994). Unfortunately, as pointed out by Erzurumlu and Killackey (1982), the terms *critical period* and *sensitive period* have been used interchangeably to refer to periods that appear to correspond to temporally and mechanistically distinct phases of development (see e.g., Crowley and Katz, 2000).

Most studies of the effects of retinal deafferentation on the development of visual corticocortical connections have focused on the visual callosal pathway (Olavarria et al., 1987; Olavarria and Li, 1995; Olavarria and Hiroi, 2003). Thus, little information is available about the susceptibility of striate-extrastriate connections to neonatal enucleation, and whether or not the effects of enucleation on these connections resemble in some manner those on the callosal pattern. In the present study we have therefore examined the effects that early enucleation has on the overall organization of striate-extrastriate connections. We addressed the following questions in a group of adult rats bilaterally enucleated at birth: Are projections emerging from restricted loci in striate cortex of enucleated rats patchy as in control rats, or are they distributed in a diffuse fashion? If patchy, do the patches form consistent projection patterns associated with known subdivisions of extrastriate cortex? Are the abnormalities observed in the feedforward projection also present in the feedback extrastriate-striate pathway? Do striate-extrastriate projections originating from acallosal striate cortex maintain a close, complementary relationship with callosal connections in enucleated animals, as they do in normal rats? Finding that anomalies in striate-extrastriate connections correlate closely with anomalies in the callosal

pathway would suggest that the eyes guide the development of both inter- and intrahemispheric connections through common, or linked, mechanisms.

In a second group of animals we delayed the age at which enucleation was performed in order to determine whether the critical period for the effect of enucleation on the pattern of striate-extrastriate projections is similar to that for callosal connections. A recent study in mice showed that feedback pathways develop later than striate-extratriate feedforward projections (Dong et al., 2004), raising the possibility that the critical period for feedback extrastriate-striate projections is delayed with respect to that for the feedforward, striate-extrastriate projections. To test this possibility, in some animals we injected striate cortex with both anterogradely and retrogradely transported tracers to investigate the effect of delayed enucleation on the distribution and critical period of both feedforward and feedback pathways. We also assessed the effect of delayed enucleation on the size of visual cortex (Olavarria et al., 1987) in order to compare the critical periods for the effects of enucleation on the pattern of striate extrastriate projections and on the size of visual cortex. Finally, in a third experimental group we examined the initial growth of striate-extrastriate projections into grey matter of young pups enucleated at birth to assess whether the definition and time course of the initial invasion of axons into grey matter differs from a recent description of the development of these projections in normal rats (Ruthazer et al., 2010).

MATERIALS AND METHODS

Our study is based on data obtained from a total of 36 Long-Evans pigmented rats. Pregnant animals were monitored several times daily and the births of the litters were determined to within 12 hours. Twenty-eight rat pups were anesthetized with isoflurane (2–4% in air) and binocularly enucleated either within 24 hours of birth (BE0, n = 17) or at the following postnatal ages: P4 (BE4, n = 6) and P6 (BE6, n = 5). After recovering from the anesthesia, pups were returned to their dams. Enucleations at P4 and P6 were performed to determine when enucleation no longer affects the development of striate-extrastriate projections. These ages were chosen because previous studies in the rat have shown that the period during which development of callosal connections depends on retinal input ends by P6 (Olavarria and Hiroi, 2003). In addition, eight rats were used for analyzing striate-extrastriate projections in normal adult animals. All

surgical procedures were performed according to protocols approved by the Institutional Animal Care and Use Committee (IACUC) at the University of Washington.

Tracer injections

In both control and enucleated animals, patterns of striate extrastriate projections were analyzed in tangential sections through the flattened cortical hemisphere following restricted tracer injections into striate cortex, while the distribution of callosal connections was revealed in the same hemisphere following multiple injections of a different tracer in the opposite hemisphere. In some animals, brains were analyzed in the coronal plane. In normal rats, callosal connections occupy approximately the lateral third of area 17, while in area 18a they form more or less continuous bands on either side of this area, as well as a series of callosal bridges dividing area 18a in a number of compartments that correspond closely to visual areas described physiologically (Olavarria and Van Sluyters, 1985; Montero, 1973; Montero et al., 1973a,b; Olavarria and Montero, 1984; Espinoza and Thomas, 1983; Thomas and Espinoza, 1987). Callosal and callosal-free regions have also been described in striate and extrastriate cortex of enucleated rats (Olavarria et al., 1987). To facilitate the description of procedures and results, in the present report we use the terms “callosal” or “acallosal” to refer to regions in striate and extrastriate cortex that either contain, or are largely devoid of callosal connections, respectively. For reasons explained in “Discussion”, here we describe patterns of striate-extrastriate projections resulting from tracer injections aimed at acallosal regions of striate cortex. Anatomical experiments in all normally reared animals (n = 8) and in twenty-two rats enucleated at different postnatal ages took place when they were at least 1 month old. In addition, six rats enucleated at P0 were injected either at P4 (n=3) or P6 (n=3) and studied at P6 or P8, respectively. Tracer injections were made under isoflurane anesthesia (2–4% in air). To study the patterns of striate-extrastriate projections, all animals received a single injection of biotinylated dextran amine (BDA, 10% in DW, Molecular Probes, Eugene, OR), which is predominantly transported anterogradely. To reveal the pattern of feedback extrastriate-striate projections, some control and enucleated animals studied at adulthood also received restricted injection of fluorescent tracers (Rhodamine beads, RB, or Green beads, GB), LumaFluor, Naples, FL, concentrated stock solution), which are transported retrogradely. Small volumes (0.05–0.1 μl) of BDA or fluorescent tracers were injected into striate cortex of the right hemisphere (adults:

approx. 2.9 –3.5 mm from the midline; 0.1–1.7 mm anterior to the lambda suture, neonates: approx. 3.0 mm from the midline and 0.5 mm anterior to the lambda suture). In all cases analyzed the tracer injections were restricted to grey matter. To reveal the overall pattern of callosal connections, multiple (12-15) injections (total volume approx. 4.0 μL) of horseradish peroxidase (HRP, Sigma Co, 25% in saline) were placed over visual cortex of the left hemisphere (Olavarria and Van Sluyters, 1985). All tracers were pressure-injected through glass micropipettes (50–100 μm tip diameter).

Histochemical processing

After a survival period of 2 days, the animals were deeply anesthetized with pentobarbital sodium (100 mg/kg i.p.) and perfused through the heart with 0.9% saline followed by 4% paraformaldehyde in 0.1 M phosphate buffer (PB, pH 7.4). After being removed from the skull, the brains from adult control and enucleated rats were analyzed in histological sections cut either tangentially to the flattened cortex (control, n = 5, enucleated, n = 19) or in the coronal plane (control, n = 3, enucleated, n = 3). All brains of rats perfused at P6 (n = 3) or P8 (n = 3) were studied in coronal sections. In the cases studied in the tangential plane, the cortical mantle of the injected hemisphere was separated from the brainstem, flattened between glass slides and left overnight in 0.1M PB, while the thalamus was left overnight in 20% sucrose in 0.1M PB. The flattening procedure was done with great care to ensure that both striate and extrastriate cortices were contained in the tangential sections. The following day flattened cortices were removed from the glass slides and placed in 30% sucrose in 0.1M PB for one hour, and 60 μm thick sections were cut tangential to the cortical surface using a freezing microtome. The thalamus was cut into 60 μm thick coronal sections. Brains to be studied in the coronal plane were left overnight in 20% sucrose and 0.1 M PB. In adult brains the data were analyzed in a series of 60 μm thick coronal sections, while in neonate rats the sections were 80 μm thick. If present in the same brain, fluorescent and BDA labeling patterns were analyzed in alternate series of sections. Sections in the series examined only for fluorescence were mounted on slides and analyzed under epifluorescence without further processing. However, sections in the series processed for BDA were often also analyzed for epifluorescence because the fluorescent labeling in these sections was similar to that in sections not processed for BDA. This allowed a direct correlation of the spatial location of retrograde and anterograde labeling in the same section. The sites

injected with fluorescent tracers often appeared as dark areas in the sections processed for BDA (sites marked with asterisks in Fig. 2.1). However, inspection of BDA labeling patterns in target areas revealed that BDA had no been uptaken at these sites, indicating that the dark staining at these sites was artifactual. For instance, Figure 2.7B, C shows that fields of fluorescently labeled cells were displaced with respect of BDA-labeled fields in accordance with the topography of extrastriate visual areas (see Results). In contrast, when both tracers were injected at adjacent sites, the fields labeled by each tracer tended to overlap with each other (Fig. 2.7A). Similarly, if uptake of BDA had occurred at the fluorescent injection sites, two or more BDA labeled fields, instead of one, would be observed in the dorsal lateral geniculate nucleus (dLGN), but this was not the case (Fig. 2.1). A detailed account of the data from multiple tracer injections in striate cortex will be part of a future report. BDA labeling was revealed using the standard Avidin-Biotin-Peroxidase protocol (Vectastain Elite ABC kit, Vector Laboratories, Burlingame, CA) and 0.01% H_2O_2 in 0.05% 3-3′ diaminobenzidine, with cobalt or nickel intensification; sections were then mounted, dehydrated, defatted, and coverslipped. In the young rats studied, we have assumed that the pattern of projections revealed with BDA is that present at the time of perfusion (Simon and O'Leary, 1992). HRP labeling was revealed using tetramethyl benzidine as the chromogen (Mesulam, 1978).

Data acquisition and analysis

Digital images of the BDA and HRP labeling patterns in tangential sections were obtained by scanning the sections at 2400 dpi using an Epson 4990 scanner. These data were used for characterizing the effect of enucleation on these patterns, and for measuring the size of the overall BDA labeled projection in area 18a. High magnification images of selected BDA labeled fields in tangential or coronal sections were obtained using a Leica light microscope coupled to a digital camera. The distribution of cells labeled retrogradely with fluorescent tracers in adult rats, and of striate-extrastriate axons labeled antrogradely by BDA in neonatal rats were analyzed using a microscope equipped with a motorized stage (LEPCO) controlled by a Dell XPS T500 computer and a graphic system (Neurolucida, MicroBrightField, Williston, VT). Identifying the borders of areas 17 and 18a. Previous studies have shown that scanning unstained sections can readily reveal myelin patterns (Richter and Warner, 1974; Bock and Olavarria, 2011), and we used this procedure to identify the borders of areas 17 and 18a (Krieg, 1946,

Caviness, 1975, Zilles et al., 1980) in tangential sections from control and enucleated rats (Fig 5; Olavarria and Van Sluyters, 1985; Olavarria et al., 1987). Immediately lateral to area 17 lays an area of less dense myelination (Fig. 2.5B; Olavarria and Van Sluyters, 1985), which previous studies have identified as area 18a (Krieg, 1946, Caviness, 1975). In normal rats, it is generally accepted that area 18a contains the visual areas that have been described in lateral extrastriate cortex of the rat, including the most lateral areas (areas laterointermediate, LI, and laterolateral, LL) (Montero, 1973; 1993; Montero et al., 1973a,b; Olavarria and Montero, 1981; 1984; 1989; Espinoza and Thomas, 1983; Thomas and Espinoza, 1987; Coogan and Burkhalter, 1993). Although myelination is less dense in visual cortex of enucleated animals (Olavarria et al., 1987), the lateral profile of area 18a can also be recognized in enucleated animals (Fig. 2.5F; Olavarria et al., 1987), and, as in normal rats, this area is the target of virtually all projections from striate cortex to lateral extrastriate cortex (see Results). Further information for identifying the location of the border of areas 17 and 18a in control and enucleated rats came from analyzing landmarks provided by the overall callosal pattern in visual cortex, and the relation that these landmarks have with the borders of areas 17 and 18a as revealed in the myelination patterns (Fig. 2.5; Olavarria and Van Sluyters, 1985; Olavarria et al., 1987). However, although the lateral border of area 18a can be readily recognized from myelin and callosal patterns, there are no clear criteria for recognizing the anterior border of this area. In order to compare the size of area 18a across all experimental groups, we outlined an area that was identified using similar landmarks in normal and enucleated animals (see Fig. 2.4A). The lateral border of this area followed the lateral border of the myelinated region lying immediately lateral to area 17, as well as callosal bands overlapping this border and extending posteriorly, roughly parallel to the posterior half of the lateral border of area 17 (Fig. 2.5D, E). The anterior border of this area was drawn as a mediolateral line extending from the most anterior point in area 17 to the most posterior point of the barrel field, as visualized in the myelin or callosal pattern (Fig. 5), while its posterior border followed the edge of the histological section. Although similar in general shape and location, the area delimited by these criteria does not necessarily correspond exactly to areas "18a", "Oc2.1", or "Oc2L" of other studies (Krieg, 1946, Caviness, 1975, Zilles et al., 1980; Zilles and Wree, 1995).

Location and size of tracer injections in area 17

The location of the injection site determined with reference to the border of area 17 was confirmed by analyzing the distribution of retrogradely labeled fields within the ipsilateral dLGN (Montero et al., 1968; Godement et al., 1979; Kaiserman-Abramof et al., 1980; Guillery et al., 1985; Warton et al., 1988). We also estimated the size of the tracer injection in area 17 in order to analyze how the size of the tracer injection relative to the size of area 17 relates to the size of the overall projection in area 18a relative to the size of area 18a in both control and enucleated rats. In normal animals, estimates of the effective size of injections in visual cortex are usually obtained by measuring the sizes of the projections to targets such as the superior colliculus or dLGN. However, comparing injections sizes determined this way between control and enucleated animals would not be appropriate because thalamo-cortical connections are affected by neonatal enucleation in rodents (Warton et al., 1988). We therefore estimated the size of injections using two approaches based on the staining surrounding the injection sites. One approach consisted in outlining the perimeter where an abrupt transition in the staining density was observed. We also used the public domain NIH Image program (written by Wayne Rasband, National Institutes of Health) to analyze density profiles at the injection sites obtained from digitized images of the BDA-processed tangential sections. We found that area measurements performed at 50% of the peak intensity level (after subtracting the background density value) were not significantly different ($p < 0.05$) from our estimates of the area encircled by the perimeter drawn around the injection site by visual inspection. The analysis performed using the NIH Image program was independent of adjustments in the contrast or other parameters of the digitized images. For each injection, the size used in our quantitative analysis was the average of the values obtained with these two approaches.

To illustrate the variability of striate-extrastriate projections in each experimental group, outlines of the injection sites and patterns of 17-18a projections in each group were superimposed and merged after they had been carefully aligned with reference to the location and orientation of the lateral border of area 17.

Quantitative analysis

Using Adobe Photoshop CS2 (Adobe Systems), digitized images of anatomical tracer and myelin labeling patterns from the same animal were carefully aligned with each other using the border of area 17, the edges of the sections, blood vessels and other fiducial marks. To facilitate the quantitative analysis of the patterns of striate extrastriate projections among the different

experimental groups studied, thresholded version of these patterns were compared within and across groups. Thresholded versions of these patterns were prepared after first applying a median filter to reduce noise, and a high pass filter to remove gradual changes in staining density across the entire image. The labeling density profiles were highly similar across cases, and no significant differences ($p < 0.05$) were found between groups in the mean, median, or range of pixel values. The same filter parameters and thresholding levels were applied to all control and enucleated animals, and thresholded versions were visually inspected to confirm they accurately represented the labeling pattern observed in the tissue sections. Quantitative comparisons of the sizes of area 17, 18a, tracer injections and projection patterns in area 18a were performed using an ANOVA with α set at 0.05; post hoc comparisons were made using the Tukey HSD test. Figures were prepared using Adobe Photoshop CS2.

RESULTS

Striate-extrastriate projections in normal rats and in rats enucleated at birth

Analysis of striate-extrastriate projections in normal and enucleated animals was performed in animals receiving single injections of an anterogradely transported tracer at restricted sites within acallosal regions of striate cortex. The pattern of striate-extrastriate projections in normal rats is illustrated in Fig. 2.1A. As described previously (Olavarria and Montero, 1984; Coogan and Burkhalter, 1993; Montero, 1993), following single tracer injections, projections from striate cortex are distributed into multiple extrastriate fields located lateral, anterior and medial to striate cortex. These fields represent projections to separate visual areas that have been identified with physiological and anatomical methods (Montero, 1973; 1993; Montero et al., 1973a,b; Olavarria and Montero, 1981; 1984; 1989; Espinoza and Thomas, 1983; Thomas and Espinoza, 1987; Coogan and Burkhalter, 1993; Wang and Burkhalter, 2007; Wang et al., 2011).

In rats bilaterally enucleated at birth (BE0), we observed that single, restricted injections of anterogradely transported tracer into striate cortex did not produce diffuse labeling of fibers in extrastriate cortex. Instead, as in normal animals, these injections produced multiple labeled fields that were distributed throughout broad regions of lateral, anterior and medial extrastriate cortex (Fig. 2.1B). High magnification views of fields analyzed in the tangential plane revealed that the borders of extrastriate projection fields in BE0 rats were well defined (Fig. 2.2B), as in

control rats (Fig. 2.2A). Furthermore, in sections cut in the coronal plane, we observed that labeled fibers in area 18a formed dense, radially oriented, column-like projection fields in both control (Fig. 2.2C) and BE0 rats (Fig. 2.2D), and that the laminar distribution of labeled axonal terminations was similar in both groups of animals.

However, striking differences between control and BE0 rats became evident when the overall patterns of area 18a projections were compared. In what follows we will focus our attention to the effect of enucleation on the projections to lateral extrastriate cortex. Figure 2.3A shows thresholded versions of the projection patterns from five control rats, while Figure 3B shows the patterns from five BE0 rats (the cases shown first in Fig. 2.3A, B correspond to those shown in Fig. 2.1A, B, respectively). The thin line within area 17 delineates the injection sites, while the thin line in lateral extrastriate cortex indicates the lateral border of area 18a. The black patches represent the resulting labeled projection fields in area 18a. In order to facilitate the comparison of the patterns shown in Figure 2.3, the patterns were scaled so that the profile of area 17 in each case matched the profile of area 17 in the first case shown in Fig. 2.3A as closely as possible. Particular attention was paid to matching the size of area 17 along its anteroposterior axis. In agreement with previous studies, we found in normal rats that virtually all projection fields fell within area 18a as defined in Materials and Methods (Fig. 2.3A, 2.4I, 2.5D). In addition, the pattern of 17-18a projections in control rats was remarkably constant from animal to animal, and projections to lateral areas LI and LL were nearly always smaller than projections fields to more medial areas AL, LM, and PL. Moreover, comparing data from animals with injections in different loci within striate cortex (Fig. 2.4B, C) illustrates that changes in the location of the injection site in striate cortex produced relatively small displacements of the extrastriate projection fields, and that these displacements were in accord with the topography of the extrastriate visual areas (Olavarria and Montero, 1984; Coogan and Burkhalter, 1993; Montero, 1993). For instance, Figure 2.4B illustrates that projections fields in areas AL and LM tend to fuse when injections are placed anteriorly in area 17, but they separate in the anteroposterior axis when the injections move posteriorly. Likewise, Figure 2.4C illustrates that the maps in lateral visual areas mirror the topography in V1, i.e., projection fields in most areas translocate medially as the injection site moves from medial to lateral within area 17.

In BE0 rats, as in control rats, projections fields from restricted loci in area 17 were largely restricted to area 18a as defined in Materials and Methods (Fig. 2.3B, 2.4J, 2.5E, F).

However, projection fields within area 18a were not arranged into medial and lateral tiers as clearly as in controls, and fields removed from the 17/18a border were not always smaller than fields close to this border. Also in marked contrast to controls, the patterns of 17-18a projections in BE0 rats were very variable from animal to animal, and it was typically not possible to transform the pattern in one animal into that of another simply by displacing the fields in a consistent manner, as is often the case in normal animals. For instance, Figure 2.4D illustrates a displacement of injection sites along the anteroposterior axis. However, unlike Figure 2.4B, the projection patterns resulting from each injection in Figure 2.4D are very different from each other with no simple way of transforming one pattern into the other. Moreover, Figure 2.4E illustrates that projection patterns can be very different even if they originate from injections placed at similar locations in different animals. These observations suggest that the variability in the overall pattern of 17-18a projections in BE0 rats is not primarily due to changes in the location of the injection sites.

To gain further appreciation of the variability in the overall spatial distribution of the patterns of striate-extrastriate projections in each of the four experimental groups analyzed, the thresholded patterns in each group shown in Figure 2.3 were merged after their orientation had been adjusted so that the lateral border of striate cortex coincided as closely as possible within each group. In addition to using the border of striate cortex identified in the myelin and/or callosal patterns, this adjustment was facilitated by using other landmarks such as the border of area 18a, the location of auditory cortex and of the barrel field in somatosensory cortex, which were often visible in sections analyzed for myelin or HRP-labeling (Fig. 2.5). The merged injection sites and striate projection patterns for each group are shown in Figure 2.4I-L, and for clarity, a single area 17 border representative of all borders in each group was drawn. Inspection of Figure 2.4J illustrates that the merged striate projection pattern was very different in BE0 animals compared to that in control cases (Fig. 2.4I). Moreover, the merged pattern in the control group bears a general resemblance to the individual patterns in this group (compare with control cases in Figs 2.1 and 2.3), whereas the merged pattern in the BE0 group bears little resemblance to any of the individual patterns in the group (compare with BE0 cases in Figs 2.1 and 2.3).

Abnormalities of striate-extrastriate projections correlate with abnormal features of the callosal pattern in lateral extrastriate cortex

In normal rats, previous studies have shown that loci in acallosal regions of striate cortex project virtually exclusively into acallosal islands within extrastriate cortex (Fig. 2.5D; Olavarria and Montero, 1984; Coogan and Burkhalter, 1993). This correlation suggests that the distributions of both ipsilateral and interhemispheric connections are regulated by a common mechanism. To determine whether enucleation disrupts the correlation between both systems of corticocortical connections, we compared the distributions of striate-extrastriate projections with the pattern of callosal connections revealed in the same animals following multiple injections of HRP in the contralateral hemisphere. As described previously (Olavarria et al., 1987), we observed that while the overall arrangement of callosal and acallosal regions seen in extrastriate cortex of normal rats is still recognizable in rats enucleated at birth, it is often distorted and highly variable. For instance, bridge-like callosal bands that normally separate the various callosal rings (arrows in Figure 2.5A,C) are often interrupted, appearing instead as stumps protruding into acallosal regions at irregular locations (see asterisks in Figs. 2.5E, 2.6A, D, G). Sometimes isolated, labeled callosal patches appear in the middle of acallosal regions (indicated by arrows in Fig. 2.6A, D). We found a striking correlation, illustrated in Figures 5 and 6, between anomalous patterns of striate-extrastriate projections and abnormal features of the callosal pattern. For instance, labeled striate-extrastriate projection fields often extend across gaps in the bridge-like callosal bands, and protrude/invade from one acallosal compartment to another. This is particularly well illustrated in Figure 2.6D-F. In this case, an extremely long labeled field crosses at least three such gaps, extending uninterruptedly through three acallosal compartments (marked 1 - 3 in Fig. 2.6D). In this case it is also interesting to observe that, in the acallosal compartment #3, a labeled extension emanating from the long 17-18a projection field wraps around the isolated callosal patch indicated by an arrow (Fig 2.6E, F). The case shown in Figure 2.7A-C also illustrates a protrusion of labeled projections (asterisk) occurring between acallosal compartments 3 and 4, as well as wrapping of labeled 17-18a projections around an isolated callosal patch located in the middle of an acallosal region (indicated with an arrow in Fig. 2.6A, C). The existence of gaps in the bridge-like callosal bands suggests that enucleation often interferes with the development of the middle portions of the bridges. In some cases, gaps may appear because the callosal protrusions on either side of area 18a become misaligned with each other. The latter is illustrated in Figure 2.5E, in which asterisks mark two finger-like protrusions that would have formed a bridge had they developed in alignment with each other. It

is interesting to note that a field of labeled striate-extrastriate projections is "wedged" between these two finger-like protrusions (indicated with an arrow in Fig. 2.5E). This suggests that not only complete callosal bridges, but also callosal protrusions can be associated with separate 17-18a projection fields. This phenomenon may underlie some of the variability in the patterns of projection fields observed among cases enucleated at birth. For example, in normal animals, a single acallosal island, associated with visual area Anterolateral (AL, Olavarria and Montero, 1984; Montero, 1993; Coogan and Burkhalter, 1993), is typically observed in anterolateral area 18a (see Fig. 2.5D). As in normal animals, in the enucleated case illustrated in Fig. 2.6A, a single acallosal island is visible in this region (marked "2" in Fig. 2.6A). (The acallosal island marked "1" in Fig. 2.6A likely corresponds to the anterior callosal ring observed in normal rats, marked with a cross in Fig. 2.5A, C). In contrast, in the enucleated case illustrated in Fig. 2.6D-F, a callosal protrusion marked with a black asterisk in Fig. 2.6D separates this anterolateral region into two acallosal compartments (marked 2 and 2' in Fig. 2.6D), and each of these compartments accommodates separate projection fields (marked with white asterisks in Figure 2.6E). The fact that these two projection fields lie within the boundaries of area 18a provides evidence that they represent anomalous projections in the region normally occupied by area AL. Finally, Figure 6D, E illustrates that anomalous projection fields (marked with arrowheads in Figs. 2.1B, 2.6E, H) often develop along the 17/18a border, occupying abnormal acallosal islands that are often visible in BE0 rats (marked with arrowheads in Fig. 2.6D) (Olavarria et al. 1987; Ankaoua and Malach, 1993). In summary, our data show that while neonatal enucleation induces the development of anomalous patterns of striate-extrastriate and callosal connections, it does not significantly degrade the basic correlation observed between these projections in control rats. These results indicate that the mechanisms responsible for this correlation do not depend on retinal input, and suggest that a combination of retinally dependent as well as independent mechanisms is required for the development of normal patterns of striate-extrastriate and callosal connections.

Critical period

To determine the period during which the eyes are critically needed for normal development of striate-extrastriate projections, we studied these projections in animals that were enucleated at P4 (n = 5) or P6 (n = 5). Figure 3C shows the projection pattern in five adult rats

enucleated at P4. The first case in Figure 2.3C is also shown in Figure 2.1C. Comparison of these patterns with those in normal rats and in rats enucleated at birth suggests that, overall, anomalies in the distribution of projections induced by enucleation at P4 can still be recognized, although they appear less severe than those observed in BE0 rats (cf. Fig 2.3C and B). Moreover, Figure 2.4F illustrates that changes in the projection patterns observed when comparing BE4 cases with injections displaced along the anteroposterior axis do not resemble the changes observed in control animals (cf. Fig 2.4B), suggesting that the topography of striate-extrastriate projections is abnormal in BE4 rats. We also examined the pattern of callosal connections in extrastriate cortex of BE4 rats and observed that gaps in the callosal bridges are less prevalent and not as obvious as in BE0 rats. Figure 2.6I shows relatively small gaps in some callosal bridges, and a large callosal patch that seems to be roughly in the position of the callosal patches indicated by arrows in Figure 2.6A,D. These observations are consistent with our data from normal and BE0 rats showing that the patterns of striate-extrastriate projections correlate closely with the pattern of callosal connections. Figures 2.1D and 2.3D illustrate the striate-extrastriate patterns of projections in 5 rats enucleated at P6 (the first case in Fig. 2.3D is also shown in Figure 2.1D). These projection patterns appear very similar to those in normally reared rats (cf. Figs. 1D, 1A and Figs. 2.3D, 2.3A), suggesting that the period during which binocular enucleation disrupts the development of striate-extrastriate projections ends around 6 days of age. Consistent with these observations, comparison of data from animals with injections in different loci within striate cortex (Figs. 2.4G, H) reveals that, as in control animals (Figs. 2.4B, C), changes in the location of the injection site in striate cortex produced relatively small displacements of the extrastriate projection fields, and that these displacements were in accord with the topography of the extrastriate visual areas (Olavarria and Montero, 1984; Coogan and Burkhalter, 1993; Montero, 1993). For instance, Figure 2.4G illustrates that projections fields in areas AL and LM separate from each other along the anteroposterior axis when the injections is placed in posterior area 17, but they tend to approach each other as the injection moves anteriorly. Also, as in Figure 2.4C, Figure 2.4H illustrates that the maps in lateral visual areas mirror the topography in V1, i.e., projection fields in most areas translocate medially as the injection site moves from medial to lateral within area 17. Moreover, Figure 2.4K illustrates that the variability in the striate-extrastriate projection patterns appears reduced in BE4 rats compared to BE0 rats (cf. Fig. 2.4J),

while the variability of the patterns in BE6 rats (Fig. 2.4L) appears comparable to that observed in control rats (cf. 2.4I).

Feedforward vs. feedback striate-extrastriate pathways

Previous studies in the rat have shown that the distribution of striate-extrastriate feedforward projections closely matches that of feedback projections (Olavarria and Montero, 1981). To compare the effects of enucleation on the distribution and critical period of feedforward and feedback pathways, in some animals we injected striate cortex with both BDA and a retrogradely transported fluorescent tracer. Figure 2.7A compares the distributions of retrogradely labeled cells (grey dots) and of anterogradely BDA-labeled projection fields (black areas) in lateral extrastriate cortex following closely placed injections of BDA (large black dot) and red latex fluorescent beads (RB, large grey dot) into striate cortex of a BE0 rat. This diagram illustrates that retrogradely labeled cells tend to accumulate in regions targeted by feedforward projections, and that the overall distribution of feedback projections closely resembles that of feedforward projections. Data from this and two additional cases provide evidence that enucleation at birth has similar effects on both feedforward and feedback pathways. We also compared the distributions of feedback connections in rats enucleated at P6 with the distribution of feedforward projections in order to determine whether the age at which the eyes are no longer necessary for normal development of feedback projections differs from P6. Data from two animals enucleated at P6 (Fig. 2.7B, C) show that retrogradely labeled cells (grey dots) accumulate in clusters whose number and general distribution resembles those of anterogradely, BDA-labeled projections (black areas). Moreover, these clusters of labeled cells are displaced with respect to the fields of feedforward projections in a way that is consistent with the topography of extrastriate visual areas in normal rats and mice (Montero, 1973; 1993; Montero et al., 1973a,b; Olavarria and Montero, 1984; 1989; Thomas and Espinoza, 1987; Coogan and Burkhalter, 1993; Wang and Burkhalter, 2007). For example, Figure 7B illustrates that a displacement of the injection site from anterior (BDA, large black dot) to posterior (RB, large grey dot) causes the clusters of labeled cells to displace anteriorly in visual areas AL and PL, but posteriorly in area LM with respect to the feedforward projection fields, as it would be expected in normal rats. In Figure 2.7C, a displacement of the injection sites from medial (BDA, large black dot) to lateral (RB, large grey dot) causes the clusters of labeled cells to displace medially

in visual areas AL, LM and PL, in accord with these areas' normal maps, which mirror the map in V1 in the medio-lateral direction (cf. Fig. 2.4C; Olavarria and Montero, 1984; Thomas and Espinoza, 1987; Montero, 1993; Coogan and Burkhalter, 1993; Wang and Burkhalter, 2007; Wang et al., 2011). Results from these and an additional case (not shown) provide evidence that enucleation at P6 does not prevent the development of normal patterns of feedback connections.

Development of striate-extrastriate projections in neonatally enucleated rats

In newborn rats, parental axons originating in striate cortex and navigating laterally in white matter give off interstitial branches that begin invading grey matter in lateral extrastriate cortex a few days after birth. By P6, many fibers of simple architecture reach the newly formed supragranular cortical layers, and by P8, fibers labeled anterogradely from restricted injections into striate cortex form projection fields that, although sparse, appear to be as well-defined as those observed in adult rats (Ruthazer et al., 2010). To determine whether enucleation at birth changes the time course and definition of the initial invasion of striate-extrastriate projections, we made restricted injections of BDA into striate cortex of BE0 pups at P4 and P6, and analyzed the distribution of anterogradely labeled fibers in lateral striate cortex at P6 and P8, respectively. As in normal pups, parental axons in BE0 animals labeled by the injection of BDA navigate toward area 18a predominantly through deep cortical layers and white matter. Figure 2.8A illustrates that, as in normal rats, many fibers of simple architecture reach upper layers of the cortex by P6. Moreover, in subsequent days the invasion of additional fibers is not diffuse; instead, invading fibers, many of which are developing terminal arborization patterns, form focused fields (Fig. 2.8B) whose columnar appearance in coronal sections resembles that of mature projection fields, although the latter appear denser (Fig. 2.2D). These data provide evidence that neonatal binocular enucleation does not induce obvious changes in the time course of the initial invasion of axon fibers into grey matter, and that, as in normal rats, invading fibers form focused projection fields from the beginning of the invasion.

Quantitative analysis

Our qualitative analysis presented above provides evidence that neonatal enucleation induces the development of abnormal and highly variable patterns of striate extrastriate projections, and that these effects are no longer obvious when enucleation is delayed until P6.

We also analyzed our data quantitatively to investigate whether or not enucleation compromises the relationship between the overall size of the projection in area 18a and the size of the injection sites in striate cortex. In normal animals, the existence of topographically organized striate-extrastriate projections implies that the size of the projections in area 18a with respect to the size of area 18a increases in proportion to the increase in the size of the injection sites with respect to the size of area 17. If this rule were compromised by enucleation, it could lead to a reduction, or even lack of topography in striate-extrastriate projections. To investigate this possibility it was necessary to determine the effects of enucleation on the sizes of area 17 and 18a, and to measure the sizes of the injection sites and of the projection fields in area 18a of control and enucleated animals (see Materials and Methods). We found that the size of striate cortex measured from tangential sections was significantly larger ($p < 0.05$) in control rats (M = 14.89 mm^2, SD = 0.95, n = 6; see also Olavarria et al., 1987) compared to BE0 (M = 9.08 mm^2, SD = 1.3, n = 6), BE4 (M =10.63 mm^2, SD = 1.18, n = 5) and BE6 (M = 12.49 mm^2, SD = 0.72, n = 5) (Fig. 9A). Expressed as % of the size of area 17 in control rats, on average, the size of area 17 was 61 %, 71.4%, and 83.95 % in BE0, BE4 and BE6 rats, respectively. Figure 2.9A also shows that while enucleation performed at later ages had less effect on the size of area 17, the size of area 17 in rats enucleated at P6 was still significantly smaller than that in control rats. In agreement with a recent study in the ferret (Bock et al., 2012), these results indicate that the critical period for the effect of enucleation on the size of area 17 extends beyond the critical period for the effect of enucleation on the pattern of corticocortical projections. In sharp contrast to the effects of enucleation on the size of area 17, we found that area 18a, as defined in Materials and Methods (Fig. 4A), was not significantly larger ($p < 0.05$) in controls (M = 9.70 mm^2, SD = 0.45) compared to BE0 (M = 8.91 mm^2, SD = 1.39), BE4 (M = 9.05 mm^2, SD = 1.18) and BE6 rats (M = 8.79 mm^2, SD = 0.50) rats (Fig. 2.9A). Figure 2.9B, which plots the ratio between the sizes of areas 18a and area 17, shows that in normal rats area 18a is about 65% of the size of area 17, while in BE0 rats, due to the nearly 39% reduction in the size of area 17, the size of area 18a approximates (98%) the size of area 17. Thus, as illustrated in Figure 2.10B, area 17 projects to a target area that is relatively much larger in BE0 than in control rats. Does this significant increase in the size of area 18a relative to the size of area 17 in BE0 rats alter the normal relationship between the size of the projections in area 18a and the size of the injections into area 17? To answer this question, we calculated the ratio between the fraction of area 18a occupied by

the overall size of the projection and the fraction of area 17 occupied by the injection site in control and enucleated rats. This ratio was not significantly different ($p < 0.05$) between control rats (1.5, SD = 0.24) and any of the enucleated groups of rats (BE0 = 1.6, SD = 0.44; BE4 = 1.4, SD = 0.39; BE6 = 1.38, SD = 0.31). Moreover, as shown in the scatter plot in Figure 9C, the data from all four groups could be fit by a regression line ($r^2 = 0.78$) with slope = 1.46 (formula: Y = 1.46X + 0.004). These results therefore indicate that early enucleation does not alter the normal relationship that exists between the relative sizes of the projection fields in area 18a and the relative sizes of the injection sites in area 17. These results further suggest that altering this relationship is not necessary for the development of anomalous topographic projections in enucleated animals. Moreover, as illustrated in the diagram of Figure 10, these data suggest that maintenance of this proportionality in enucleated animals is achieved through a corresponding increase in the divergence of projections from area 17 to area 18a, i.e., an increase in the ratio between the overall size of the projection in 18a and the size of the tracer injection in area 17. For example, Figure 10 illustrates that a tracer injection that occupies, for instance, 10% of area 17 in control rats (Fig. 2.10A) would occupy approximately 16.4% of area 17 in BE0 rats (Fig. 10B) due of the reduction in the size of this area observed in these animals (Fig. 2.9A). From the correlation shown in Figure 2.9C it follows that the proportion of area 18a occupied by the resulting projections would be correspondingly greater in BE0 rats than in control rats. However, because area 18a is approximately the same size in both control and BE0 rats (Figure 2.9A), the absolute size of the 18a projection produced by an injection of the same size would be greater in BE0 than in control rats (cf. Fig. 2.10A,B). Indeed, we found that the ratio between the overall size of the projection in area 18a and the size of the injection site in area 17 was significantly larger ($p < 0.05$) in BE0 rats (M = 1.69, SD = 0.6) compared to control rats (M = 0.97, SD = 0.15), confirming that enucleation causes an increase in the divergence of striate-extrastriate projections.

DISCUSSION

Studies from several laboratories have shown that the pattern of striate-extrastriate projections in the rat is remarkably consistent from animal to animal (Olavarria and Montero, 1984; Malach, 1989; Montero, 1993; Coogan and Burkhalter, 1993). Moreover, these studies

showed that tracer injections into different regions of V1 produce essentially the same projection patterns, except that the projection fields translocate locally according to the retinotopic organization of extrastriate visual areas. In contrast, in the present study we found that bilateral enucleation at birth leads to the development of striate-extrastriate projections patterns that are highly anomalous and variable from animal to animal. Unlike control rats, it was often not possible to transform the patterns observed in different rats by displacing the overall set of projection fields. A highly variable pattern of cortical projections to area 17 has also been described in neonatally enucleated opossums (Karlen et al., 2006). As in this previous study, the variability we observed does not seem to be due to differences in the location of injection sites because animals with injections in similar locations often showed widely different projection patterns. If extrastriate cortex in BE0 rats were subdivided into multiple striate-recipient areas, our observations would suggest that, unlike normal rats, the arrangement of these areas would vary considerably among animals. Our results are in agreement with a previous study describing anomalous striate-extrastriate projections in both neonatally enucleated and anophthalmic rats (Bravo and Inzunza, 1994), and are consistent with experiments in hamsters (Kingsbury et al., 2002) and cats (Carić and Price, 1999) showing that early ablation of thalamic input leads to abnormal corticocortical connections. Moreover, our data from animals injected with both anterogradely and retrogradely transported tracers into striate cortex showed that enucleation at birth induces similar anomalies on both feedforward and feedback pathways. These results provide evidence that the development of normal striate-extrastriate connections depends critically on retinal influences.

Our quantitative analysis revealed that the size of area 17, but not that of area 18a, is markedly smaller in early enucleates compared to controls, leading to a pronounced mismatch between the sizes of area 17 and 18a. This mismatch is compensated by an increase in the divergence of striate-extrastriate projections, which prevents enucleation from altering the normal relationship that exists between the proportion of area 18a occupied by the projection from area 17, and the proportion of area 17 occupied by the tracer injection. In order to calculate the relationship between the relative sizes of the projection fields in area 18a and the relative sizes of the injection sites in area 17, it was necessary that we measure the sizes of areas 17, 18a, the overall projection in area 18a, and the size of the tracer injections. Our measurements of the size of area 17 are likely to be accurate because they are based on the profile of area 17 as

revealed by myelin and callosal patterns in tangential sections of the flattened cortex. In addition, they are in good agreement with previous estimates of the size of area 17 (Olavarria et al., 1987). Likewise, we believe that our measurements of the overall size of the projection in area 18a are accurate because they are based on BDA-staining patterns that could be readily scanned and processed by imaging programs. However, although the lateral border of area 18a can be readily recognized from myelin and callosal patterns, there are no clear criteria for recognizing the anterior border of this area. In order to compare the size of area 18a across all experimental groups, we traced the anterior border of area 18a using common landmarks identifiable in all animals, but which were somewhat arbitrary (see Materials and Methods). It is therefore possible that we underestimated the size of area 18a. Similarly, we estimated the sizes of the injection sites using two approaches that were highly consistent with each other, but it is possible that the sizes we measured do not correspond to that of the effective injection sites. As explained in Materials and Methods, striate projections to the superior colliculus or lateral geniculate nucleus could not be used to compare the effective injection site between control and enucleated animals because striate-subcortical connections are abnormal in neonatally enucleated rodents (e.g., Warton et al., 1988). However, since the same procedures were used to measure the size of the tracer injections and area 18a in all experimental groups, potential differences between our measurements and the actual sizes of area 18a and of the effective tracer injections would not necessarily invalidate our comparative analysis across groups.

The increase in the divergence of striate-extrastriate projections that we observed in early enucleated rats is consistent with a recent study reporting that neonatal enucleation increases the divergence/convergence of callosal connections in rat visual cortex (Bock and Olavarria, 2011), which raises the possibility that increases in the divergence/convergence of connections is a common plastic response to early deafferentation in the central nervous system. It is also interesting to note that our finding that area 17, but not area 18a, is reduced in enucleated rats contrasts with a recent report that early enucleation in the ferret is associated with a reduction in the size of both striate and extrastriate visual areas (Bock et al., 2012). Projections from the dLGN have been implicated in the regulation of the size of visual areas (see Bock et al., 2012, for references relevant to this issue). In this context, the difference between our results in the rats and those reported in the ferret is probably related to the fact that projections from the dLGN are largely restricted to area 17 in the rat (Ribak and Peters, 1975; Schober and Winkelmann, 1977;

Olavarria, 1979), while in the ferret, in addition to area 17, direct retino geniculate projections also innervate area 18 and possibly other extrastriate visual areas (Innocenti et al., 2002; Redies et al., 1990; Ruthazer et al., 1999; White et al., 1999).

Retinal influences specify normal patterns of striate-extrastriate connections by postnatal day six

Our data from delayed enucleations show that the patterns of 17-18a projections appear less disrupted when enucleation is performed at P4 than when enucleation is performed at P0. However, delaying enucleation by only two more days results in 17-18a projection patterns that closely resemble the patterns in control animals. Our data show that the patterns of projections in adult rats enucleated at P6 are very similar to the patterns in control rats in the overall arrangement and relative location of the projection fields, as well as in the consistency of the overall pattern from animal to animal. Moreover, we showed that the feedback projection from lateral extrastriate cortex to striate cortex also appears immune to enucleation by P6. These results indicate that retinal input ceases to influence the development of feedforward and feedback striate-extrastriate projections by postnatal day 6. Previous studies have reported that both binocular and monocular neonatal enucleation alter the overall distribution of callosal connections in the 17/18a callosal zone of rats and mice (Cusick and Lund, 1982; Olavarria and Van Sluyters, 1984; Olavarria et al., 1987). Moreover, the appearance of the overall visual callosal pattern (Olavarria et al., 1987), as well as its point-to-point topography (Olavarria and Hiroi, 2003), abruptly becomes immune to the effects of eye removal at P6. Thus, our present results together with those from previous studies of the callosal pathway indicate that the overall distributions of callosal connections and ipsilateral striate-extrastriate connections become specified at about the same time during early stages of development, possibly by similar retinally driven mechanisms. If these mechanisms depended on ganglion cell activity, the likely source would be spontaneous activity because the eyes open by P13, ruling out a role for visual experience in the development of striate-extrastriate projection patterns. Although enucleation at P6 did not have an obvious effect on the patterns of striate-extrastriate connections, it still had a significant effect on the size of striate cortex. Similar observations have been reported in a recent study of the effects of neonatal enucleation on the pattern of callosal connections and the size of visual areas in the ferret (Bock et al., 2012). These observations suggest that retinal

influences regulate several aspects of cortical development through mechanisms that do not necessarily operate during the same time window. Moreover, they indicate that the pattern of visual corticocortical connections can develop without obvious abnormalities even if the size of striate cortex is somewhat smaller than normal.

At first sight, our results show that the critical period for the feedback pathway coincides with that for the feedforward pathway may seem at odds with reports that development of feedback pathways in humans (Burkhalter, 1993) and mice (Dong et al., 2004) is delayed by several days when compared to that for the feedforward pathway. Assuming that the development of the feedback pathway is also delayed in normal rats, our finding of a common critical period for both pathways suggests that the timing of the critical period for the effect of the eyes does not primarily depend on the timing of axon arrival at the target region. For example, during the critical period, chemical cues induced by retinally driven processes could lay down a "blue print" for normal patterns of feedforward and feedback projections. In this scenario, fibers from extrastriate cortex would still be able to "read" the instructions in the blue print even if they arrive at their targets with some delay. In the present study we found that the development of feedforward striate-extrastriate projections in neonatally enucleated rats proceeds with a time course that is similar to that of feedforward projections in normal-eyed animals (Ruthazer et al., 2010). If in normal rats the development of the feedback projection were delayed relative to the development of feedforward projections, as it is in humans (Burkhalter, 1993) and mice (Dong et al., 2004), it would be of interest to determine whether the time course for the development of the feedback projection is similarly delayed in neonatally enucleated rats. Finding that this is indeed the case would provide further evidence that the timing of axon growth and invasion of grey matter for different pathways is likely triggered by mechanisms depending on central, rather than retinal, factors.

Role of retinal input on the development of striate-extrastriate projection patterns

A recent study of the development of the 17-18a projection in normal rat pups found that axonal interstitial branches of simple architecture reach superficial layers by P6, and that by P8 fibers originating from a single, small injection of BDA in area 17 formed well-defined, focused projection fields at the correct topographical locations in area 18a (Ruthazer et al., 2010). In the present study we observed that striate-extrastriate projections in pups enucleated at birth also reach superficial cortical

layers by P6, providing evidence that the timing of fiber invasion and growth in area 18a is independent from retinal influences. A similar schedule for fiber invasion and growth in grey matter has been reported for visual callosal connections in both normal rats and in rats enucleated at birth (Olavarria and Safaeian, 2006). Moreover, as in normal pups (Ruthazer et al., 2010), our data from pups enucleated at birth and studied at P6 or P8 show that fibers invading area 18a from area 17 form well-defined projection fields from the beginning of the invasion, suggesting that the highly variable projection patterns observed in area 18a of mature neonatally enucleated rats do not result from anomalous pruning of exuberant distributions of 17-18a fibers in grey matter. These results in young enucleated pups, together with our finding that lack of retinal influences during the critical period results in highly variable patterns of striate-extrastriate connections in adult rats suggest that retinal influences regulate the spatial arrangement of striate-extrastriate projection patterns, but not the timing and definition of the initial invasion of area 18a by striate projection axons.

What may account for the high variability of striate-extratriate projections observed in neonatally enucleated rats? Ruthazer et al. (2010) also performed a time-lapse analysis of the development of 17-18a projections in normal pups and reported that many filopodium-like branches emerged along parental axons in white matter or deep layers in area 18a. Most of these filopodial branches were transient, often disappearing after several minutes to hours of exploratory extension and retraction. On the basis of their fixed tissue and time-lapse observations, Ruthazer et al. (2010) proposed that the development of topographically organized corticocortical projections in rats involves extensive exploratory branching along parental axons and invasion of cortex by only a small number of interstitial branches which grow toward the pia at topographically correct places. Ruthazer at al. (2010) further suggested that the growth of branches at topographically correct places could be specified both by a combination of local mapping cues, such as the graded expression patterns of ephrinA (Cang et al., 2005), and cues from the eyes, either in the form of patterned neural activity (Ruthazer et al., 2003; Cang et al., 2008) or thalamic afferent-derived molecular signals (Sugiyama et al., 2008). The observation that small, dynamic filopodium-like branches also emerge from 17-18a parental axons in neonatally enucleated rats (E. Ruthazer and J. Olavarria, unpublished observations), together with our present data from BDA-labeled fibers in neonatal rats, suggest that striate-extrastriate projections go through similar developmental stages in both control and enucleated rats, except that the arrangement and topography of the projections are anomalous in enucleated rats. This lack of topography could result from the loss of retinal topographic cues caused by enucleation, which

would leave only local cues in charge of specifying the places along the parental axons where small dynamic branches are to grow toward the pia. It is possible that the spatial distribution of these local cues varies significantly from animal to animal, leading to the development of highly variable patterns of striate-extrastriate projections in enucleated animals.

Callosal to callosal, acallosal to acallosal rule

In normal rats, callosal connections occupy approximately the lateral third of area 17, while in area 18a they form more or less continuous bands on either side of the area, as well as a series of callosal bridges dividing area 18a in a number of compartments that correspond closely to visual areas described physiologically (Fig. 5 A,C,D). Previous studies (Olavarria and Montero, 1984; Coogan and Burkhalter, 1993; Ankaoua and Malach, 1993), as well as our present results illustrate that projections from area 17 to ipsilateral area 18a obey the general rule "callosal to callosal, acallosal to acallosal", i.e., medial, acallosal regions of area 17a project to acallosal islands in area 18a, while the lateral, callosal region of area 17 projects to callosal regions located preferentially at the border of visual areas in lateral extrastriate cortex. In normal rats, this rule likely reflects the fact that projections from restricted loci in striate cortex are distributed according to the topography of extrastriate visual areas identified physiologically (Montero, 1973; Montero et al., 1973b; Thomas and Espinoza, 1987). Thus, the lateral, callosal region in area 17 represents portions of the visual field located close to, or on the vertical meridian of the visual field, and this region projects to the medial, as well as other callosal regions in ipsilateral area 18a, which represent the same central regions of the visual field. Similarly, medial, acallosal regions in area 17 represent more peripheral portions of the visual field, and they project to acallosal islands in ipsilateral area 18a, which also represent peripheral fields. In the present report we focused our attention on the projections from medial, acallosal regions of area 17 to highlight the close complementarity of these projections with the pattern of callosal connections in area 18a (Fig. 5 C,D), and to examine whether this relationship is affected by the removal of topographic cues from retinal origin. Our results indicate that enucleation leads to the development of anomalous striate-extrastriate and callosal connections. However, the abnormalities in 17-18a projections mirror the abnormalities in the callosal pattern in such a way that projections from medial, acallosal regions of striate cortex remain confined to acallosal territories in area 18a, thereby maintaining the complementarity between these pathways that is

observed in normal animals. These results indicate that this complementarity does not depend on topographic cues from the retina, and provide evidence that, in spite of abnormalities in the topography of striate-extrastriate projections, the rule "callosal to callosal, acallosal to acallosal" remains valid in neonatally enucleated rats. Mechanisms underlying this complementary may relate to central cues specifying the distribution of callosal and non-callosal territories, and several scenarios are possible. For instance, callosal and non-callosal territories may be "marked" by cues that attract projections from callosal and non-callosal territories, respectively. Alternatively, callosal and no-callosal territories may be specified by cues that are mutually repulsive. In this case, projections originating from acallosal regions in area 17 would be confined to acallosal territories in area 18a because callosal regions in areas 17 and 18a would repel them. A similar mechanism would restrict projections originating from callosal regions in area 17 to callosal territories in area 18a. However, these mechanisms require that both pathways be specified by specific markers, making it hard to explain how the distribution of separate markers would vary in tandem to induce variability in the distribution of striate-extrastriate and callosal connections without loss of complementarity. Perhaps central cues only specify the territory for one of these pathways, which would then act as a template to passively mold the distribution of the other one through repellent interactions. This would allow variability in the template without loss of complementarity. The cues involved are not known at present, but they may be similar to guidance labels that have been implicated in the establishment of topographically organized thalamocortical projections. For instance, Cang et al. (2005) showed that EphA/ephrin-A interactions are involved at central levels of the visual pathway, including primary visual cortex, and suggested that they may have a role in mapping projections from primary to non-primary visual areas. Further research is necessary to determine the mechanisms regulating the patterns of striate extrastriate and callosal connections, and how they give rise to ensembles of topographically organized visual areas that are highly constant from animal to animal. Our data suggest that retinal input may not only specify the normal arrangement of extrastriate visual areas, but also their normal internal topography, a question we are currently investigating in more detail using injections of multiple tracers in the same animal. Finally, studying how striate extrastriate and callosal connections interact during development may yield important clues toward understanding evolutionary changes in the segmentation and arrangement of cortical visual areas across species.

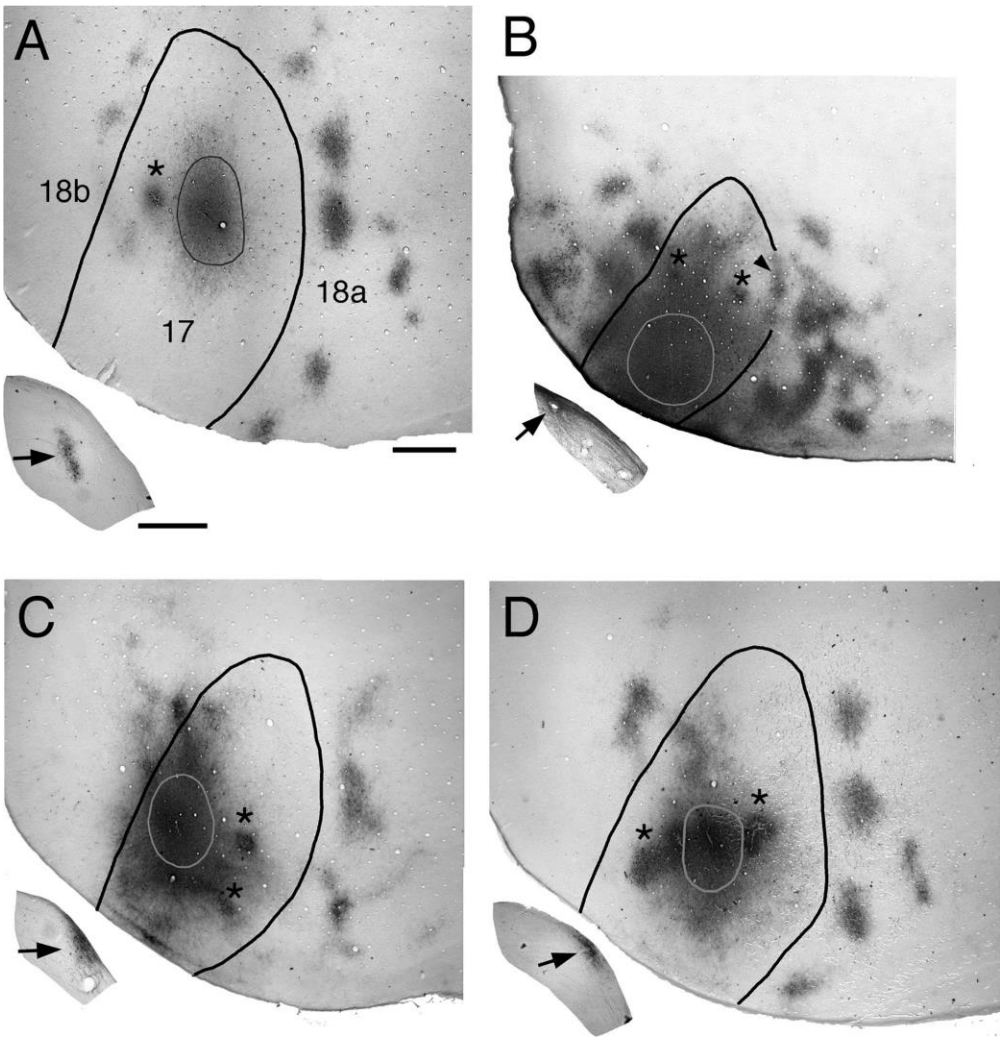

Figure 2.1. Effect of bilateral enucleation at different postnatal ages on the pattern of striate-extrastriate projections. Photographs of tangential tissue sections cut through the flattened occipital cortex illustrate the anterogradely labeled projection patterns in extrastriate cortex (areas 18a and 18b, Krieg, 1946; Caviness, 1975) resulting from a single injection of BDA into medial, acallosal regions of striate cortex (area 17). Lateral is to the right, anterior is up. Outlines inside area 17 indicate the injections of the tracer BDA. Asterisks indicate artifactual staining produced by injections of fluorescent tracers. Black arrows in insets indicate the patterns of antrogradely transported BDA labeling in the ipsilateral dLGN. (A) Control animal. (B) Enucleation at postnatal day 0 (BE0). Arrowhead indicates labeling at the 17/18a border. (C) Enucleation at postnatal day 4 (BE4). (D) Enucleation at postnatal day 6 (BE6). Scale for flattened tissue = 1.0 mm; scale for dLGN = 0.5 mm.

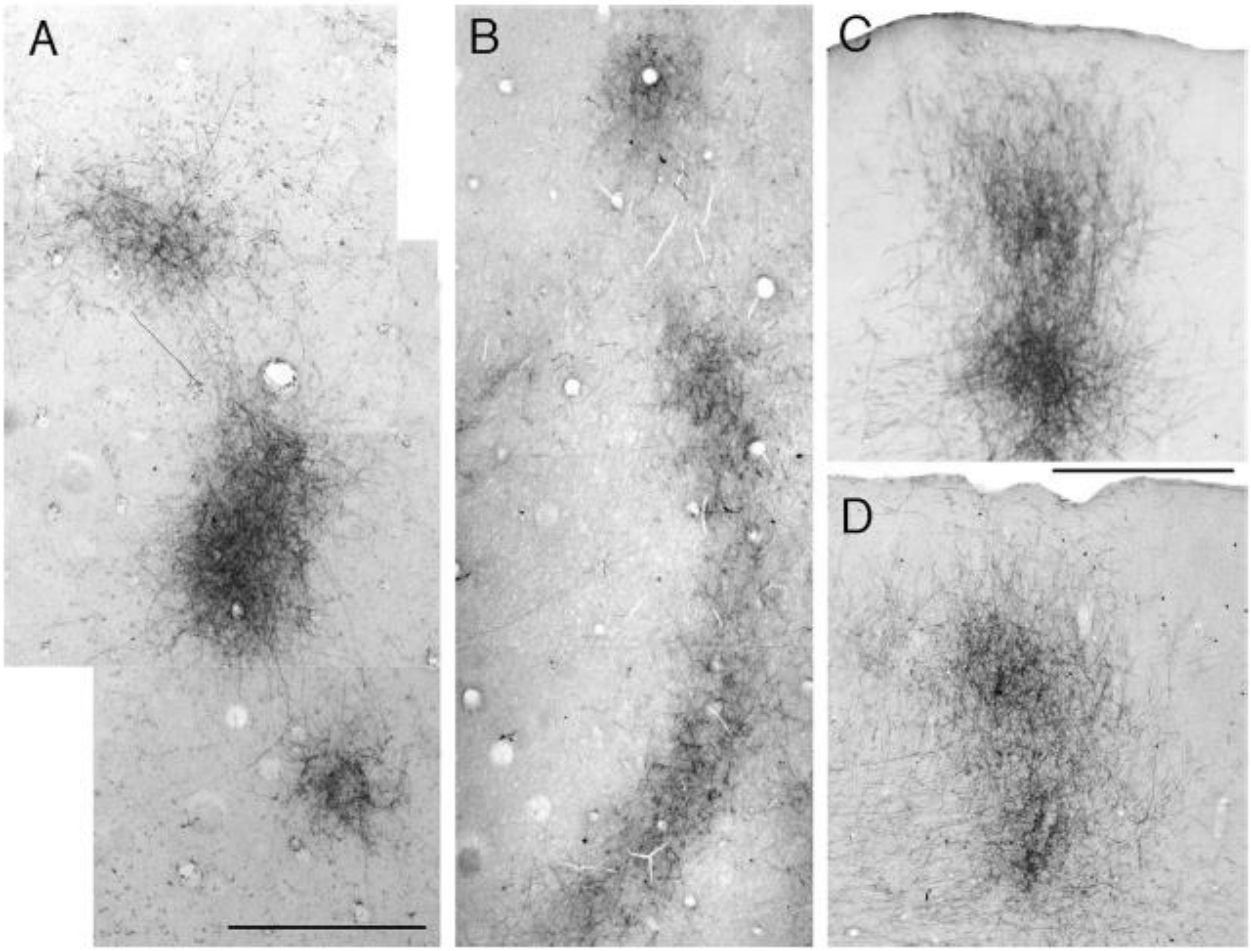

Figure 2.2. Effect of bilateral enucleation at birth (BE0) on projections from striate cortex to lateral extrastriate cortex. High magnification photographs of striate projection fields observed after single injections of BDA into medial, acallosal regions of striate cortex. (A, B) Projections fields revealed in tangential sections in control (A) and BE0 (B) animals. Lateral is to the right, anterior is up. (C, D) Projection fields revealed in coronal sections through lateral extrastriate cortex in a control (C) and a BE0 (D) animal. Lateral is to the right. Scale bar in A = 1.0 mm; scale bar in C = 0.5 mm.

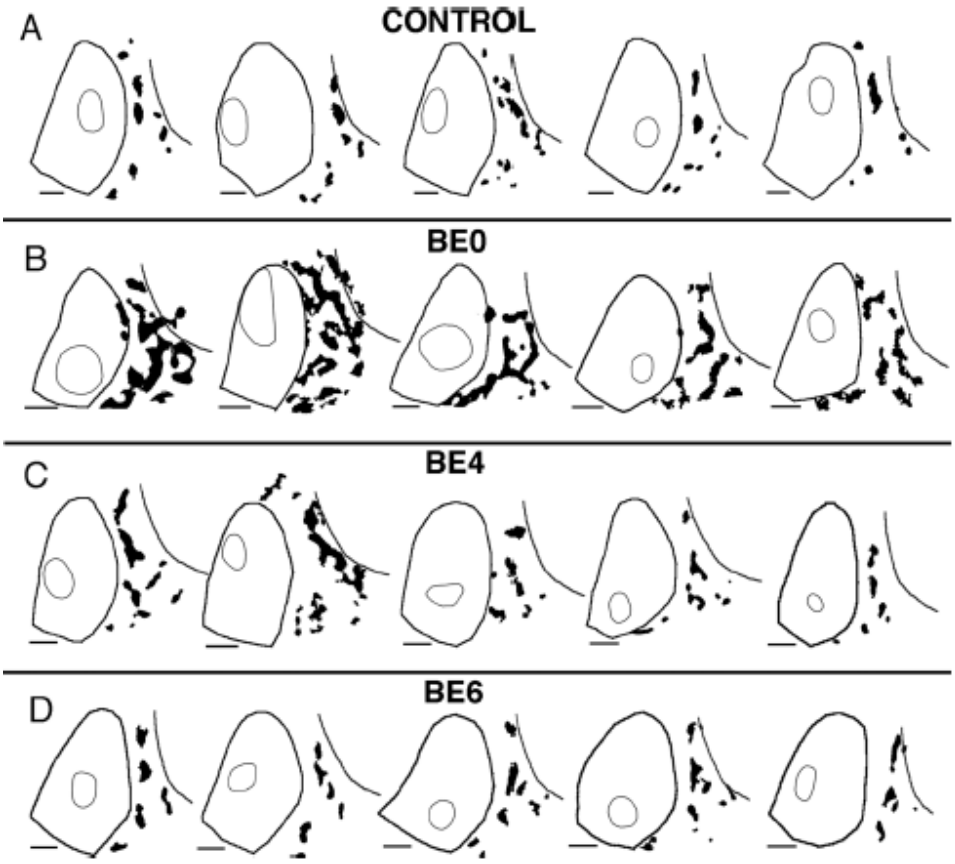

Figure 2.3. Patterns of BDA labeled projections from striate cortex to area 18a in control rats and in rats enucleated at different ages. Lateral is to the right, anterior is up. Thresholded versions of the projection patterns are represented in black. Thick lines delineate the borders of areas 17 and the lateral border of area 18a, while thin outlines outline the BDA injection sites. The injection outlines were drawn at the perimeter where an abrupt transition in the labeling density was observed (see Materials and Methods). The patterns were scaled so that the profile of area 17 in each case matched the profile of area 17 in the first case shown in A as closely as possible. (A) Control rats. (B) Rats enucleated at birth (BE0). (C) Rats enucleated at postnatal day 4 (BE4). (D) Rats enucleated at postnatal day 6 (BE6). Scale bars = 1.0 mm.

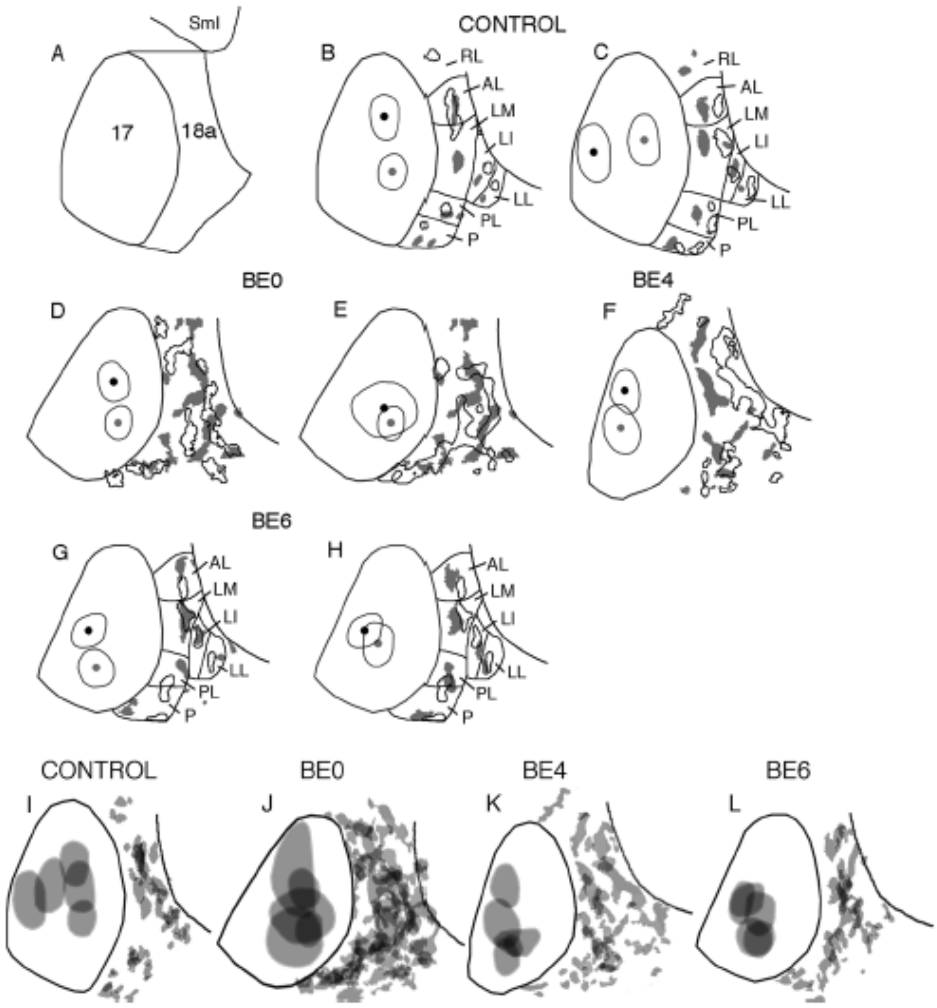

Figure 2.4. (A) Diagram illustrating the borders of area 18a in both control and enucleated rats, as defined by criteria used in this study (see Materials and Methods). Lateral is to the right, anterior is up. (B-H) Comparison of 18a projection patterns from pairs of animals with BDA injections in different loci within striate cortex. Black outlines in area 18a indicate projections from injection sites marked by black dot and thin outline in area 17; grey patches in area 18a indicate projections from injection sites marked by grey dot and thin outline in area 17. Lateral border of area 18a is indicated by black line. Control (B, C); BE0 (D, E); BE4 (F); BE6 (G, H). (I-L) Variability of the patterns of projections from striate cortex to lateral extrastriate cortex in control (I) and enucleated rats (J-L). The injection sites within striate cortex and the striate-extrastriate projection patterns in each group shown in Figure 3 were merged after their orientation had been adjusted so that the lateral border of striate cortex coincided as closely as possible within each group. The lateral border of area 18a is indicated by a black line. SmI,

Somatosensory cortex; lateral extrastriate visual areas are named as reported previously: AL, anterolateral; LM, lateromedial; LI, laterointermediate; LL, laterolateral; PL, posterolateral; P, posterior (Montero, 1993; Olavarria and Montero, 1981; 1984; 1989; Espinoza and Thomas, 1983; Thomas and Espinoza, 1987; Coogan and Burkhalter, 1993; Wang and Burkhalter, 2007); other conventions as in Figure 3.

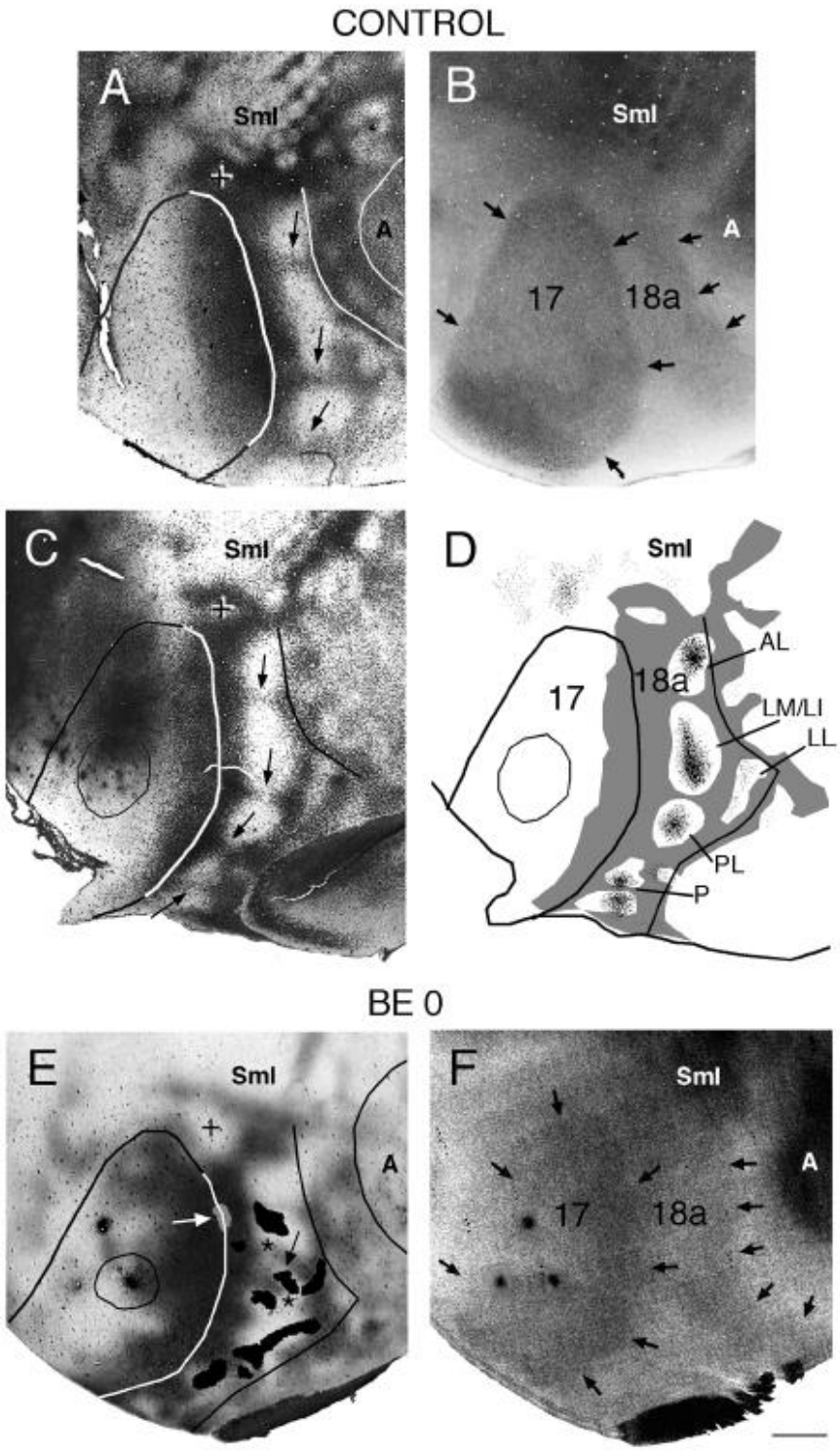

Figure 2.5. Correlating the patterns of striate-extrastriate and visual callosal connections. Lateral is to the right, anterior is up. (A, B) Callosal (A) and myelin (B) patterns in normal adult rats. In A, dark areas correspond to dense accumulations of retrogradely labeled somas and anterogradely labeled axons; the profiles of areas 17, 18a and auditory cortex were drawn

following myelin boundaries in the myelin pattern (B). Arrows in A indicate callosal bridges across area 18a, which separate several acallosal ring-like regions; the cross indicates the anterior callosal ring (Olavarria and Montero, 1984); black arrows in B indicate myelin boundaries. (C) Callosal pattern in normal adult rat. Arrows point to callosal bridges separating several acallosal ring-like regions in area 18a. The cross indicates the anterior callosal ring. (D) Thresholded version of callosal pattern in A is shown in grey. Fine black dots in extrastriate cortex indicate anterograde transport of tritiated proline from an injection of this tracer into striate cortex (thin outline). Lateral border of area 18a is delineated by black line. (Modified from Olavarria and Montero, 1984). (E) Callosal pattern revealed following multiple injections of HRP in adult rat enucleated at birth. Dark areas correspond to dense accumulations of retrogradely labeled somas and anterogradely labeled axons. The cross indicates the anterior callosal ring. Asterisks mark two interrupted callosal bridges; striate extrastriate projections are represented as black patches in area 18a, and arrow indicates striate projection field "wedged" between the two interrupted callosal bridges. White arrow points to small projection field (grey) contained in an area of reduced callosal labeling at the 17/18a border. The profiles of areas 17, 18a and auditory cortex were drawn from the callosal pattern in E and the myelin pattern in F. (F) Myelin pattern from case shown in E. Arrows indicate borders of areas 17 and18a. A, auditory cortex; other conventions as in Figure 4. Scale bar = 1.0 mm.

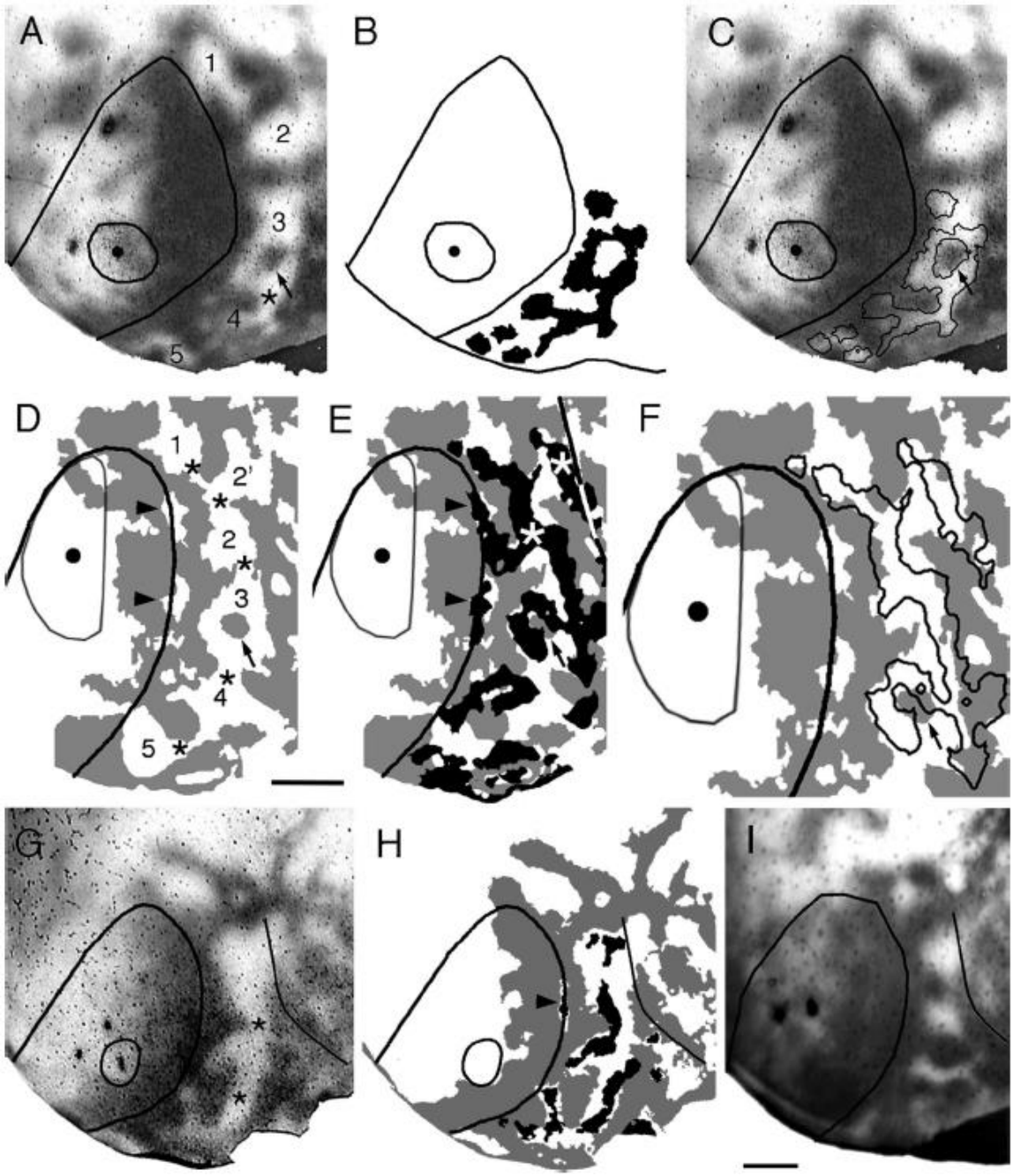

Figure 2.6. Correlating the patterns of striate-extrastriate and visual callosal connections. The callosal patterns were revealed in adult rats following multiple injections of HRP in the contralateral hemisphere, and the striate extrastriate projections were revealed following single injections of BDA into striate cortex. Injection site is represented by the dot and the fine outline. Lateral is to the right, anterior is up. (A, B, C) Rat enucleated at birth. Dark areas in A and C correspond to dense accumulations of retrogradely labeled callosal somas and anterogradely labeled callosal axons. Numbers in A indicate acallosal regions. Asterisk in A indicates

interrupted callosal bridge. Arrows in A and C indicate an island of densely labeled callosal connections. Striate extrastriate projections are represented in black in B, and as outlines in C. (D, E, F) Rat enucleated at birth. Callosal pattern is represented in grey. Striate extrastriate projections are represented in black in E and as outlines in F. Numbers in D represent acallosal islands. Asterisks in D mark interrupted callosal bridges. Arrow in D, E and F marks an island of densely labeled callosal connections. Arrowheads in D mark acallosal regions at the 17/18a border, while arrowheads in E mark anomalous striate projections into these 17/18a acallosal regions. A portion of the lateral border of area 18a is indicated by a black/white line in E. (G) Callosal pattern revealed following multiple injections of HRP in adult rat enucleated at birth. Dark areas correspond to dense accumulations of retrogradely labeled somas and anterogradely labeled axons. (H) Thresholded version of callosal pattern in G is shown in grey. Black areas in extrastriate cortex indicate anterograde transport of BDA from an injection of this tracer into striate cortex (thin outline). Arrowhead points to a small projection field within an area of reduced callosal connections at the 17/18a border. (I) Callosal pattern in adult rat enucleated at P4. Lateral border of area 18a is indicated by black line in G-I. Scale bars = 1.0 mm.

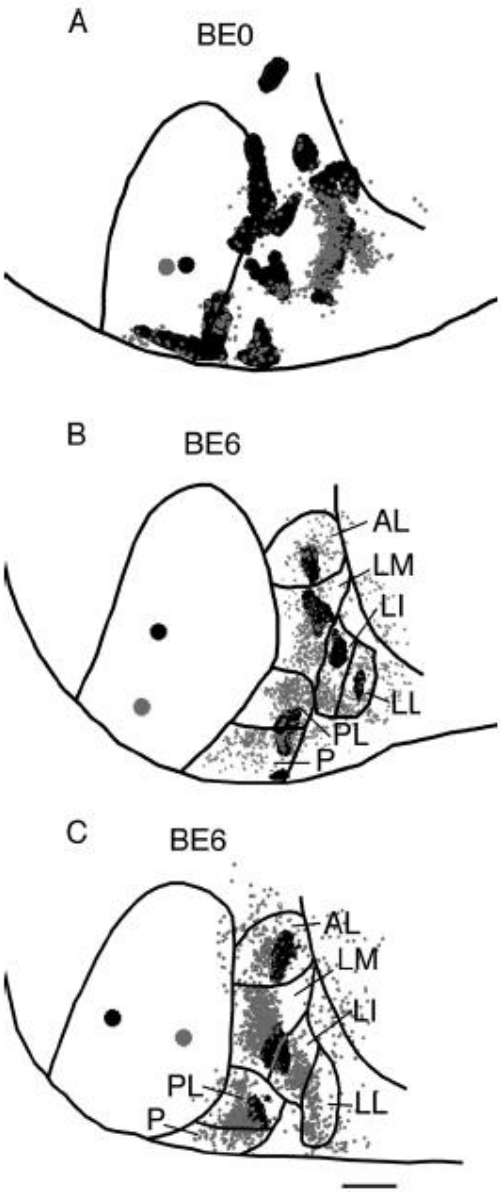

Figure 2.7. Feedforward and feedback patterns of connections in area 18a of rats enucleated at P0 (BE0) (A) and P6 (BE6) (B, C). Lateral is to the right, anterior is up. Lateral border of area 18a is indicated by a black line. Large black dot in striate cortex represents a single injection of BDA, while the grey dot represents a single injection of rhodamine latex beads. Anterograde projections in area 18a are represented by the black areas, while the small grey dots represent cells labeled retrogradely by the transport of rhodamine latex beads. Visual areas are named as in Fig. 4. Scale bar = 1.0 mm.

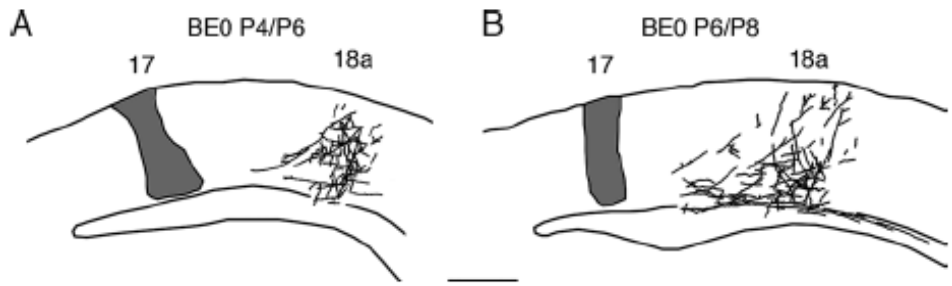

Figure 2.8. Development of 17-18a projections in rats enucleated at birth. Lateral is to the right. Projections were studied following single injections of BDA into area 17 and the distribution of anterogradely labeled fibers was studied forty-eight hours later in coronal sections cut through occipital cortex. The injection site is represented in grey, and labeled fibers are represented as black lines. (A) Case injected at P4 and studied at P6. (B) Case injected at P6 and studied at P8. Scale bar = 0.5 mm.

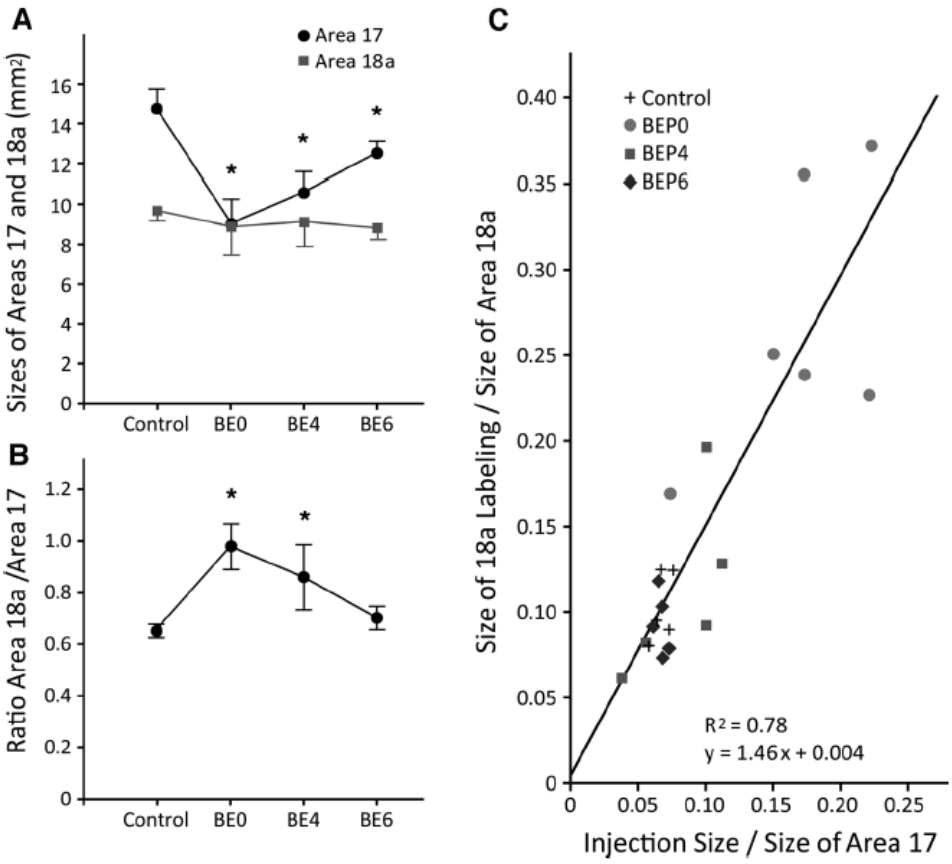

Figure 2.9. (A) Comparison of the sizes of areas 17 and 18a in control and in BE0, BE4 and B6 rats. Asterisks indicate that area 17 was significantly ($P < 0.05$) larger in control compared to each group of enucleated rats. In contrast, area 18a was not significantly different in control rats compared to any of the groups of enucleated rats. Error bars indicate SD. (B) Comparison of the ratio of the size of area 18a to the size of area 17 in control and in BE0, BE4 and B6 rats. Asterisks indicate that this ratio was significantly ($P < 0.05$) smaller in control compared to BE0 and BE4 rats. Error bars indicate SD. (C) Scatter plot correlating the overall proportion of area 18a occupied by the BDA-labeled projection from area 17 with the proportion of area 17 occupied by the injection of BDA into area 17.

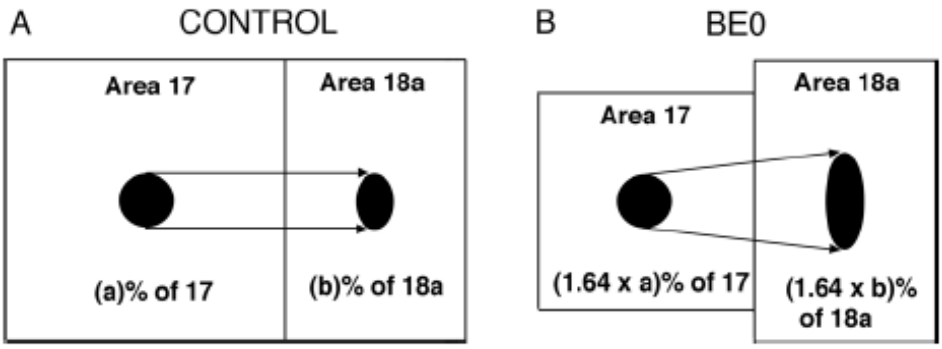

Figure 2.10. Diagram summarizing the effects of BE0 on the sizes of areas 17 and 18a, and on the relation between the overall proportion of area 18a occupied by BDA labeling and the proportion of area 17 occupied by the BDA injection. The diagram illustrates that, on average, BE0 causes a 39% reduction in the size of area 17, while it does not have a significant effect on the size of area 18a. The BDA injection in area 17 of the control case (A), represented by the black circle, occupies (a)% of area 17, while in the BE0 case (B), the proportion of area 17 occupied by an injection of the same size increases by a factor of 1.64 due to the reduction in the size of area 17. For example, if the injection site occupied 10% of area 17 in the control rat, an injection of the same size would occupy 16.4% of area 17 in the B0 rat. Similarly, the proportion (b%) of area 18a occupied by the projection from area 17 in control rats (black oval in area 18a, Fig. 10A) increases by the same factor in area 18a of BE0 rats (black oval in area 18a, Fig. 10B). Thus, the diagram in B illustrates that, for an injection of the same size, the absolute size of the BDA labeling in area 18a is greater in BE0 than in control rats (cf. black ovals in areas 18a in A and B), indicating that enucleation leads to an increase in the divergence of the projections from 17 to 18a.

CHAPTER 3 TOPOGRAPHY OF STRIATE-EXTRASTRIATE CONNECTIONS IN NEONATALLY ENUCLEATED RATS

ABSTRACT

It is known that retinal input is necessary for the normal development of striate cortex and its corticocortical connections, but there is little information on the role that retinal input plays in the development of retinotopically organized connections between V1 and surrounding visual areas. In nearly all lateral extrastriate areas, the anatomical and physiological representation of the naso-temporal axis of the visual field mirrors the representation of this axis in V1. To determine whether the mediolateral topography of striate-extrastriate projections is preserved in neonatally enucleated rats, we analyzed the patterns of projections resulting from tracer injections placed at different sites along the mediolateral axis of V1. We found that the correlation between the distance from injection sites to the lateral border of V1 and the distance of the labeling patterns in area 18a was strong in controls and much weaker in enucleates. Data from pairs of injections in the same animal revealed that the separation of area 18a projection fields for a given separation of injection sites was more variable in enucleated than in control rats. Our analysis of single and double tracer injections suggests that neonatal bilateral enucleation weakens, but not completely abolishes, the mediolateral topography in area 18a.

This chapter was previously published in Biomedical Research International (August, 2013) and used with permission.

INTRODUCTION

Visual information is processed along ascending neuronal pathways that maintain the point-to-point topography of the retinofugal projections. Much work has focused on understanding how topography is established in the projections from ganglion cells to the superior colliculus and thalamus (Simon and O'Leary, 1992; McLaughlin et al., 2003; Flanagan, 2006), but less is known about how higher order pathways develop. In particular, there is little information about the mechanisms guiding the development of retinotopically organized connections, known as topographic maps, between primary visual cortex (V1, striate cortex, area 17) and higher extrastriate visual areas. Recent studies support the idea that development of cortical areas and their organized interconnections may depend on a combination of activity-independent cortical factors, such as genetically determined guidance labels, and activity-dependent mechanisms driven by sensory input (Katz and Shatz, 1996; Miyashita-Lin et al., 1999; Vanderhaeghen et al., 2003; Cang et al., 2005).

During development, interhemispheric callosal connections in V1 are established between opposite cortical loci that are retinotopically matched (i.e., they represent the same visual coordinates; Olavarria, 1996; Olavarria, 2001; Bosking et al., 2000). Olavarria and colleagues proposed that the temporal retina, through a system of bilateral projections, promotes the stabilization of callosal linkages that, while retinotopically corresponding, are arranged in a nonmirror-symmetric pattern with respect to the brain midline (Olavarria, 1996; Olavarria, 2001; Olavarria and Li, 1995). However, in the absence of retinal input callosal connections are established between opposite cortical loci that are mirror- symmetric with respect to the midline (Olavarria and Hiroi, 2003). This reversal in the callosal map provides evidence that retinal input can specify cortical topography. However, it remains unclear whether or not retinal input plays a major role on the establishment of topographically organized *intra*hemispheric connections between V1 and surrounding extrastriate visual areas.

Numerous anatomical and physiological studies in normal rats have shown that V1 is surrounded by at least 10 extrastriate visual areas (Montero et al., 1973a; Montero et al., 1973b), which have been named according to their location relative to V1 (see Fig. 2A). Each of these areas contains a representation of the opposite visual hemifield and receives direct, retinotopically organized, projections from V1 (see Montero, 1993 and Bravo and Wang and Burkhalter, 2007, for reviews). Moreover, callosal connections form a dense band that straddles

the V1/18a border, and a series of ring-like callosal bands that separate adjoining extrastriate visual areas in area 18a (Olavarria and Montero, 1984; Espinoza and Thomas, 1983; Thomas and Espinoza, 1987; Coogan and Burkhalter, 1993; Laing et al., 2012) (Fig. 2A). These callosal rings provide fixed reference landmarks for locating and identifying the various visual areas in area 18a of normal rats.

The pattern of striate-extrastriate projections in normal rats is remarkably consistent from animal to animal (Olavarria and Montero, 1984; Montero, 1993). Moreover, tracer injections placed into different loci in V1 produce essentially the same extrastriate projection patterns, except that the projection fields translocate locally according to the retinotopic map in each extrastriate visual area. This has made it possible to obtain information about the topography of striate-extrastriate connections in normal rats using single tracer injections into V1 (Olavarria and Montero, 1984). In contrast to normal rats, we recently reported that neonatal enucleation induces highly irregular and variable patterns of striate-extrastriate and callosal projections (Laing et al., 2012). However, this previous study, based on the analysis of projection patterns produced by single, restricted injections of anatomical tracers into V1, did not report the effects of enucleation on the topography of these projections. In the present study we have addressed this issue by analyzing data from single tracer injections into V1, as well as connection patterns resulting from pairs of discrete tracer injections placed at different locations in V1 of the same animal.

MATERIALS AND METHODS

Our study is based on data obtained from a total of 24 Long-Evans pigmented rats. Pregnant animals were monitored several times daily and the births of the litters were determined to within 12 hours. Sixteen rat pups were anesthetized with isoflurane (2–4% in air) and binocularly enucleated within 24 hours of birth (BE0). After recovering from the anesthesia, pups were returned to their dams. In addition, 8 rats were used for analyzing striate-extrastriate projections in normal adult animals. All surgical procedures were performed according to protocols approved by the Institutional Animal Care and Use Committee (IACUC) at the University of Washington.

Tracer injections

In both control and enucleated animals, striate-extrastriate projections were revealed following restricted tracer injections into striate cortex, while the distribution of callosal connections was demonstrated in the same hemisphere following multiple injections of a different tracer in the opposite hemisphere. Anatomical experiments in all normally reared and enucleated rats took place when the animals were at least 1 month old. Tracer injections were made under isoflurane anesthesia (2–4% in air). To study the topography of striate-extrastriate connections, animals received restricted injections of various tracers into different places of striate cortex, including biotinylated dextran amine (BDA, 10% in DW, Molecular Probes, Eugene, OR), which is predominantly transported anterogradely, horseradish peroxidase (HRP, Sigma Co, 25% in saline), which is transported both anterogradely and retrogradely, and fluorescent tracers (Rhodamine beads, RB, or Green beads, GB, LumaFluor, Naples, FL, concentrated stock solution), which are transported retrogradely. Small volumes (0.05–0.1 μl) of these tracers were injected into striate cortex of the right hemisphere (approx. 2.9 – 4.2 mm from the midline; 0.1–2.0 mm anterior to the lambda suture). In all cases analyzed the tracer injections were restricted to grey matter. The size of single injections of BDA and HRP was estimated as described previously (Laing et al., 2012). High levels of fluorescence from GB and RB injections were typically restricted to the injection sites because diffusion of these tracers is low. To reveal the overall pattern of callosal connections, multiple (Olavarria and Li, 1995; Olavarria and Hiroi, 2003; Montero et al., 1973a; Montero et al., 1973b) injections (total volume approx. 4.0 μL) of either HRP or bisBenzimide (BB, Sigma Co, 10% in DW) were placed over visual cortex of the left hemisphere (Olavarria and Van Sluyters, 1985). All tracers were pressure-injected through glass micropipettes (50–100 μm tip diameter). Data from some cases injected with BDA were presented in Laing et al., 2012.

Histochemical processing

After a survival period of 2 days, the animals were deeply anesthetized with pentobarbital sodium (100 mg/kg i.p.) and perfused through the heart with 0.9% saline followed by 4% paraformaldehyde in 0.1 M phosphate buffer (PB, pH 7.4). After the brain was removed from the skull, the cortical mantle to be analyzed was separated from the brainstem, flattened between glass slides and sectioned tangentially (60 μm thick sections) as described previously (Laing et

al., 2012). The flattening procedure was done with great care to ensure that both striate and extrastriate cortices were contained in the tangential sections. The thalamus was cut into 60 μm thick coronal sections. If present in the same brain, fluorescent and BDA or HRP labeling patterns were analyzed in alternate series of sections. Sections in the series examined only for fluorescence were mounted on slides and analyzed under epifluorescence without further processing. However, sections in the series processed for BDA or HRP were often also analyzed for epifluorescence because the fluorescent labeling in these sections was similar to that in sections not processed for these tracers. This allowed a direct correlation of the spatial location of both fluorescent and non-fluorescent labeling in the same section. BDA labeling was revealed using the standard Avidin-Biotin-Peroxidase protocol (Vectastain Elite ABC kit, Vector Laboratories, Burlingame, CA) and 0.01% H_2O_2 in 0.05% 3-3′ diaminobenzidine, with cobalt or nickel intensification; sections were then mounted, dehydrated, defatted, and coverslipped. HRP labeling was revealed using tetramethyl benzidine as the chromogen (Mesulam, 1985).

Data acquisition and analysis

Digital images of the BDA and HRP labeling patterns in histological sections were obtained by scanning the sections at 2400 dpi using an Epson 4990 scanner. The distribution of cells labeled with fluorescent tracers were analyzed using a microscope equipped with a motorized stage (LEPCO) controlled by a Dell XPS T500 computer and a graphic system (Neurolucida, MicroBrightField, Williston, VT). The borders of areas 17 and 18a (Krieg, 1946; Caviness, 1975; Zilles et al., 1980) were identified in the myelin pattern by scanning unstained tangential sections (Laing et al., 2012; Richter and Warner, 1974) (Fig. 3.1A). In both normal and enucleated rats, area 18a is the target of virtually all projections from V1 to lateral extrastriate cortex (Laing et al., 2012), so in this report we will consider the terms “lateral extrastriate cortex” and “area 18a” as synonymous. Further information for identifying the location of the border of areas 17 and 18a in control and enucleated rats came from analyzing landmarks provided by the overall callosal pattern in visual cortex, and the relation that these landmarks have with the borders of areas 17 and 18a as revealed in the myelination patterns (Laing et al., 2012; Olavarria and Van Sluyters, 1985; Olavarria et al., 1987) (Fig. 3.1).

The locations of the injection sites within striate cortex were confirmed by analyzing the distribution of labeled fields within the ipsilateral dorsal lateral geniculate nucleus of the

thalamus (dLGN) (Montero et al., 1968; Godement et al., 1979; Kaiserman-Abramof et al., 1980; Guillery et al., 1980; Warton and Harvey, 1988). The distance between injections of different tracers ranged form 0.8 to 1.6 mm. These distances were judged adequate for studying the topography of striate projections because the injections produced separate labeling fields in the dLGN (Fig. 3.2B,C). Tangential sections throughout the depth of the cortex were analyzed to ensure that injections were restricted to grey matter.

Using Adobe Photoshop CS2 (Adobe Systems), digitized images of anatomical tracer and myelin labeling patterns from the same animal were carefully aligned with each other using the border of V1, the edges of the sections, blood vessels and other fiducial marks. Cells labeled retrogradely by the injections of RB and GB were represented by red and green dots, respectively. Callosal patterns labeled with BB were represented by outlining the areas containing dense accumulations of labeled cells. To illustrate the patterns of callosal connections labeled with HRP or striate projections resulting from restricted injections of HRP or BDA, thresholded versions of these patterns were prepared after first applying a median filter to reduce noise, followed by a high pass filter to remove gradual changes in staining density across the entire digital image. The same filter parameters and thresholding levels were applied to all control and enucleated animals, and thresholded versions were visually inspected to confirm they accurately represented the labeling pattern observed in the tissue sections. Figures were prepared using Adobe Photoshop CS2, and all imaging processing used, including contrast enhancement and intensity level adjustments, were applied to the entire images.

Quantitative analysis

We restricted our analysis to the distribution of labeled fields in lateral extrastriate cortex resulting from injections placed at different medio-lateral locations in V1. The distance of the injection sites from the lateral border of V1 was expressed as the % of the width of V1 measured along a line passing through the injection site and perpendicular to the V1/18a border (Fig. 3.1C,F). To evaluate the overall distribution of the labeling pattern in area 18a with respect to the lateral border of V1, we divided lateral extrastriate cortex into four compartments (C) of equal width and numbered C1 to C4 from medial to lateral. These compartments were drawn parallel to the lateral border of V1 and to each other (Fig. 3.1C,F). For each tracer injection, we calculated a Laterality Index (LI) using the formula:

LI = [(C4-C1) + 2/3 (C3-C2) + N]/2N, where Cn is the number of labeled pixels within compartment n, and N is total number of labeled pixels in area 18a. This index ranges from 0.0 to 1.0, values that indicate that 100% of the labeling produced by a particular injection in V1 is contained within C1 or C4, respectively. Changes in LIs produced by pairs of tracer injections into V1 of the same animal were evaluated statistically using paired *t* tests.

RESULTS

The diagram in Figure 3.2A, based on numerous anatomical and physiological studies in normal rats (see Refs. above), illustrates the arrangement of visual areas in lateral extrastriate cortex, their internal topography, and their relationship to the overall pattern of callosal connections. This diagram shows that, with the exception of the small area LI, the maps in all lateral extrastriate areas are mirror images of the map in V1 along the medio-lateral axis (from temporal to nasal visual field representation). In contrast, the maps of the antero-posterior axis in V1 (from lower to upper visual field representation) differ among the areas: while the maps in areas LM, P, LI and LL show the same polarity as the map in V1, the polarity is inverted in areas AL and PL.

As it is difficult to identify with certainty specific extrastriate areas in enucleated rats due to marked abnormalities in striate-extrastriate and callosal connections (Bravo and Inzunza, 1994; Laing et al., 2012), we did not pursue the study of the effect of enucleation along the anteroposterior axis. Instead, we focused our attention on studying whether or not displacements of the injections along the mediolateral axis of V1 in enucleated rats lead to mirror image displacements of the overall labeling patterns in lateral extrastriate cortex. To this end we correlated the distances from the injection sites to the V1/18a border with the LI calculated for each labeling pattern in area 18a of control and enucleated rats (see Materials and Methods).

As expected, in control rats we observed a high correlation ($R^2 = 0.81$) between the distance of injection sites from the lateral border of V1 and the LIs of the resulting labeling patterns in area 18a (Figure 3.3A, 14 injection sites from 8 rats). This Figure shows that, as the distance of the injections increased, the overall labeling patterns moved more laterally in lateral extrastriate cortex, resulting in higher LIs. A positive, although weaker, correlation ($R^2 = 0.36$) was observed in enucleated rats (Fig. 3.3B, 24 injections from 16 rats). These results are

consistent with the high variability of striate-extrastriate projections in enucleated rats (Laing et al., 2012), and suggest that, in spite of this variability, the overall labeling patterns in area 18a of enucleated rats tend to move laterally when the injection sites are displaced medially in V1.

Due to the high animal-to-animal variability of striate-extrastriate projection patterns in BE0 rats, it is typically not possible to transform the pattern in one animal into that of another simply by displacing the fields in a consistent manner, as is often the case in normal animals (Laing et al., 2012). This variability may to some extent obscure the mediolateral topography in area 18a of BE0 rats when the data from different animals are pooled together, as in Figure 3B. To examine this possibility, we compared the changes in LIs resulting from pairs of injections placed at different locations in V1 of the same animals.

Figure 3.2B presents the results from a control rat that received restricted injections of GB and RB at different distances from the lateral border of V1. The arrangement of the injection sites (red dot = RB, green dot = GB) permits analyzing the mapping along the mediolateral axis in V1. In lateral extrastriate cortex, red and green dots represent individual cells retrogradely labeled with RB or GB, respectively. Figure 3.2B shows that when the injection site is displaced from lateral (green dot) to medial (red dot) in V1, the labeled fields in extrastriate cortex move in a mirror image fashion with respect to the border of V1, as predicted from the mapping summarized in Figure 3.2A. Thus, the cells labeled by the GB injections accumulate in medial portions of lateral extrastriate cortex, near the lateral border of V1, while the cells labeled by the RB injection accumulate more laterally in extrastriate cortex. Consistent with these observations, the LI associated with the GB injection (0.19) is smaller than that associated with the RB injection (0.45).

Results from a double injection experiment in a BE0 rat are shown in Figure 3.2C. This animal received an injection of RB close to the lateral V1 border and an injection of BDA further medially. Both injections produced labeled fields distributed over broad regions in lateral extrastriate cortex, and the overall arrangement of labeled fields was similar for both tracers. The LI calculated for the distribution of RB labeled cells (0.28) is smaller than that for the BDA labeled pattern (0.38), suggesting that the mediolateral displacement of the overall pattern of labeling in area 18a mirrors the displacement of the injection sites in V1 with respect to the lateral border of V1.

Analysis of pairs of injections in control rats (Fig. 3.3C) reveals a significant increase of the LIs ($p < 0.01$) calculated for the medial injections (M = 0.49, SD= 0.14) compared to the LIs calculated for the lateral injections (M = 0.27, SD = 0.12) ($n = 5$, paired t test). In BE0 rats (Fig. 3d), the LIs calculated for the medial injections (M = 0.50, SD = 0.15) were also significantly larger ($p < 0.01$) than the LI calculated for the lateral injections (M = 0.32, SD = 0.10) ($n = 8$, paired t test). However, comparison of the slopes of the lines connecting each pair in the data sets shows that the slopes tend to be more variable in BE0 rats than in control (slopes range from 0.49 to 1.39 in control rats and from -0.23 to 1.41 in BE0 rats). These data suggest that, in spite of abnormalities in the projection patterns (Laing et al., 2012), the basic mirror image topography of area 18a is largely preserved in BE0 rats. They also suggest that for a given separation of the injection site in V1, there is more variability in the separation of extrastriate labeled fields in BE0 than in control rats.

In the dLGN, we observed that restricted injections in striate cortex produced separate labeled fields in the dLGN (insets in Figs. 3.2B,C), confirming that the areas of effective tracer uptake associated with the cortical tracer injections did not overlap significantly. Compared with normal rats, the labeled fields in the dLGN of enucleated rats appeared larger relative to the size of the dLGN, possibly because neonatal enucleation reduces the size of both striate cortex (Laing et al., 2012) and dLGN (Warton et al., 1998; Heumann and Rabinowicz, 1993). Our observations in the dLGN are consistent with previous studies indicating that the geniculocortical pathway in enucleated rats and other animals maintains the gross topography observed in normal animals (Godement et al., 1979; Kaiserman-Abramof et al., 1980; Guillery et al., 1980; Warton and Harvey, 1988).

DISCUSSION

A recent study in adult rats neonatally enucleated at birth showed that single tracer injections into different regions of V1 produce anomalous and highly variable patterns of striate-extrastriate and callosal projections (Laing et al., 2012). This previous study noted that it was typically not possible to transform the pattern in one animal into that of another simply by displacing the fields in a consistent manner. In contrast, in normal animals the arrangement as well as the retinotopic organization of extrastriate areas is highly consistent from animal to

animal (Olavarria and Montero, 1984; Montero, 1993). Although the distributions of callosal and striate-extrastriate projections in enucleated rats have an overall resemblance to those in normal rats (Laing et al., 2012), the anomalies and variability in these projections impede the identification of specific visual areas in extrastriate cortex with certainty. It is therefore difficult to analyze the effect of enucleation on the topography of individual visual areas. In the present study, we took advantage of the fact that the representation of the naso-temporal axis of the visual field in nearly all lateral extrastriate visual areas mirrors the representation of this axis in V1 with respect to the lateral V1 border. We were interested in determining whether the basic medio-lateral topography in the striate-extrastriate projections was preserved in spite of abnormalities in the projection patterns. Rather than analyzing how injections into different mediolateral locations in V1 change the projections to specific extrastriate regions, we analyzed the displacements of the overall pattern of labeling produced by changes in injection sites. We assessed these changes using a laterality index LI, which is based on the proportion of the total labeling pattern that is contained in 4 equally spaced compartments oriented parallel to the lateral border of V1. The value of the LI increased or decreased as the labeling tended to accumulate in lateral or medial regions of area 18a, respectively.

In normal rats we found a strong correlation between the mediolateral location of the injections and the corresponding LIs, indicating that the sensitivity of this index is adequate for detecting displacements of the labeling patterns produced by even relatively small displacements of the injection sites. A positive correlation was also observed in enucleated rats, but it was weaker than in normal rats. Since this result was based on the analysis of single injections from different animals, the weaker correlation may simply reflect the variability of projection patterns across rats. To examine this possibility, we compared the separation of labeling patterns produced by injections of different tracers into different regions of V1 in the same animals. We found significant, mirror image separations of area 18a labeling patterns in both control and enucleated rats. However, our data suggest that the separation of labeling patterns in area 18a for a given separation of the V1 injections was somewhat more variable in enucleated rats than in control rats.

Thus, in enucleated rats we were able to detect mirror image changes in the distribution of overall labeling patterns in area 18a in response to changes in the mediolateral location of tracer injections into V1. However, these changes tended to be more variable in enucleated than

in control rats. Together, our analyses of single and double tracer injections suggest that neonatal bilateral enucleation weakens, but does not completely abolish the mediolateral topography in area 18a.

It is possible that the difference we found between normal and enucleated rats reflects differences in the injections placed in the two groups of animals. This is unlikely because the injections were small compared to the size of striate cortex, arranged similarly along the mediolateral axis in both groups, and similar results were observed with different combinations of tracers. Moreover, the separations between the injection sites were judged to be adequate because they produced separate labeled fields in the dLGN.

Previous studies have shown that neonatal bilateral enucleation reverses the topography of visual callosal connections. In normal rats callosal connections interlink opposite cortical loci that are retinotopically matched, but located asymmetrically with respect to the brain midline. In contrast, in neonatally enucleated rats callosal links are established between opposite cortical loci that are mirror symmetric with respect to the midline (Olavarria and Li, 1995). Moreover, the callosal topography in enucleated rats is less precise than in control rats. These results have led to the proposal that retinal input guides the retinotopically precise ingrowth of callosal axons in visual cortex, whereas the cues that determine the mirror-symmetric callosal maps in enucleates exert only a weak control on the topography of callosal fiber ingrowth (Olavarria and Li, 1995; Olavarria and Safaeian, 2006). Thus, under normal conditions, these weaker cues would be superseded by stronger influences of retinal origin, leading to a non-symmetric, retinotopically matched callosal map.

Our present results suggest that hierarchical topographic cues may also regulate the organization of striate-extrastriate connections, but in this case the maps that develop in both normal and enucleated rats show similar mediolateral topography, rather than opposite topography as is the case with callosal maps. Although mediolateral topography develops in area 18a under either retinally driven (in normally-eyed rats) cues or cues of central origin (in enucleated rats), it is important to note that retinal cues appear to be critical for the development of connections patterns that are highly consistent from animal to animal (i.e. similar from animal to animal, even when injections are placed in different regions of V1). Thus retinal input may not only specify the normal internal topography of extrastriate visual areas but may also have an important role in the parcellation of extrastriate visual areas in normal animals.

How does retinal input influence the development of striate-extrastriate maps? Projections from the dLGN are primarily confined to striate cortex (Ribak and Peters, 1975; Schober and Winkelmann, 1977; Olavarria, 1979), so retinal input from the dLGN could reach area 18a via the projections from V1. However, although enucleation reduces the size of both the dLGN and V1 (Laing et al., 2012; Warton et al., 1988; Heumann and Rabinowicz, 1980; Karlen and Krubitzer, 2009), it does not change the basic topography of the dLGN projection to V1 (Godement et al., 2979; Kaiserman-Abramof et al., 1980; Warton et al., 1980). Retinal input can also reach area 18a via the lateroposterior nucleus of the thalamus (LP) (Olavarria, 1979; Hughes, 1977), which receives direct projection from the superior colliculus (Jones, 1985). In normal animals, these two pathways (from LGN vs. LP) could mediate synchronous neural activity to establish normal topography through Hebbian-like mechanisms. Enucleation could interfere with the layout of topographic cues in area 18a by disrupting this alternative pathway. Indeed, Negyessy et al., 2000 reported that cortical projections from LP were abnormal in neonatally enucleated rats. Alternatively, retinal input may regulate the normal arrangement and topography of extrastriate visual areas by specifying the normal distribution of cortical guidance labels through activity independent cues. For instance, interactions between gradients of EphA/ephrin-A could guide the formation of topographically organized projections from V1 to each extrastriate visual area in a manner similar as they guide the development of the thalamocortical pathway (Cang et al., 2005). Central cues operating in the absence of retinal input could specify reduced or distorted gradients leading to the development of anomalous and variable topographic projections between V1 and area 18a. Detecting these gradients and possible changes induced by neonatal enucleation or other manipulations will be specially challenging given the small size of the extrastriate visual areas. Finally, it should be noted that whatever are the mechanisms by which retinal input guides cortical topography, they must exert their effect by postnatal day 6 (P6) because enucleation at P6 or later no longer prevents the development of normal patterns of striate-extrastriate connections (Laing et al., 2012).

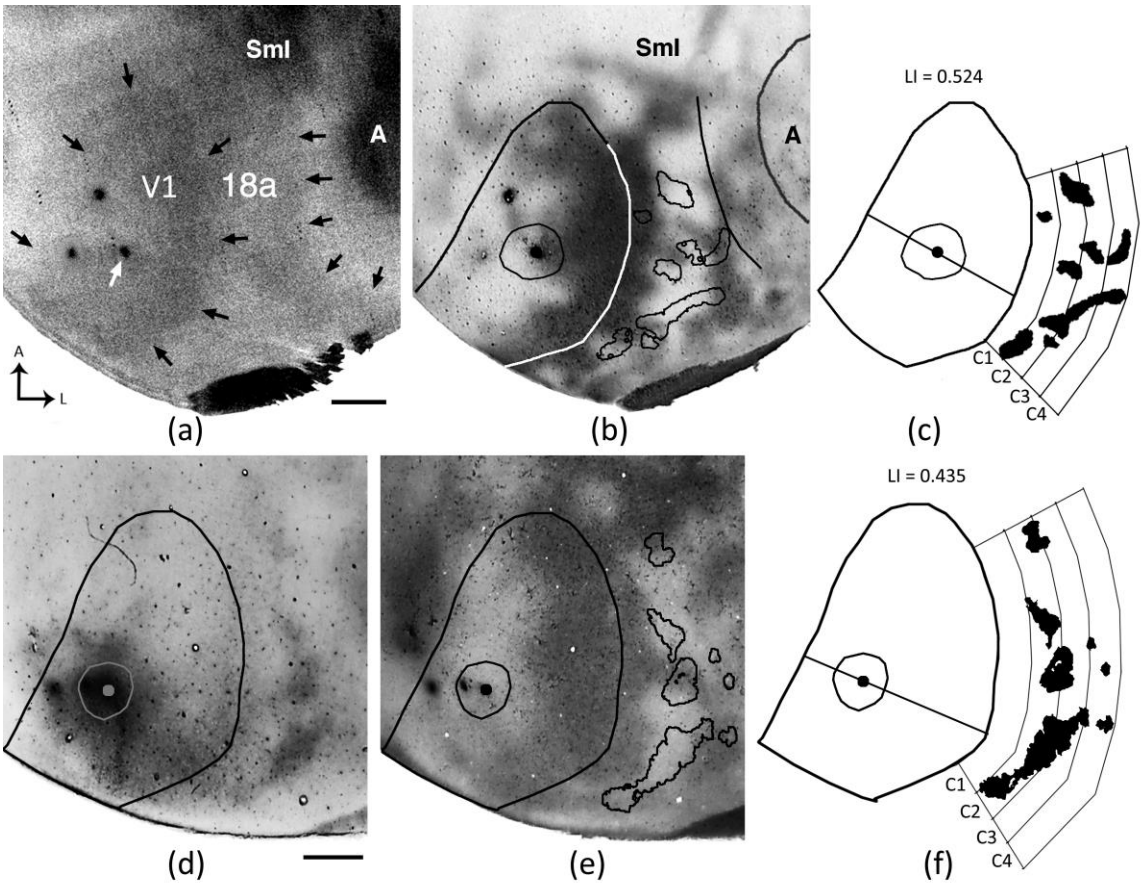

Figure 3.1. Correlating the patterns of striate–extrastriate projections with the patterns of myelination and visual callosal connections, and procedure for calculating LI. (A) Myelin pattern from a rat (BEM-2) enucleated at birth. Black arrows indicate borders of V1 and area 18a. A, auditory cortex; Sml, somatosensory cortex. White arrow indicates BDA injection site. Neighboring dark spots correspond to injections of other tracers. (B) Callosal pattern revealed following multiple injections of HRP in the contralateral hemisphere in the same enucleated rat. Dark areas correspond to dense accumulations of retrogradely labeled somas and anterogradely labeled axons. The profiles of V1, 18a, and auditory cortex were drawn from the myelin pattern in A. Regions outlined in black represent BDA-labeled projection fields drawn from a section processed for BDA. Black dot indicates the location of the BDA injection and the circular outline estimates the size of tracer diffusion (see Materials and Methods). (D) Pattern of BDA-labeled projections in another enucleated rat (case M6e4). Grey dot and grey outline indicate the injection and diffusion of BDA, respectively. Border of V1, outlined in black was determined

from the callosal pattern in E from the same case. (E) Pattern of HRP-labeled callosal connections (case M6e4). Black lines in lateral extrastriate cortex outline the BDA-labeled projections shown in D. (C, F) Diagrams illustrating the compartments (C1-C4) in area 18a used in LI calculations. The LI for each case is indicated. Line passing through injection site was used to calculate the distance from the injection site to the lateral border of V1. Inset in A indicates orientation, A: anterior, L: lateral. Scale bars = 1.0 mm.

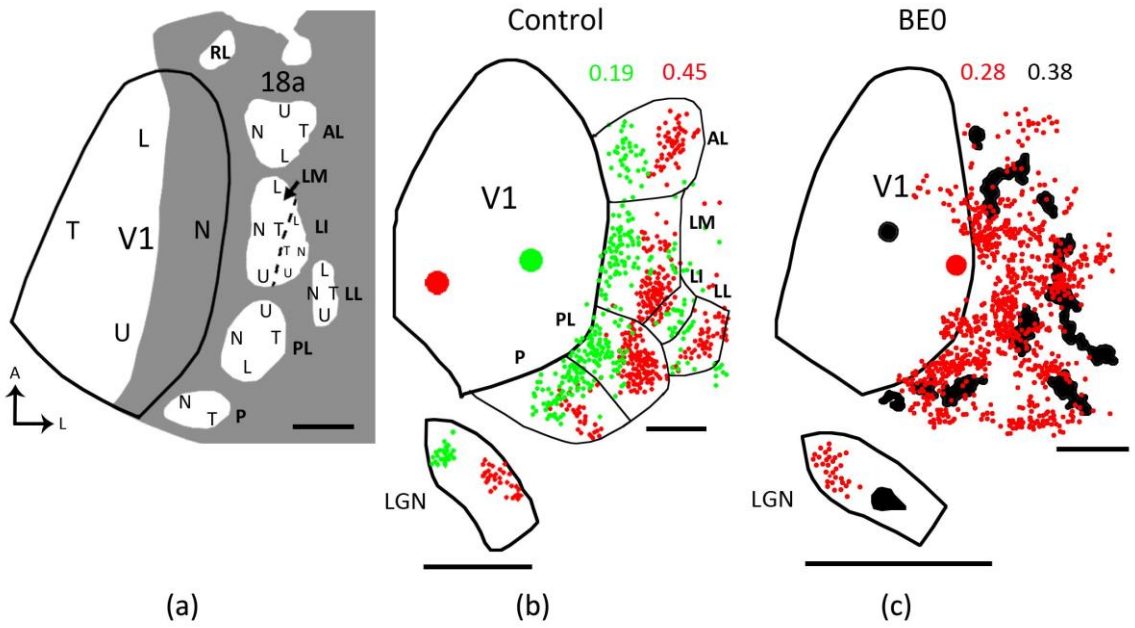

Figure 3.2. Topography of striate-extrastriate connections in normal and enucleated rats. (A) Diagram of the distribution of callosal connections and of visual areas in lateral striate cortex of normal rats. The border of V1 is outlined in black; callosal pattern is indicated in grey, while acallosal areas are indicated in white. The diagram summarizes previous studies (see Refs. in text) of the overall topographic organization of V1 and of some visual areas in lateral extrastriate cortex (area 18a). Cortical regions representing upper, lower, nasal and temporal portions of the visual field are indicated by U, L, N and T, respectively. RL: rostrolateral, AL: anterolateral, LM: lateromedial, LI: laterointermediate, LL: laterolateral, PL: posterolateral, P: posterior. Modified from [45]. (B) Data from a normal rat (case C21) that received injections of GB (green dot) and RB (red dot) in V1. Cells labeled by RB or GB are indicated by small red or green dots, respectively. Approximate location of the border of visual areas in area 18a is indicated by thin black lines. (C) Data from an enucleated rats (case M4e9) that received injections of RB (red dot) and BDA (black dot) in V1. BDA-labeled fields are indicated in black. The LI for each tracer injection in B and C are indicated. Insets in B and C show labeled fields in the dLGN. Callosal connections and striate projection fields in medial extrastriate cortex are not represented. Inset in A indicates orientation, A: anterior, L: lateral. Scale bars = 1.0 mm.

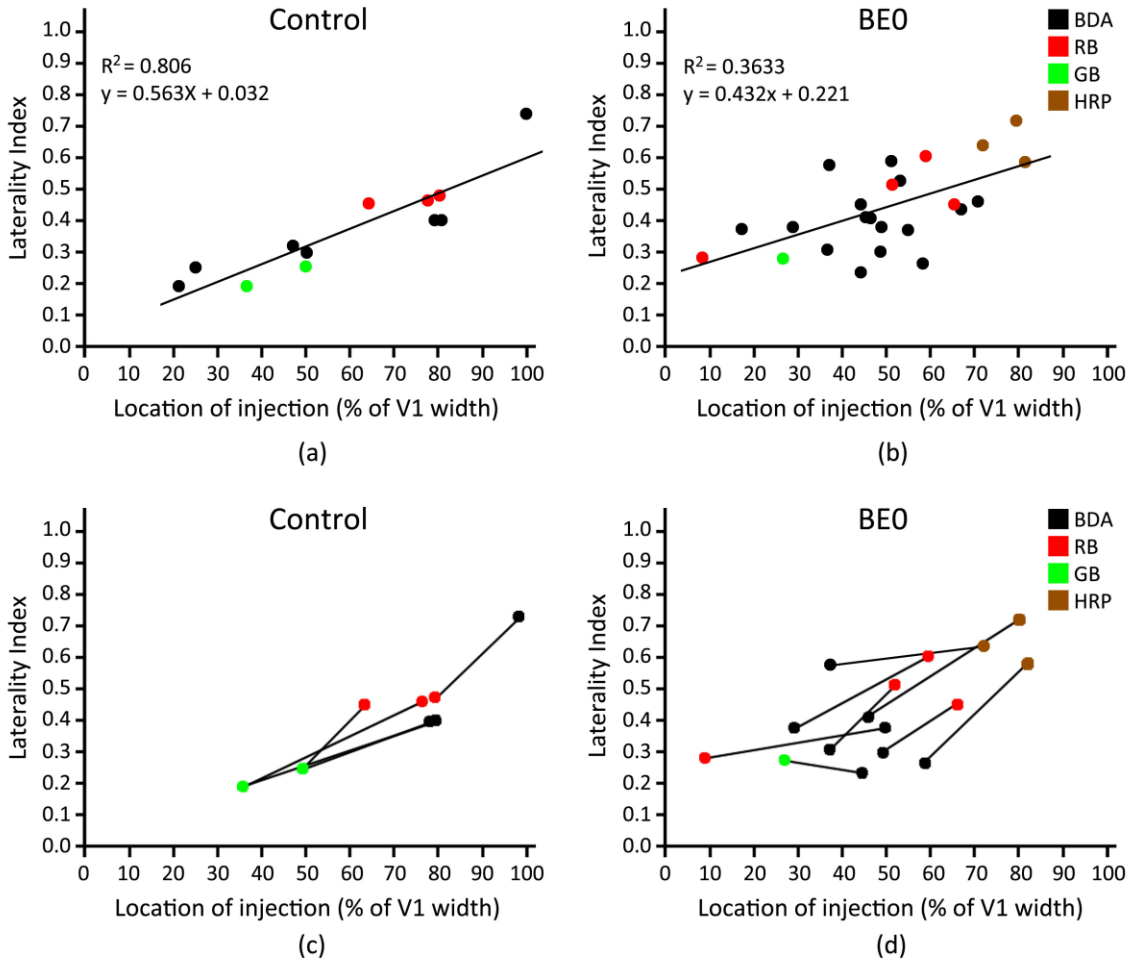

Figure 3.3. Laterality indices for normal and enucleated rats. (A, B) Scatterplots correlating the LI values calculated for single injections with the distance of the injection sites to the lateral border of V1, expressed as a percentage of the width of V1 (see Fig. 1 C, F). Black, red, green and brown dots represent injections of BDA, RB, GB and HRP, respectively. (B, C) Comparing the separation of labeling patterns produced by injections of different tracers into different regions of V1 in the same animal. Black lines connect data from the pair of injections in the same animal.

CONCLUSIONS

Chapter 1 challenged the notion that rodents lack columnar organization in the visual cortex, and specifically, ODCs. Here, we used transneuronal tracing, in situ hybridization and electrophysiology to demonstrate that Long Evans rats have anatomically and functionally segregated ODCs in V1. In addition, we found that V1 can be divided into 3 sub regions including a medial, monocular segment (MS), a central, binocular segment (CS), and a lateral, monocular segment (LS). Finally, we demonstrated that these rats have patchy callosal connections, and that, similar to a relationship that was shown previously in the cat (Olavarria, 2001), that callosal patches in the rat overlap with ipsilateral ODCs in the CS and with contralaterally dominated territories in the LS. Our data also provided new insight into connectivity as well as the role of the corpus callosum in V1 and why the LS is largely monocular in the Long Evans rat (see Fig. 1.12). Overall, these results demonstrate that cortical modular architecture is more conserved among rodents, carnivores and primates than previously thought.

If ODCs do serve any functional role in visual system processing, it has yet to be found, as is the case with the cortical column (reviewed by Horton and Adams, 2005). However, ODCs are still important in that they have provided scientists with a model to study activity- and experience-dependent cortical plasticity and development. While ODCs may not be involved in stereopsis, questions still remain about their plasticity as well as formation during early life. For example, what mechanisms mediate the clustering of eye-specific territories? There is still controversy as to whether ODCs develop independent of activity or are a result of competition-based mechanisms. Optical imaging techniques have shown a strong bias toward the contralateral eye during early development, suggesting that they may not develop initially through competition-based mechanisms (reviewed by Crowley and Katz, 2002). In 1986, Stryker and Harris used TTX to block retinal activity of 2-week-old kittens and found no ODCs later in life, though it was later found that cats already have ODCs by 2 weeks (Crair et al., 2001), suggesting that they may have only affected ODC plasticity. Crowley and Katz (1999) removed the eyes of ferret kits and found that ODCs develop in the absence of retinal input. In contrast, data from the rat have shown that ODCs fail to develop by 2 weeks of age after monocular enucleation performed at 7 days of age, but develop normally when TTX is applied monocularly

during the 2nd week of life (Laing et al., unpublished data). If this form of development is activity-independent, then what molecular mechanisms are necessary? As many questions still remain about the nature of ODCs, much work still needs to be performed on this system.

In Chapter 2, we investigated the role that retinal input plays in the development of interhemispheric callosal connections and ipsilateral striate-extrastriate connections. We focused on 7 different regions which have previously been described in area 18a. We found that after bilateral enucleation performed before P6, the patterns of striate-extrastriate connections and interhemispheric callosal connections were abnormal. While striate-extrastriate projections consisted of multiple well-defined fields that were largely confined to acallosal regions as they are in normal rats, these projections were highly irregular and variable, as were the acallosal regions observed in extrastriate cortex. Furthermore, we also found that area 17, but not area 18, was smaller in enucleates compared to controls, resulting in an increase in the divergence of striate projections.

In Chapter 3, we focused our investigation on the role that the eyes play in the topography of striate-extrastriate connections. Using multiple, single injections of different tracers placed at different locations in striate cortex, we were able to map out the patterns of projections to extrastriate cortex. In lateral extrastriate cortex of normal rats, the representation of the naso-temporal axis of retinal loci mirrors the representation of this axis in V1. We found that the correlation between the distance from injection sites to the lateral border of V1 and the distance of the labeling patterns in area 18a was strong in controls and much weaker in neonatally enucleated rats. Furthermore, data from pairs of injections in the same animal revealed that the separation of area 18a projection fields for a given separation of injection sites was more variable in enucleated than in control rats.

Our results demonstrated that the eyes play a role in the development of mediolateral topography as well as the parcellation of extrastriate areas during neonatal life. However, the eyes alone are not necessary for this development, as some basic topography was preserved in enucleates. Moreover, multiple extrastriate areas were still identifiable and largely confined to acallosal regions in these animals. Taken together, these findings suggest that molecular cues may also be involved in specifying mediolateral topography and parcellation in extrastriate cortex. Additional studies examining the interactions between chemical gradients such as EphA/ephrin-As (Cang et al., 2005) will be necessary to better address these questions.

REFERENCES

Adams AD, Forrester JM. 1968. The projection of the rat's visual field on the cerebral cortex. Q J Exp Physiol Cogn Med Sci. 53:327-336.Belford GR, Killackey HP. 1980. The sensitive period in the development of the trigeminal system of the neonatal rat. J Comp Neurol 193:335-350.

Adams DL, Horton JC. 2009. Ocular dominance columns: Enigmas and challenges. Neuroscientist 15: 62-77.

Alekseenko SV, Toporova SN, Makarov FN. 2005. Neuronal connection of the cortex and reconstruction of the visual space. Neurosci Behav Physiol. 35:435–442.

Anderson PA, Olavarria J, Van Sluyters RC. 1988. The overall pattern of ocular dominance bands in cat visual cortex. J Neurosci. 8:2183-2200.

Ankaoua D, Malach R. 1993. Evidence for plasticity of intrinsic horizontal connections in area 17 of the rat. Isr J Med Sci 29:555-569.

Antonini A, Fagiolini M, Stryker MP. 1999. Anatomical correlates of functional plasticity in mouse visual cortex. J Neurosci. 19:4388–4406.

Bock AS, Kroenke CD, Taber EN, Olavarria JF. 2012. Retinal input influences the size and cortico-cortical connectivity of visual cortex during postnatal development in the ferret. J Comp Neurol 520:914–932.

Bock AS, Olavarria JF. 2011. Neonatal enucleation during a critical period reduces the precision of cortico-cortical projections in visual cortex. Neurosci Lett 501:152-156.

Bosking WH, Kretz R, Pucak ML, Fitzpatrick D. 2000. Functional specificity of callosal connections in tree shrew striate cortex. J Neurosci. 20:2346-2359.

Berlucchi G, Rizzolatti G. 1968. Binocularly driven neurons in visual cortex of split-chiasm cats. Science. 159:308-310.

Bosking WH, Kretz R, Pucak ML, Fitzpatrick D. 2000. Functional specificity of callosal connections in tree shrew striate cortex. J Neurosci. 20:2346-2359.

Bravo H, Inzunza O. 1994. Effect of pre- and postnatal retinal deprivation on the striate-peristriate cortical connections in the rat. Biol Res 27:73-77.

Burkhalter A. 1993. Development of forward and feedback connections between areas V1 and V2 of human visual cortex. Cereb Cortex 3:476-487.

Caleo M, Lodovichi C, Pizzorusso T, Maffei L. 1999. Expression of the transcription factor Zif268 in the visual cortex of monocularly deprived rats: effects of nerve growth factor. Neurosci 91:1017-1026.

Cang J, Kaneko M, Yamada J, Woods G, Stryker MP, Feldheim DA. 2005. Ephrin-As guide the formation of functional maps in the visual cortex. Neuron 48:577-589.

Cang J, Wang L, Stryker MP, Feldheim DA. 2008. Roles of ephrin-As and structured activity in the development of functional maps in the superior colliculus. J Neurosci 28:11015-23.

Carić D, Price DJ. 1999. Evidence that the lateral geniculate nucleus regulates the normal development of visual cortico-cortical projections in the cat. Exp Neurol 156:353-362.

Caviness VS. 1975. Architectonic map of neocortex of the normal mouse. J Comp Neurol 164:247-263.

Cerri C, Restani L, Caleo M. 2010. Callosal contribution to ocular dominance in rat primary visual cortex. Eur J Neurosci 32:1163-1169.

Chaudhuri A, Matsubara JA, Cynader MS. 1995. Neuronal activity in primate visual cortex assessed by immunostaining for the transcription factor Zif268. Vis Neurosci 12:35-50.

Chaudhuri A, Nissanov J, Larocque S, Rioux L. 1997. Dual activity maps in primate visual cortex produced by different temporal patterns of Zif268 mRNA and protein expression. Proc Natl Acad Sci USA. 94:2671-2675.

Coogan TA, Burkhalter A. 1993. Hierarchical organization of areas in rat visual cortex. J Neurosci 13:3749-3772.

Crowley JC, Katz LC. 2000. Early development of ocular dominance columns. Science 290:1321-1324.

Cusick DG, Lund RD. 1981. The distribution of the callosal projections to the occipital visual cortex in rats and mice. Brain Res 214:239-259.

Cusick CG, Lund RD. 1982. Modification of visual callosal projections in rats. J Comp Neurol 212:385-398.

Dehay C, Giroud P, Berland M, Killackey H, Kennedy H. 1996. Contribution of thalamic input to the specification of cytoarchitectonic cortical fields in the primate: effects of bilateral enucleation in the fetal monkey on the boundaries, dimensions, and gyrification of striate and extrastriate cortex. J Comp Neurol 367:70-89.

Dehay C, Horsburgh G, Berland M, Killackey H, Kennedy H. 1989. Maturation and connectivity of the visual cortex in monkey is altered by prenatal removal of retinal input. Nature 337:265-267.

Diao YC, Wang YK, Pu ML. 1983. Binocular responses of cortical cells and the callosal projection in the albino rat. Exp Brain Res 49:410-418.

Dong H, Wang Q, Valkova K, Gonchar Y, Burkhalter A. 2004. Experience-dependent development of feedforward and feedback circuits between lower and higher areas of mouse visual cortex. Vision Res 44:3389-3400.

Dräger UC. 1974. Autoradiography of tritiated proline and fucose transported transneuronally from the eye to the visual cortex in pigmented and albino mice. Brain Res 82:284-292.

Dräger UC. 1975. Receptive fields of single cells and topography in mouse visual cortex. J Comp Neurol 160:269–290.

Dufour A, Seibt J, Passante L, Depaepe, Ciossek VT, Frisen J, Kullander K, Flanagan JG, Polleux F, Vanderhaeghen P. 2003. Area specificity and topography of thalamocortical projections are controlled by ephrin/Eph genes. Neuron 39: 453-465.

Erzurumlu RS, Killackey HP, 1982. Critical and sensitive periods in neurobiology. Curr Top Dev Biol 17:207-40.

Espinoza SG, Thomas HC. 1983. Retinotopic organization of striate and extrastriate visual cortex in the hooded rat. Brain Res 272:137-144.

Fagiolini M, Pizzorusso T, Berardi N, Domenici L, Maffei L.1994. Functional postnatal development of the rat primary visual cortex and the role of visual experience: dark rearing and monocular deprivation. Vision Res 34: 709–720.

Fish SE, Rhoades RW, Bennett-Clarke CA, Figley B, Mooney RD. 1991. Organization, Development and Enucleation-induced Alterations in the Visual Callosal Projection of the Hamster: Single Axon Tracing with Phaseolus vulgaris leucoagglutinin and Di-I. Eur J Neurosci 3:1255-1270.

Flanagan JG. 2006. Neural map specification by gradients. Curr Opin Neurobio. 16:59–66.

Gallyas F. 1979. Silver staining of myelin by means of physical development. Neurol Res 1:203-209.

Gerfen CR, O'Leary DD, Cowan WM. 1982. A note on the transneuronal transport of wheat germ agglutinin-conjugated horseradish peroxidase in the avian and rodent visual systems. Exp Brain Res 48:443-448.

Girman SV, Sauve Y, Lund RD. 1999. Receptive field properties of single neurons in rat primary visual cortex. J Neurophysiol. 82:301–311.Godement P, Saillour P, Imbert M. 1979. Thalamic afferents to the visual cortex in congenitally anophthalmic mice. Neurosci Lett 13:271-278.

Gordon JA, Stryker MP. 1996. Experience-dependent plasticity of binocular responses in the primary visual cortex of the mouse. J Neurosci 16:3274-3286.

Guillery RW, Ombrellaro M, LaMantia AL. 1985. The organization of the lateral geniculate nucleus and of the geniculocortical pathway that develops without retinal afferents. Brain Res 352:221-233.

Hata Y, Stryker MP. 1994. Control of thalamocortical afferent rearrangement by postsynaptic activity in developing visual cortex. Science 265:1732-1735.

Heumann D, Rabinowicz T. 1980. Postnatal development of the dorsal lateral geniculate nucleus in the normal and enucleated albino mouse. Experimental Brain Research 38:75–85.

Hirokawa J, Watakabe A, Ohsawa S, Yamamori T. 2008. Analysis of area-specific expression patterns of RORbeta, ER81 and Nurr1 mRNAs in rat neocortex by double in situ hybridization and cortical box method. PLoS One 3:e3266.

Horton JC, Adams DL. 2005. The cortical column: a structure without a function. Phil Trans R Soc B 360:837–862.

Horton JC, Hocking DR. 1996. Anatomical demonstration of ocular dominance columns in striate cortex of the squirrel monkey. J Neurosci 16:5510–5522.

Horton JC, Hocking DR, Adams DL. 2000. Rapid identification of ocular dominance columns in macaques using cytochrome oxidase, Zif268, and dark-field microscopy. Vis Neurosci 17:495-508.

Hubel DH, Wiesel TN. 1962. Receptive fields, binocular interaction and functional architecture in the cat’s visual cortex. J Comp Physiol 160:106-154.

Hughes HC. 1977. Anatomical and neurobehavioral investigations concerning the thalamocortical organization of the rat’s visual system. J Comp Neuro 175:311-336.

Ichinohe N, Fujiyama F, Kaneko T, Rockland KS. 2003. Honeycomb-like mosaic at the border of layers 1 and 2 in the cerebral cortex. J Neurosci 23:1372-1382.

Innocenti GM. 1991. The development of projections from cerebral cortex. In, pp 65-114. Progr Sens Physiol.

Innocenti GM, Frost DO. 1980. The postnatal development of visual callosal connections in the absence of visual experience or of the eyes. Exp Brain Res 39:365-375.

Innocenti GM, Manger PR, Masiello I, Colin I, Tettoni L. 2002. Architecture and callosal connections of visual areas 17, 18, 19 and 21 in the ferret (*Mustela putorius*). Cereb Cortex 12:411-422.

Itaya SK. 1988. Transneuronal transport of WGA-HRP in immature rat visual pathways. Brain Res 466:83-88.

Itaya SK, Van Hoesen GW. 1982. WGA-HRP as a transneuronal marker in the visual pathways of monkey and rat. Brain Res 236:199-204.

Jones EG. 1985. The Thalamus. Plenum Press, New York.

Kaiserman-Abramof IR, Graybiel AM, Nauta WJ. 1980. The thalamic projection to cortical area 17 in a congenitally anophthalmic mouse strain. Neurosci 5:41-52.

Kageyama GH, Gallivan ME, Gallardo KA, Robertson RT. 1990. Relationships between patterns of acetylcholinesterase activity and geniculocortical terminal fields in developing and mature rat visual cortex. Dev Brain Res 53:139-144.

Kalatsky VA, Stryker MP. 2003. New paradigm for optical imaging: temporally encoded maps of intrinsic signal. Neuron 38:529-545.

Karlen SJ, Kahan DM, Krubitzer L. 2006. Early blindness results in abnormal and thalamocortical connections. Neurosci 142:843-858.

Karlen SJ, Krubitzer L. 2009. Effects of bilateral enucleation on the size of visual and non-visual areas of the brain. Cereb Cortex 19:1360-1371.

Katz LC, Burkhalter A, Dreyer WJ. 1984. Fluorescent latex microspheres as a retrograde neuronal marker for *in vivo* and *in vitro* studies of visual cortex. Nature 310:498-500.

Katz LC, Shatz CJ. 1996. Synaptic activity and the construction of cortical circuits. Science 274:1133–1138.

Kingsbury MA, Lettman NA, Finlay BL. 2002. Reduction of early thalamic input alters adult corticocortical connectivity. Brain Res Dev Brain Res 138:35-43.

Krieg WJS. 1946. Connections of the cerebral cortex I. The albino rat. A. Topography of the cortical areas. J Comp Neurol 84:221-275.

Laing RJ, Bock AS, Lasiene J, Olavarria JF. 2012. Role of retinal input on the development of striate-extrastriate patterns of connections in the rat. J Comp Neurol 520: 3256-3276.

Lepore F, Guillemot JP. 1982. Visual receptive field properties of cells innervated through the corpus callosum in the cat. Exp Brain Res 46:413-424.

LeVay S, Gilbert CD. 1976. Laminar pattern of geniculocortical projection in the cat. Brain Res 113:1-19.

Lewis JW, Olavarria JF. 1995. Two rules for callosal connectivity in striate cortex of the rat. J Comp Neurol 361:119-137.

Lund RD, Lund JS, Wise RP. 1974. The organization of the retinal projection to the dorsal lateral geniculate nucleus in pigmented and albino rats. J Comp Neurol 158:383-404.

Malach R. 1989. Patterns of connections in rat visual cortex. J Neurosci 9:3741-3752.

Markstahler U, Bach M, Spatz WB. 1998. Transient molecular visualization of ocular dominance columns (ODCs) in normal adult marmosets despite the desegregated termination of the retino-geniculo-cortical pathways. J Comp Neurol 393:118-134.

Maunsell JH. 1992. Functional visual streams. Curr Opin Neurobiol 2:506-510.

McLaughlin T, Torborg CL, Feller MB. 2003. Retinotopic map refinement requires spontaneous retinal waves during a brief period of development. Neuron 40:1147–1160.

Merlin S, Horng S, Marotte LR, Sur M, Sawatari A, Leamey CA. 2012. Deletion of Ten-m3 induces the formation of eye dominance domains in mouse visual cortex. Cereb Cortex 23:763-774.

Mesulam MM. 1978. Tetramethyl benzidine for horseradish peroxidase neurohistochemistry: A non-carcinogenic blue reaction product with superior sensitivity for visualizing neural afferents and efferents. J Histochem Cytochem 26:106-117.

Metín C, Godement P, Imbert M. 1988. The primary visual cortex in the mouse: receptive field properties and functional organization. Exp Brain Res 69:594-612.

Minciacchi D, Antonini A. 1984. Binocularity in the visual cortex of the adult cat does not depend on the integrity of the corpus callosum. Behav Brain Res 13:183-192.

Miyashita-Lin EM, Hevner R, Wassarman KM, Martinez S, Rubenstein JLR. 1999. Early neocortical regionalization in the absence of thalamic innervation. Science 285: 5429:906–909.

Montero VM. 1973. Evoked responses in the rat's visual cortex to contralateral, ipsilateral, and restricted photic stimulation. Brain res 53:192-196.

Montero VM. 1993. Retinotopy of cortical connections between the striate cortex and extrastriate visual areas in the rat. Exp Brain Res 94:1-15.

Montero VM, Bravo H, Fernández V. 1973a. Striate-peristriate cortico-cortical connections in the albino and gray rat. Brain Res 53:202-207.

Montero VM, Brugge JF, Beitel RE. 1968. Relation of the visual field to the lateral geniculate body of the albino rat. J Neurophysiol 31:221-236.

Montero VM, Rojas A, Torrealba F. 1973b. Retinotopic organization of striate and peristriate visual cortex in the albino rat. Brain Res 53:197-201.

Morgan JE, Henderson Z, Thompson ID. 1987. Retinal decussation patterns in pigmented and albino ferrets. Neurosci 20:519-535.

Mountcastle VB. 1957. Modality and topographic properties of cat's somatic sensory cortex. J Neurophysiol 20:408–434.

Mrsic-Flögel TD, Hofer SB, Ohki K, Reid RC, Bonhöffer T, Hübener M. 2007. Homeostatic regulation of eye-specific responses in visual cortex during ocular dominance plasticity. Neuron 54:961-972.

Negyessy L, Gal V, Farkas T, Toldi J. 2000. Cross-modal plasticity of the corticothalamic circuits in rats enucleated on the first postnatal day. Euro J Neurosci 12:1654–1668.

O'Brien BJ, Olavarria JF. 1995. Anomalous patterns of callosal connections develop in visual cortex of monocularly enucleated hamsters. Biol Res 28:211-218.

Ohki K, Chung S, Ch'ng YH, Kara P, Reid RC. 2005. Functional imaging with cellular resolution reveals precise micro-architecture in visual cortex. Nature 433:597-603.

Ohki K, Reid RC. 2007. Specificity and randomness in the visual cortex. Curr Opin Neurobiol 17:401-407.

Olavarria J. 1979. A horseradish peroxidase study of the projections from the latero-posterior nucleus to three lateral peristriate areas in the rat. Brain Res 173:137-141.

Olavarria JF. 1996. Non-mirror-symmetric patterns of callosal linkages in areas 17 and 18 in cat visual cortex. J Comp Neurol 366: 643-655.

Olavarria JF. 2001. Callosal connections correlate preferentially with ipsilateral domains in cat areas 17 and 18, and with contralateral domains in the 17/18 transition zone. J Comp Neurol 433:441-457.

Olavarria JF. 2002. Influence of topography and ocular dominance on the functional organization of callosal connections in cat striate cortex. In: Payne B, Peters A, editors. The cat primary visual cortex. New York (NY): Academic Press. p. 259-294.

Olavarria J, Bravo H, Ruiz G. 1988. The pattern of callosal connections in posterior neocortex of congenitally anophthalmic rats. Anat Embryol (Berl) 178:155-159.

Olavarria JF, Hiroi R. 2003. Retinal influences specify cortico-cortical maps by postnatal day six in rats and mice. J Comp Neurol 459:156-172.

Olavarria JF, Li CP. 1995. Effects of neonatal enucleation on the organization of callosal linkages in striate cortex of the rat. J Comp Neurol 361:138-151.

Olavarria J, Malach R, Van Sluyters RC. 1987. Development of visual callosal connections in neonatally enucleated rats. J Comp Neurol 260:321-348.

Olavarria J, Montero VM. 1981. Reciprocal connections between the striate cortex and extrastriate cortical visual areas in the rat. Brain Res 217:358-363.

Olavarria J, Montero VM. 1984. Relation of callosal and striate-extrastriate cortical connections in the rat: morphological definition of extrastriate visual areas. Exp Brain Res 54:240-252.

Olavarria J, Montero VM. 1989. Organization of visual cortex in the mouse revealed by correlating callosal and striate-extrastriate connections. Vis Neurosci 3:59-69.

Olavarria JF, Safaeian P. 2006. Development of callosal topography in visual cortex of normal and enucleated rats. J Comp Neurol 496:495-512.

Olavarria J, Van Sluyters RC. 1984. Callosal connections of the posterior neocortex in normal-eyed, congenitally anophthalmic, and neonatally enucleated mice. J Comp Neurol 230:249-268.

Olavarria J, Van Sluyters RC. 1985. Organization and postnatal development of callosal connections in the visual cortex of the rat. J Comp Neurol 239:1-26.

Olavarria JF, Van Sluyters RC. 1995. Overall pattern of callosal connections in visual cortex of normal and enucleated cats. J Comp Neurol 363:161-176.

Pettigrew JD, Ramachandran VS, Bravo H. 1984. Some neural connections subserving binocular vision in ungulates. Brain Behav Evol 24:65-93.

Redies C, Diksic M, Riml H. 1990. Functional organization in the ferret visual cortex: a double-label 2-deoxyglucose study. J Neurosci 10:2791-2803.

Reese BE, Cowey A. 1987. The crossed projection from the temporal retina to the dorsal lateral geniculate nucleus in the rat. Neurosci 20:951-959.

Reiner A, Veenman CL, Medina L, Jiao Y, Del Mar N, Honig MG. 2000. Pathway tracing using biotinylated dextran amines. J Neurosci Meth 103:23-37.

Restani L, Cerri C, Pietrasanta M, Gianfranceschi L, Maffei L, Caleo M. 2009. Functional masking of deprived eye responses by callosal input during ocular dominance plasticity. Neuron 64:707-718.

Rhoades RW, Dellacroce DD. 1980. Neonatal enucleation induces an asymmetric pattern of visual callosal connections in hamsters. Brain Res 202:189-195.

Richter CP, Warner CL. 1974. Comparison of Weigert stained sections with unfixed, unstained sections for study of myelin sheaths. Proc Natl Acad Sci USA 71:598-601.

Ribak CE, Peters A. 1975. An autoradiographic study of the projection from the lateral geniculate body of the rat. Brain Res 92:341-368.

Richter CP, Warner CL. 1974. Comparison of Weigert stained sections with unfixed, unstained sections for study of myelin sheaths. Proc Natl Acad Sci U S A 71:598-601.

Rochefort NL, Buzas P, Kisvarday ZF, Eysel UT, Milleret C. 2007. Layout of transcallosal activity in cat visual cortex revealed by optical imaging. Neuroimage 36:804-821.

Ruthazer ES, Akerman CJ, Cline HT. 2003. Control of axon dynamics by correlated activity *in vivo*. Science 301:66-70.

Ruthazer ES, Bachleda AR, Olavarria JF. 2010. Role of interstitial branching in the development of visual corticocortical connections: A time-lapse and fixed-tissue analysis. J Comp Neurol 518:4963-4979.

Ruthazer ES, Baker GE, Stryker MP. 1999. Development and organization of ocular dominance bands in primary visual cortex of the sable ferret. J Comp Neurol 407:151-165.

Ruthazer ES, Basker GE, Stryker MP. 1999. Development and organization of ocular dominance bands in primary visual cortex of the sable ferret. J Comp Neurol 407:151-165.

Schlingensiepen KH, Lüno K, Brysch W. 1991. High basal expression of the zif/268 immediate early gene in cortical layers IV and VI, in CA1 and in the corpus striatum--an in situ hybridization study. Neurosci Lett 122:67-70.

Schober W, Winkelmann, 1977. Die geniculo-kortikale Projektion bei Albinoratten. J Hirnforsch 18:1-20.

Shatz CJ, Lindstrom S, Wiesel TN. 1977. The distribution of afferents representing the right and left eyes in the cat's visual cortex. Brain Res 131:103-116.

Sheng M, Greenberg ME. 1990. The regulation and function of c-Fos and other immediate early genes in the nervous system. Neuron 4:477-485.

Silveira LC, Heywood CA, Cowey A. 1989. Direct and transcallosal contribution to the cortical visual evoked response in rats. Behav Brain Res 31:291-294.

Simon DK, O'Leary DD. 1992. Development of topographic order in the mammalian retinocollicular projection. J Neurosci 12:1212-1232.

Sugiyama S, Di Nardo AA, Aizawa S, Matsuo I, Volvovitch M, Prochiantz A, Hensch TK. 2008. Experience-dependent transfer of Otx2 homeoprotein into the visual cortex activates postnatal plasticity. Cell 134:508-20.

Takahata T, Higo N, Kaas JH, Yamamori T. 2009. Expression of immediate-early genes reveals functional compartments within ocular dominance columns after brief monocular inactivation. Proc Natl Acad Sci USA 106:12151-12155.

Takahata T, Miyashita M, Tanaka S, Kaas JH. 2014. Identification of ocular dominance domains in New World owl monkeys by immediate-early gene expression. Proc Natl Acad Sci USA 111:4297-4202.

Thomas HC, Espinoza SG. 1987. Relationships between interhemispheric cortical connections and visual areas in hooded rats. Brain Res 417:214-224.

Thurlow GA, Cooper RM. 1988. Metabolic activity in striate and extrastriate cortex in the hooded rat: contralateral and ipsilateral eye input. J Comp Neurol 274:595-607.

Tootell RB, Hamilton SL, Silverman MS, Switkes E. 1988. Functional anatomy of macaque striate cortex. I. Ocular dominance, binocular interactions, and baseline conditions. J Neurosci 8:1500-1530.

Trojanowski JQ, Gonatas J, Gonatas NK. 1981. A light and electron microscopic study of the intraneural transport of horseradish peroxidase and wheat germ agglutinin-peroxidase conjugates in the rat visual system. J Neurocytol 10:441-456.

Van Brussel L, Gerits A, Arckens L. 2009. Identification and localization of functional subdivisions in the visual cortex of the adult mouse. J Comp Neurol 514:107-116.

Van Essen DC, Maunsell JHR. 1983. Hierarchical organization and functional streams in the visual cortex. Trends Neurosci 6:370-375.

Van Hooser SD. 2007. Similarity and diversity in visual cortex: is there a unifying theory of cortical computation? Neuroscientist 13:639-656.

Van Hooser SD, Heimel JA, Chung S, Nelson SB, Toth LJ. 2005. Orientation selectivity without orientation maps in visual cortex of a highly visual mammal. J Neurosci 25:19-28.

Van Hooser SD, Heimel JA, Chung S, Nelson SB. 2006. Lack of Patchy Horizontal Connectivity in Primary Visual Cortex of a Mammal without Orientation Maps. J Neurosci 26:7680–7692.

Vanderhaeghen P, Lu Q, Prakash N, Frisen J, Walsh CA. Frostig RD, Flanagan JG. 2000. A mapping label required for normal scale of body representation in the cortex. Nature Neuroscience. 3:358-365.Wang Q, Burkhalter A. 2007. Area map of mouse visual cortex. J Comp Neurol 502:339-357.

Vitek DJ, Schall JD, Leventhal AG. 1985. Morphology, central projections, and dendritic field orientation of retinal ganglion cells in the ferret. J Comp Neurol 241:1-11.

Wang Q, Burkhalter A. 2007. Area map of mouse visual cortex. J Comp Neurol 502:339-357.

Wang Q, Gao E, Burkhalter A. 2011. Gateways of ventral and dorsal streams in mouse visual cortex. J Neurosci 31:1905-1918.

Warton SS, Dyson SE, Harvey AR. 1988. Visual thalamocortical projections in normal and enucleated rats: HRP and fluorescent dye studies. Exp Neurol 100:23-39.

White LE, Bosking WH, Williams SM, Fitzpatrick D. 1999. Maps of central visual space in ferret V1 and V2 lack matching inputs from the two eyes. J Neurosci 19:7089-7099.

Zilles K, Wree A. 1995. Cortex: areal and laminar structure. In: The rat nervous system (Paxinos G, ed.). San Diego: Academic Press. p. 649-685.

Zilles K, Zilles B, Schleicher A. 1980. A quantitative approach to cytiarchitectonics. Anat Embryol 159:335-360.